THE UNIVERSITY OF MANITOBA

BIOELECTRIC ASPECTS OF THE RHODNIUS PROLIXUS OVARIOLE: EXTRACELLULAR CURRENT MAPPING DURING OOGENESIS

WADE JOHANNES SIGURDSON

A THESIS

SUBMITTED TO THE FACULTY OF GRADUATE STUDIES

IN PARTIAL FULFILMENT OF THE REQUIREMENTS FOR THE

DEGREE OF MASTER OF SCIENCE

DEPARTMENT OF ZOOLOGY

WINNIPEG, MANITOBA

FALL, 1984

BIOELECTRIC ASPECTS OF THE RHODNIUS PROLIXUS OVARIOLE: EXTRACELLULAR CURRENT MAPPING DURING OOGENESIS

BY

WADE JOAHANNES SIGURDSON

A thesis submitted to the Faculty of Graduate Studies of the University of Manitoba in partial fulfillment of the requirements of the degree of

MASTER OF SCIENCE

The effects of the juvenile hormone analogue Altosid, on extracellular currents were assessed in ovarioles from mated and virgin females. Altosid caused increases in the current flux at the T follicle posterior, lateral surface, interfollicular plug and the base and lateral tropharium surface. Altosid did not stimulate extracellular current flux on the lateral T follicle surface of virgin female ovarioles and caused depressed current efflux at the follicle's anterior end.

The germ cell plasmalemma, is continuous with oocytes and nurse cells, and may be regionally differentiated. Membrane surface charge distribution on denuded somatic and germ cell membranes was examined using native and cationic ferritin. The oocyte binds some ferritin, the nurse cells none. The follicle and tropharium inner sheath cells bind cationic ferritin in areas of cell to cell contact, often in linear arrays.

These results suggest the electrophysiological properties of the ovariole are correlated with events in oogenesis and may be involved in intercellular electrophoretic transport, intraovariole regulation and the maintenance of germ cell differentiation. Anionic site distribution suggests that the basal lamina and inner sheath cells may act as charge-selective barriers restricting access to the germ cells.

Acknowledgements

I wish to thank Dr. Erwin Huebner for the many stimulating discussions, constructive criticism and for instilling in me, a sense of the excitement of doing research. I also thank him for the help and patience during many trying "probe" experiences.

I also would like to thank Drs. P. McKay and T. Hara for their critical reading of the thesis and the many helpful comments and sugestions.

I sincerely thank Dr. Richard Nuccitelli for the numerous helpful discussions concerning the care and feeding of the vibrating probe.

I thank Dr. Jean Himms-Hagen for the generous use of her word processing facilities during thesis preparation.

I would also like to thank Andrew J. Watson and Greg M. Kelly for many discussions, scientific or otherwise.

I thank the University of Manitoba for the U. of M. Graduate Felowship.

Last but not least, I thank my wife Lynn, for her constant moral support throughout this work.

Abstract

Previous work on Rhodnius prolixus telotrophic ovarioles revealed an electropotential difference of 10 mV between the tropharium and oocyte. This coincides with the restricted movement within the tropharium of microinjected labelled basic proteins, suggesting an electrical polarity in the ovariole may be important during oogenesis. Further characterization of these properties were made with the highly sensitive, extracellular vibrating probe to determine if events occurring in oogenesis could be correlated with modulation of extracellular currents. Extracellular currents occur in two patterns of consistent current flow. The first is a current leaving the terminal follicle anterior and posterior ends and moving tangentially towards the lateral follicle surface, where weak influx currents occur. The current magnitude at the T follicle anterior and the interfollicular connective increased dramatically (4-5X) upon vitellogenesis. The strong efflux was maintained until chorionation when a significant decrease in efflux occurred at the connective. The second pattern consists of strong efflux at the connective, moving tangentially towards the tropharium where weaker currents entered along the entire surface. The previtellogenic region was variable as to current direction and magnitude, indicating this area is physiologically dynamic. Statistical analysis of the net current fluxes at 3 positions in this region indicated the development of a new current pattern around the penultimate follicle as the T oocyte completes vitellogenesis. There is a correlation between the current properties at specific positions with severence of the trophic cord.

Table of Contents

List of Figures

page

page

List of Tables

Chapter 1

General Introduction and Overview

The relationships between the structure and function of the cell types comprising insect reproductive tissues, have provided the impetus for much exciting and informative research in the areas of cell differentiation, interaction and cellular physiology.

Oogenesis in meroistic ovarioles is the result of the interaction between germ cells, the nurse cells and oocytes and mesodermally derived epithelial cells (see Huebner, 1984b; Telfer, 1975). There are two morphological types of meroistic ovarioles, polytrophic and telotrophic. Briefly, the polytrophic type is structurally simpler and consists of a germ-cell syncytium; the anterior cap of nurse cells are connected to the oocyte by intercellular bridges (Telfer, 1975; King and Aggarwal, 1965; Koch and King, 1966). The syncytium is encased in a layer of mesodermally derived, epithelial cells consisting of follicle cells around the oocyte and squamous inner epithelial cells around the nurse cell cap (King and Aggarwal, 1965; Koch and King, 1966). The telotrophic ovariole, characteristic of hemipterans, polyphage coleopterans and megalopterans is morphologically more complex (Telfer, 1975; Bünning, 1978, 1979a, 1979b; Huebner, 1984b). The germ cell syncytium consists of a single anterior common chamber (the tropharium) housing all the nurse cells connected to all the oocytes by cytoplasmic channels, the trophic cords (Huebner and Anderson, 1972c; Bünning, 1979a; Huebner, 1981a; 1984b).

Knowledge of the development and morphology of the hemipteran telotrophic ovary is essential to the elucidation of the underlying physiological processes. The nurse cell nuclei occupy common cytoplasmic lobes or extensions

off the acellular, microtubule filled trophic core (Huebner and Anderson, 1972c; Huebner, 1981a; Huebner, 1984a). The differentiation of this structure is the result of incomplete cytokinesis of germ cells forming intercellular bridges and the drastic structural reorganization of the trophic core region during the larval-adult moult (Huebner and Anderson, 1972c; Lutz and Huebner, 1980; Lutz and Huebner, 1981). Cytoplasmic continuity is maintained with the oocytes by long trophic cords which extend posteriorly to the developing oocytes within the vitellarium (Huebner and Anderson, 1972b; Huebner and Anderson, 1972c; Huebner, 1981a; Huebner, 1984b). This continuity has been maintained since post-embryonic development ie., before oocyte and nurse cells have differentiated. First instar ovarioles have presumptive germ cells connected by intercellular bridges (Huebner, 1982; Huebner, 1984b) and these connections are apparently maintained, although modified well into the development of the mature egg in the adult (Huebner, 1984b).

Oocytes differentiate in the basal region of the germarium during the larval-adult transformation and therefore all oocytes originate from the base of the tropharium in the adult insect (Lutz and Huebner, 1980; Lutz and Huebner, 1981; Huebner, 1984b). Each oocyte undergoes a stage of previtellogenic growth followed by a rapid size increase during vitelloginesis (Huebner and Anderson, 1972a; Huebner and Anderson, 1972a; Pratt and Davey, 1972a). At the completetion of vitellogenesis the chorion is produced by the follicular epithelium and is laid down on the vitelline membrane. The egg is then ovulated (Huebner and Anderson, 1972a; Huebner and Anderson, 1972b).

The germ-cell syncytium is encompassed in a mesodermally derived cell sheath composed of follicle cells surrounding the oocytes (Huebner and

Anderson, 1972a; Huebner,1981b; Huebner, 1984b), and inner sheath cells which cover the nurse cells (Huebner and Anderson, 1972a; Huebner, 1984a).

Functional Aspects of the Telotrophic Ovariole

The epithelial covering of the ovariole can influence the germ-cell syncytium in several ways. By simply isolating the nurse cell-oocyte complex from any humoral factors in the surrounding hemolymph, the germ cell physiology can be regulated. The follicular epithelium surrounding vitellogenic oocytes can regulate the onset and rate of yolk protein uptake from the hemolymph by the oocyte (Pratt and Davey, 1972a; Davey and Huebner, 1974; Ilenchuck and Davey, 1982). The follicle cells change their shape creating spaces between themselves permitting vitellogenin to reach the oocyte surface where it is incorporated by pinocytosis (Huebner and Anderson, 1972a; Huebner and Anderson, 1972b; Telfer et al., 1982; Huebner, 1984b). The follicle cells and oocyte also can interact via gap junctions (Huebner, 1981b; Huebner and Injeyan, 1981) implying communication and possible follicle cell regulation of the oocyte.

A tightly sealed epithelium may also isolate the germ-cell syncytia from the normal ionic milieu and create in the extracellular space between the two, an environment where ionic concentrations can be manipulated. These could set up gradients of charge producing membrane potential differences. A tightly sealed epithelium could also direct the flow of a charged species to regions of leakiness thus producing a loop of charge flow. A hypothesis based on these assumptions has been presented to explain the extracellular current pattern around a polytrophic ovariole (Woodruff et al., 1984a; 1984b).

Clearly, the enveloping epithelial tissue forms an intimate association with the germ tissue not only in post embryonic development but also during normal oogenesis (Huebner and Anderson, 1972a; Lutz and Huebner, 1980; Huebner and Injeyan, 1981).

The germ tissue is highly polarized structurally and this is a reflection of the polarization of function (Telfer, 1975; Huebner, 1984b). The oocyte germinal vesicle does not actively produce RNA (Vanderburg, 1963; Zinsmeister and Davenport, 1971; Davenport, 1974) and appears to actually repress the expression of the ribosomal DNA (Telfer, 1975; see Bünning, 1984 for a dissenting view). Therefore much of the synthetic activities have been taken over by the nurse cell nuclei. The primary function of the nurse cells is the production of various RNAs, proteins and organelles which are then transported to the oocyte for use during oogenesis and embryogenesis (Vanderberg, 1963; Huebner and Anderson, 1970; Davenport, 1974, 1976; Hyams and Stebbings, 1977; Capco and Jeffrey, 1979; Telfer, 1975; Huebner, 1984b). In polytrophic ovarioles the nurse cell products pass through intercellular bridges to the oocyte (Pollack and Telfer, 1969; Telfer, 1975), while in telotrophic ovarioles these products pass down the trophic cords to the oocytes (Zinsmeister and Davenport, 1971; Davenport, 1976; Capco and Jeffrey, 1979).

Most descriptions of syncytial tissues have emphasized that their morphology ensures synchronous and "homogeneous" differentiation of the compartments (Burgos and Fawcett, 1955; Fawcett et al., 1959; Franchi and Mandl, 1962; Zamboni and Gondos, 1967; Telfer, 1975) The differentiation of meroistic germ cells into nurse cells and oocytes, while maintaining their intercellular connections, raises some important questions concerning the

distribution of factors which control the differentiation process (Telfer et al., 1981).

Not only do the compartments of the syncytium maintain different differentiated states, there is also a high degree of intraovariole regulation of follicle development in Rhodnius (Pratt and Davey, 1972a; Huebner, 1983). Only one oocyte is permitted to undergo vitellogenesis and complete its growth in each ovariole, while the penultimate follicles remain arrested in previtellogenesis (Huebner and Anderson, 1972b; Pratt and Davey, 1972a).

It is not clear how this regulation takes place, although there is evidence the terminal oocyte may communicate with the penultimate or T-1 oocyte and the rest of the ovariole by its trophic cord (Huebner, 1981a, 1983). The oocytes maintain their syncytial ties with the tropharium until mid-vitellogenesis when the trophic cord severs from the oocyte (Huebner, 1981a). Thus all nurse cell products must be transported to oocyte before mid-vitellogenesis.

During previtellogenesis through to mid-vitellogenesis functioning transport mechanisms are important to ensuring the movement of macromolecules and organelles to the oocyte. Despite detailed ultrastructural studies on the trophic cords (Hyams and Stebbings, 1977, 1979a, 1979b) the underlying mechanism(s) that cause and regulate transport are unknown. The morphological approach to elucidating the transport mechanisms has limitations (see Telfer, 1975; Huebner, 1984b) and therefore application of physiological techniques integrated with the morphological background may provide new insights. Physiological manifestations or consequences of transport could include membrane potential differences reflecting electrical polarity, ionic gradients, differences in the composition and functioning of the plasma membranes of the germ-cell syncytium and the

partitioning of biochemical factors which influence the nuclear differentiation of the germ and somatic cells.

Bioelectricity in Developmental Biology

To consider the application of electrophysiological tools to the Rhodnius ovariole, a brief review of the techniques and their applications in other developing systems is useful. The work of Lund (1923; see Jaffe and Nuccitelli, 1977) was the first significant demonstration of electrical polarity within a filament of algal cells and the ability of an electric potential gradient to induce a morphological polarity in Fucus eggs. Although this stimulated further research, progress was hampered by techniques available at that time (Jaffe and Nuccitelli, 1977).

The study of small, steady transcellular electric fields may be approached by three methods: a) direct measurements of the electric field within or across the cells using conventional intracellular microelectrodes; b) measurements of the current flows driven through the medium by the tissue, using extracellular electrodes such as the vibrating probe; c) surface measurements of the voltage gradients in tissues removed from its medium (Jaffe and Nuccitelli, 1977; Rose, 1980). The early workers in this field could only perform the third type of measurements and as a result, due to artefacts caused by the sensing electrodes and drying of the tissue surface, much of their work needs re-evaluation (Jaffe and Nuccitelli, 1977). The first method, used to study transient membrane potential changes in excitable tissue for many years, suffers from a lack of sensitivity needed to detect very small electric fields and the invasiveness of

the technique (Jaffe and Nuccitelli, 1974, 1977; Rose, 1980). The measurements of electric fields across epithelia is relatively easy, but attempting to measure fields within the cytoplasm introduces large artefacts due to injury currents and tip potentials (Slayman and Slayman, 1962; Jaffe and Nuccitelli, 1974, 1977; Rose, 1980). Only in large cells can this approach be successfully used (Jaffe and Nuccitelli, 1977; Rose, 1980).

The ultrasensitive vibrating probe technique developed by Jaffe and Nuccitelli, 1974 overcomes the above problems. It is an extracellular electrode and therefore does not damage the cells and it is 100-1000 times more sensitive to small steady extracellular electric fields than conventional static microelectrodes (Jaffe and Nuccitelli, 1974, 1977). A description of the probe's operation, fabrication and set-up is in Chapter 2 and Appendix 1.

The initial studies into small extracellular electric fields were carried out by Jaffe (1966) who measured micro-volt transcellular differences in hundreds of Fucus eggs placed in electrical series. The development of the vibrating probe allowed the examination of individual eggs, thus improving the spatial and temporal resolution and the ability to study other systems.

The vibrating probe has subsequently been applied in the measurement of electrical currents; during pulses in fucoid eggs (Nuccitelli and Jaffe, 1974, 1975; Jaffe et al., 1974), traversing pollen tubes (Weisenseel et al., 1975), during ameboid movement (Nuccitelli et al., 1977), leaving regenerating newt limbs (Borgens et al., 1977, 1979), leaving the primitive streak of chick embryos (Jaffe and Stern, 1979), through full-grown and maturing Xenopus oocytes (Robinson, 1979), as natural proton currents traversing barley root hairs (Weisenseel et al., 1979), during the growth and sporulation of water mold

(Stump et al., 1980; Kropf et al., 1983), around muscle fibers (Betz et al., 1980), entering transected lamprey spinal cords (Borgens et al., 1980), around the chloride cell of teleost opercular membranes (Foskett and Scheffy, 1981; Scheffy et al., 1983), during the cleavage of Xenopus eggs (Kline et al., 1983), and leaving during Axolotl hind limb development (Borgens et al., 1983). Extracellular electric fields have been studied in two insect systems; the polytrophic ovariole of cecropia (Jaffe and Woodruff, 1979) and the telotrophic ovariole of Dysdercus (Dittmann et al., 1981).

The initial interest in the bioelectric aspects of insect ovaries was generated by Woodruff and Telfer (1973) who found a 10 mV potential difference between the oocyte and nurse cells (more electronegative) of cecropia. This electrical polarity is supported by studies where microinjected fluorescein labelled charged proteins moved unidirectionally between nurse cells and oocytes (Woodruff and Telfer, 1973, 1980). Acidic proteins could only move from nurse cells to oocytes, while basic proteins moved only from the oocyte to the nurse cells (Woodruff and Telfer, 1973, 1980; Telfer et al., 1981). This is precisely the pattern of movement one would expect of a charged species in an electrophoretic field, and prompted Woodruff and Telfer (1980) to propose that proteins could electrophoretically move in intercellular bridges. Further characterization of the resistances of oocytes and nurse cell showed that normal cytoplasmic resistivity (100-200 Ω-cm) within the bridges could account for the observed potential difference (Woodruff and Telfer, 1974). They estimated the current flow acoss the bridges and suggested that maintenance of the potential difference was physiologically feasible.

By applying the vibrating probe technique to the cecropia follicle, Jaffe and Woodruff (1979) confirmed the above transfollicular current flow. Strong positive current (up to 20 uA/cm^2) was seen to enter the nurse cell cap and leave the rest of the follicle. To explain the apparent contradictory extracellular and intracellular observations, Jaffe and Woodruff (1979) proposed a hypothesis in which electrogenic pumps were located only in the nurse cell membrane in the cleft region between the oocyte and nurse cell. This would permit a loop of positive current to enter the oocyte from across the cleft and return through the intercellular bridges (see Jaffe and Woodruff, 1979).

Subsequent research has prompted a modified hypothesis (Woodruff et al., 1984a; Woodruff et al., 1984b), where the entire nurse cell membrane produces an outward positive current which is inhibited from flowing out into the extracellular fluid by an insulating layer of inner epithelial cells, thus forcing the current to move through the peri-nurse cell space towards the oocyte (see Woodruff et al., 1984a).

The brief foregoing description of the bioelectric events in cecropia follicles provides an introduction to the present state of this type of research. It also provides the basis on which to discuss the observations of bioelectric phenomena in other insect ovaries, since the cecropia follicle has been the best studied in this regard. Very little information concerning the presence of electrical polarity, transfollicular currents and electrophoretic transport in other insect ovarioles exists (Huebner, 1984a).

In response to the exciting work of Woodruff and Telfer, intracellular recordings of nurse cells and oocyte membrane potentials were made in Rhodnius ovarioles (Telfer et al., 1981; Huebner, 1984a; Huebner et al., in

preparation). A 3 mV potential difference was observed with the nurse cells more negative; a result very similar to that found in cecropia. The presence of 10^{-8} M juvenile hormone caused a depolarization of the oocyte equilibrium potential increasing the difference to 10 mV (Telfer et al., 1981; Huebner, 1984a; Huebner et al., in preparation). The mobilities of fluorescently charged proteins, McFLy and FLy (methylcarboxylated fluorescein labelled lysozyme and fluorescein labelled lysozyme respectively) were also tested by microinjection into oocyte and the tropharium. Due to the long trophic cords it was estimated that a 100 mV potential difference would have to exist between the oocyte and nurse cells in Rhodnuis if the same size of gradient was to exist as found in cecropia follicles (Telfer et al., 1981). For this reason, both fluorescein labelled proteins were able to freely diffuse throughout the oocyte and partly up the trophic cords, indicating that an electrophoretic gradient did not exist within the ooplasm. The mobilities of the tracers were quite different within the tropharium. The acidic McFLy could freely diffuse within the syncytial portion of the tropharium, but the basic FLy was restricted to the injection site (Telfer et al., 1981). This was an indication of greater electronegativity in the nurse cell lobes than the trophic core, a situation which may restrict the movement of basic proteins between nurse cell lobes.

Extracellular current patterns surrounding coleopteran, megalopteran and orthopteran ovarioles have been briefly described (Huebner 1984a, Huebner and Sigurdson, 1984). Comparative analysis reveals species and ovariole type differences in current patterns (Dittmann et al., 1981; Huebner, 1984a; Overall and Jaffe, unpublished abstract).

There are several major differences in both the structure and development of the ovariole in the hemipterans Rhodnius and Dysdercus. The Rhodnius ovariole is highly regulated, producing only one vitellogenic follicle at a time while Dysdercus has up to eight vitellogenic follicles simultaneously (Dittmann et al., 1981). The trophic cords maintain contact only with the small pre-vitellogenic oocytes in Dysdercus, while the cords remain connected well into mid-vitellogenesis in Rhodnius (Huebner, 1981a). Therefore Rhodnius ovarioles will undergo cycles of egg production while Dysdercus continuously produces eggs.

Given these differences, and the larger body of information concerning its electrophysiological properties, it was felt that a rigorous and detailed analysis of the extracellular current patterns during an entire Rhodnius oogenesis cycle, could provide insights into the mechanisms that characterize intraovariole regulation and physiological polarity in this insect system. A study of this type would provide the groundwork for future studies involving the molecular mechanisms of current generation, ionic components of the current and hormonal regulation of current pattern and magnitude. Not only can the mapping of current patterns be established, but also modification of currents under hormonal influence. In the insect ovary juvenile hormone (JH) plays a central role in regulation of oogenesis (Pratt and Davey, 1972a; Huebner and Davey, 1973; Engelmann, 1979). The vibrating probe technique has been used to monitor the effect of hormones in a vertebrate system (Robinson, 1979).

The relationship of electrical polarity, in terms of extracellular electric fields and intracellular potential differences, to the general question of cellular differentiation and intracellular transport mechanisms, is actively under

investigation. The application of the vibrating probe technique for the study of the bioelectric events represents a new approach in the field of insect developmental biology. It is clear from the previous discussion, the surface has only been scratched and there is great potential for further work involving the telotrophic ovariole system.

The electrical current studies exhibit one manifestation of the functional assymetry between nurse cells and oocytes. A second aspect, since this is a syncytium bound by a single plasmalemma, is the possible regional differences in the plasma membrane between oocytes and nurse cells. A widely used and valuable approach to reveal membrane charge differences morphologically, is the use of cationic and native ferritin or colloidal iron as electron dense markers (Gasic et al., 1968; Danon et al., 1972; Nicolson, 1973; DeBruyn et al., 1978; Burry and Wood, 1979 ; Simionescu et al., 1981). No previous studies on membrane charge distribution in insect ovarian tissues have been reported. Thus to augment the electrophysiological data, Rhodnius ovarian tissues were appropriately prepared for ferritin and colloidal iron binding studies. These were successful in revealing membrane charge heterogeneities (see Chapter 4).

Chapter 2

Ovariole Extracellular Current Mapping During Oogenesis

Introduction

The functional units, or ovarioles of insect meroistic ovaries, consist of germ and somatic cells in a highly polarized structural and functional arrangement (see reviews Telfer, 1975; Huebner, 1984b). Polytrophic ovarioles develop from cystocytes, which differentiate into one oocyte and several nurse cells (occupying the anterior cap) in each follicle (King and Aggarwal, 1965; Koch and King, 1966; Telfer, 1975). The oocyte and nurse cells are connected by intercellular bridges, which have arisen from incomplete cytokinesis during the differentiation of the germ cells (King and Aggarwal, 1965; Koch and King, 1966; Huebner et al., 1975. Telfer, 1975). Thus a germ-cell syncytium exists, which is maintained until the oocyte is matured (Telfer, 1975). Each follicle is covered by mesodermally derived epithelial cells, which have differentiated into follicle cells, surrounding the oocyte, and inner epithelial cells, surrounding the nurse cell cap (King and Aggarwal, 1965; Koch and King, 1966; Huebner et al., 1975; Telfer, 1975). Telotrophic ovarioles have segregated the nurse cells to an anterior chamber, the tropharium and the oocytes to the posterior vitellarium (see Huebner, 1984b; Huebner and Anderson, 1972b, 1972c; Bünning, 1978, 1979b) . The oocytes maintain long open cytoplasmic channels called, trophic cords, with the nurse cells of the tropharium thus forming a spatially exaggerated syncytium (Huebner and Anderson, 1972b, 1972c; Bünning, 1978; Huebner, 1981a). The trophic cords and nurse cell syncytial connections result from incomplete

cytokinesis of germ cells and a structural reorganization of the tropharium during the larval-adult moult (Bünning, 1978, 1979b; Lutz and Huebner, 1980, 1981; Huebner, 1982, 1984b). The entire ovariole is encased in mesodermally derived follicle and inner sheath cells (Huebner and Anderson, 1972a; Huebner, 1984a, 1984b). As each oocyte begins development it becomes encased in a single layer of follicle cells which have differentiated from a storehouse of prefolliclular cells at the tropharium base (Huebner and Anderson, 1972a, 1972b; Bünning, 1979b; Huebner, 1984b). The inner sheath cells form a complete covering over the nurse cells in the Rhodnius ovariole (Huebner and Anderson, 1972a; Huebner, 1984a, 1984b).

The germ cell syncytium is functionally polarized. Nurse cells become polyploid (Telfer, 1975) and produce primarily RNA (Bier, 1963; Vanderberg, 1963; Zinsmeister and Davenport, 1971; Telfer, 1975). These nurse cell products in the form of ribosomes and/or rRNA (Davenport, 1974, 1976; Huebner and Anderson, 1970; Telfer, 1975; Hyams and Stebbings, 1977), messenger RNA (Telfer, 1975; Capco and Jeffrey, 1979) and possibly mitochondria (Telfer, 1975; Hyams and Stebbings, 1979) are transported to the oocyte via intercellular bridges in polytrophic ovarioles (Bier, 1963; Pollack and Telfer, 1969) or down the trophic cords in telotrophic ovarioles (Zinsmeister and Davenport, 1971; Davenport, 1976; Capco and Jeffrey, 1979).

The telotrophic ovariole of the hemipteran Rhodnius prolixus, is well suited as a model for the study of the cell interactions during oogenesis. The extensive morphological background (see reviews by Huebner, 1984a, 1984b) has laid down the groundwork for the investigation of the physiological parameters which characterize the transport of nurse cell products and regulatory molecules

within the germ-cell syncytium. Recently, preliminary reports on the electrophysiological properties of the Rhodnius ovariole have shown the presence of an 10 mV electro-potential gradient between the tropharium (more negative) and oocyte (Telfer et al., 1981; Huebner, 1984a; Huebner et al., in preparation). The restricted movement of microinjected fluorescein labelled lysozme (FLy) within the nurse cell lobes indicates the possible electrophoretic movement of charged proteins within the tropharium (Telfer et al., 1981).

These initial results parallel the earlier work on the structurally simpler polytrophic ovariole of Hyalophora cecropia. Woodruff and Telfer (1973, 1974, 1980) have shown the presence of a 10 mV potential difference between the nurse cells and oocytes (nurse cells more negative) and unidirectional movement of acidic and basic proteins microinjected into the nurse cells and oocyte.

The electro-potential difference, if not due to fixed charges, would result in current flow through and around tissues which can be detected using extracellular electrodes such as the vibrating probe (Jaffe and Nuccitelli, 1974; see review by Jaffe and Nuccitelli, 1977). Jaffe and Woodruff (1979) detected extracellular current flowing around the cecropia follicle, where positive current left the oocyte and entered the nurse cell cap region, thus confirming that a transfollicular potential existed.

There is very little information available on the bioelectric properties of telotrophic ovarioles. Dittmann et al. (1981) have reported strong extracellular currents around Dysdercus ovarioles consisting of two separate circuits. The first surrounds the tropharium and pre-follicular region, where current leaves pre-follicular tissue and enters the tropharium. The second circuit surrounds each of the multiple developing follicles, in which very strong currents leave

the interfollicular connectives and enter the lateral surfaces of the follicles. Preliminary reports on extracellular electric fields around Rhodnius ovarioles, indicate current leaving the interfollicular region and entering the tropharium (Huebner, 1984a). Dysdercus and Rhodnius, although both hemipterans, differ significantly in the way their ovarioles function. Dysdercus contains multiple vitellogenic follicles in each ovariole (Dittmann et al., 1981). The trophic cords lose contact with the oocytes quite early, which produces follicles independent from the nurse cell syncytium and younger pre-vitellogenic oocytes (Dittmann et al., 1981). The Rhodnius ovariole is highly regulated producing only one vitellogenic follicle in each ovariole (Pratt and Davey, 1972a; Huebner, 1981a, 1983). The trophic cord remains connected to the terminal (T) oocyte well into mid-vitellogenesis. These facts caused Huebner (1981a, 1983) to speculate that the T oocyte inhibits the development of previtellogenic oocytes by communication with the rest of the ovariole via the trophic cord. The mechanism of this intraovariole regulation is not known. Therefore, the Rhodnius ovariole produces eggs in a cyclical manner (Pratt and Davey, 1972a) while Dysdercus will produce eggs continuously.

These differences plus the electrical polarity found in the Rhodnius ovariole has prompted a detailed examination of the extracellular current patterns and magnitudes surrounding ovarioles during a complete oogenesis cycle. This study will examine the electrophysiological events which characterize the structural and functional assymetry of the Rhodnius ovariole in an attempt to determine a possible mechanism for the transport of nurse cell products, control of germ-cell differentiation and intraovariole regulation.

This study will also provide the background for future work concerning the identification of the ions important in current generation and the location of their associated membrane pumps. The modulation of extracellular currents with hormones known to be crucial for oogenesis, may provide insight on the external regulation of the ovariole.

Materials and Methods

The insect used in this study was the hemipteran Rhodnius prolixus. The colony was maintained under controlled conditions of temperature (27^{o}) and high humidity. Animals were fed and reared as previously described by Huebner and Anderson (1972a). Ovaries were removed on successive days after feeding.

Ovaries were dissected from females under Rhodnius Ringers (Madrell, 1969) and the ovarioles separated and desheathed immediately before use. The external ovariole sheaths are quite muscular and cause the ovariole to convulsively twist and turn, which prevents making measurements in close proximity to the ovariole surface. The muscular contractions may also be a source of external electric fields which could confuse observations made on the ovariole. Dittmann et al., (1981) reported that external sheathes around Dysdercus ovarioles did not influence extracellular current measurements, although the potential problem of muscle generated electric fields was not addressed. All extracellular current measurements reported here are from desheathed ovarioles.

For purposes of comparing extracellular current values during oogenesis, ovarioles were classified on the basis of T oocyte length; starting at 300 μM to 400 μM for Ovariole Class 1, and increasing in 100 μM increments for classes 2, 3, 4, 5, 6, 7, and in 500 μM increments for stages 8 and 9 (Table 1; see also Pratt and Davey, 1972a). All measurements of ovariole dimensions employed a calibrated ocular micrometer or ocular grid. The results of the growth characteristics are in Appendix 2.

Ovarioles were placed in fresh Ringers, in specially designed chambers made of a 1.5 mm thick plexiglass ring cemented to a #1 coverslip as a bottom. The chamber rim held two diametrically opposed #23 gauge syringe needles connected to a double syringe system which permitted the exchange of fresh Ringers without changing the fluid level of the chamber. The chamber was placed on a 1 cm thick plexiglass gliding stage, greased to the standard stage of a modified Leitz Diavert inverted microscope. This facilitated the precise positioning of the ovariole in relation to the vibrating tip.

Small steady extracellular electric fields around ovarioles were measured with the vibrating probe (Jaffe and Nuccitelli, 1974; purchased from the Vibrating Probe Company, Davis CA). The sensing electrode is a 30 μM platinum black ball vibrating at 320-450 Hz (driven by a piezoelectric reed), which produces a sinusoidal output when in the presence of an electric field. This AC signal is amplified and filtered by a lock-in amplifier (Princeton Applied Research Model #5101) tuned to the vibration frequency, whose DC output drives a chart recorder. The probe is calibrated with a constant current source to permit matching the phase of the probe signal with that of the AC voltage used to drive the piezoelectric reed. This ensures the maximum sensitivity and the correct current polarity are attained. A complete description of the fabrication, operation and set-up procedures is presented in Appendix 1. Given the medium resistivity and vibration amplitude, the current density can be easily calculated (see Appendix 1). Rhodnius Ringers has a resistivity of 60 Ω-cm and the vibration amplitude was the same as the diameter of the probe tip ie., approximately 30 μM.

Sixteen positions along the ovariole surface were chosen for extracellular current measurement (Fig. 1) which coincide with morphological landmarks, permitting a consistent evaluation of the currents at particular position during the oogenesis cycle. To aid in identifying a position, reference to the numeric positions in Fig. 1 will be made. For example, P3 refers to the interfollicular connective between T and T-1 follicles, while P7 refers to the tropharium base.

The data consist primarily of measurements made perpendicular to the ovariole surface, thus indicating influx or efflux of positive current. A comprehensive collection of parallel measurements comparable to the vertical measurements was not done in this study, owing to the length of time each ovariole would be in vitro in order to accomplish both types of measurements. Tangential current directions from ovarioles from all clases have been combined and presented in Fig. 2. The data has been presented and analyzed in two ways. The mean current value and direction for each position are plotted for each ovariole class (Figs. 3-11), thus demonstrating the current distribution pattern of influx and efflux along the ovariole surface. The second approach was the comparison of the mean current values of one position for all ovariole classes (Figs. 12-27), thus showing any changes in current direction and magnitude throughout the oogenesis cycle. The second approach provides an easy way to examine dynamic changes in current properties at one region of the ovariole throughout oogenesis.

Analysis of variance and a multiple comparision test were used to determine if statistically significant differences between mean current values existed between different positions along the ovariole and between the same position, from ovarioles of different size classes. A complete description of the

statistical procedures is given in Appendix 3. Certain positions proved to be quite variable as to the direction of current flow. For this reason exiting current was designated as a negative value and entering current as a positive value. Therefore, mean current values from these positions, represent the net current flux at that position.

Results

Extracellular Current Patterns

The most consistent observable feature of current flow around the ovariole was the large efflux of current at P3 (interfollicular plug) and P2c and the smaller influx of current spread over the tropharium (P8, P8a, P8b). This pattern was consistently observed in all ovarioles examined (Figs. 3-11).

The posterior end of the T follicle, P1, consistently produced an efflux of current in 81% of the ovarioles examined. The other ovarioles were evenly split between no detectable current or small entry currents. When the probe was positioned anterior to P1, at P1a, current efflux was still detected (except for ovariole class 1) but decreased (Figs. 4-11). This decrease was shown to be statistically significant for ovariole classes 4-9, but not 2 and 3, using a Bayes Rule least significant difference, multiple comparison test (Waller and Duncan, 1969). These differences were significant at an error-seriousness ratio or K ratio of 100, which is equivalent to $\alpha = 0.05$ for a Student's t test (see Waller and Duncan, 1969). The tangential current moves anteriorly from positions P1 and P1a towards the lateral surface of the follicle (Fig. 2).

The vertical measurements on the lateral surface of the T follicle, P2, P2a and P2b demonstrate a gradual change from the strong efflux of current found at P2c and P3 to weaker effluxes at P2a and P2b and the variable current flux at P2 (eg. see Fig. 9). The decreased efflux current seen at P2b was significant (k=100) for all ovariole classes, except for class 1 which had one value (Fig. 3-11). Moving the probe less than 100 μM to P2a produced a another decrease in efflux current which was significant for for ovariole classes 4-8, but not 2, 3 or

9 (eg. see Fig. 10). The average current flux at P2 was variable during the oogenesis cycle (Fig. 14). The average efflux of current observed for ovariole classes 2, 4 and 6 were quite small, ranging from 0.2 to 0.5 $\mu A/cM^2$, while the average influxes ranged from 0.4 to 2.6 $\mu A/cM^2$. It was not possible to show a significant difference between the mean current values for each ovariole class with respect to position P2, although given the larger influx means, current appears to predominantly enter at P2, especially for the larger oocytes (see Figs. 9, 10, 11). Parallel measurements at P2c, P2b and P2a showed strong current moving posteriorly from these areas towards the mid-lateral region near P2. This tangential current was strongest at P2c and decreased as one moved toward P2 (Fig. 2). At P2, both anterior and posterior tangential current of almost equal size could be detected. In more than half of the ovarioles examined at P2 (12 out of 21) no tangential current was detected at all.

The current effluxes measured at the apical end of the T follicle (P2c) and the interfollicular plug region (P3) were the largest extracellular currents measured around the Rhodnius ovariole, attaining mean maximums of 18.6 $\pm$ 3.7 S.E. $\mu A/cM^2$ (Fig. 8) and 21.2 $\pm$2.3 S.E. $\mu A/cM^2$ (Fig. 10) respectively. Surprisingly, given the close proximity of the two positions (usually <100 μM), P3 was significantly ($k=100$) larger than P2c during the early stages of vitellogenesis ie, ovariole classes 3, 4 and 5 (Fig. 5, 6, 7). There were no differences between means during previtellogenesis; ovariole classes 1 and 2 (Figs. 3 and 4 respectively). During the later stages of vitellogenesis the position with the largest mean current efflux fluctuates between ovariole classes. P2c is greater than P3 during ovariole class 6 (Fig. 8); while there is no difference during ovariole class 7 (Fig. 9). P3 is greater than P2c for class 8

(Fig. 10) and then reverses during ovariole class 9 (Fig. 11). The tangential current measured at P3 was reversed in direction from that observed at P2c ie., strong currents moved towards the T-1 follicle. This was also observed at P4 (Fig. 2), although the size had decreased.

On the lateral surface of the T-1 follicle, P4, the large current efflux observed at P3 has dramatically decreased for all ovariole classes (Figs. 3-11). In all classes this decrease was significant (k=100). During the early stages of vitellogenesis (ovariole classes 1-6), when current was detected, it predominantly left this position with magnitudes ranging from 0.3 to 3.6 $\mu A/cM^2$ with one exception. One ovariole produced a 20.4 $\mu A/cM^2$ outward current at this position and presumably has skewed mean value shown in Fig. 5. This ovariole did not appear damaged or abnormal in any way. When current was observed to enter, it was small in magnitude (0.3 to 1.7 $\mu A/cM^2$) and was found only during ovariole classes 2, 5 and 6. During the later stages of vitellogenesis (classes 7, 8, 9), current flux was divided between influx (ranging from 0.5 to 3.2 $\mu A/cM^2$)and influx (ranging from 0.5 to 8.9 $\mu A/cM^2$). In 25 ovarioles measured at P4, no current was detected.

The positions along the younger previtellogenic follicles (T-2, T-3 etc. etc.) and up to the tropharium base (positions P5, P6, P7), were the most variable both in terms of current direction and magnitude. Therefore it is necessary to discuss these data in terms of net current flux as represented by the means, and determine if the means differ between positions during each ovariole class. A more detailed examination of current direction patterns will be given below.

The three positions do not differ significantly during ovariole class 1 and therefore the net current flux for this entire region is outwards (Fig. 3). At the beginning of vitellogenesis, class 2, the positions again do not differ from each other, but the net current flux is now inwards (Fig. 4). During class 3 all three positions become quite variable as to current direction and magnitude with P5 producing a net influx, P6 almost no current flux and P7 showing an average current efflux (Fig. 5). Later in vitellogenesis (class 4), current leaves P5 primarily, while the net current flux at P6 and P7 is close to zero (Fig. 6). As the T follicle enters mid-vitellogenesis and prior to trophic cord separation, the extracellular current around the pre-vitellogenic area of the ovariole appears as a relatively uniform current efflux (Figs. 7 and 8). During ovariole classes 5 and 6, P5 produced small current effluxes with means of 1.1 $\pm$0.4 S.E. and 0.6 $\pm$0.3 S.E. $\mu A/cM^2$ respectively. At P6 similar current effluxes were detected (0.8 $\pm$0.5 S.E. and 0.5 $\pm$0.3 S.E. $\mu A/cM^2$ respectively). P7 was more variable with means of 1.9 $\pm$2.6 S.E. and 0.3 $\pm$1.9 S.E. $\mu A/cM^2$ respectively (see Figs. 7 and 8). When the T follicle reaches a length of 900 to 1000 μM, the trophic cord begins to lose contact with the oocyte (Huebner, 1981a). At this time the previtellogenic region in the ovariole shows a net current influx at positions P6 and P7 (Fig. 9). At P5 the mean current is near zero, but variability of current magnitude and direction were quite large. Current efflux values ranged from 0.5 to 17.3 $\mu A/cM^2$ while current influx values ranged from 0.5 to 17.3 $\mu A/cM^2$ with the number of occurrences of each evenly divided. During mid-vitellogenesis (ovariole class 8), P6 becomes a region of current influx which was shown to be significantly larger than the small influxes at P5 and P7 (k=100). Both P5 and

P7 were quite variable in current direction and magnitude as evidenced by the large standard errors (see Fig. 10).

As the terminal oocyte nears the completion of vitellogenesis and begins chorion formation (ovariole class 9), the current fluxes at positions P6 and P7 become small and do not significantly differ from each other (Fig. 11). At this time P5 becomes an region of strong consistent current efflux (mean 4.9 $\pm$1.0 S.E. $\mu A/cM^2$) which differs significantly from the values obtained at P6 and P7.

The parallel measurements at P5 produced an even split (of number of occurrences), in terms of direction and current strength, with current moving posteriorly (mean 5.3 $\pm$9.3 S.D.) and anteriorly (mean 4.2 $\pm$3.8 S.D. $\mu A/cM^2$) in the 17 ovarioles examined (Fig. 2). At P6 current moved predominantly towards the tropharium (Fig. 2). The variability in the vertical measurements made at P7 is reflected in the tangential measurements as well, although the posterior directed current was stronger (4.6 $\pm$5.4 S.D. $\mu A/cM^2$) than the anterior directed current (2.7 $\pm$1.9 S.D. $\mu A/cM^2$).

The position P7a is 50-60 μM anterior to P7 and represents the posterior region of the tropharium proper (see Fig. 1). Even over this small distance, the current direction and magnitude becomes much more consistent than observed at P7 in all ovariole classes except 5 and 9 where the means are small with large standard errors; 0.2 $\pm$1.1 S.E. and 0.1 $\pm$0.9 S.E. $\mu A/cM^2$ respectively, (Figs. 7 and 8). In all other classes the mean influx of current ranged from 0.7 $\pm$0.5 S.E. to 2.1 $\pm$0.9 S.E. $\mu A/cM^2$. Due in part to the large variation observed at P7, a significant difference (k=100) between means for P7 and P7a could only be shown for ovariole class 6 (Fig. 8). The tangential current measured at P7a was also more consistent in direction than that observed at P7, and consisted almost

entirely of anterior directed current with an average strength of 4.0 ±3.3 S.D. $\mu A/cM^2$ (Fig. 2).

The lateral surface of the tropharium, represented by positions P8, P8a and P8b had a consistent influx of current during the entire oogenesis cycle (Figs. 3-11). There were no detectable differences in mean current values between any of these positions for any of the ovariole classes. The mean current influx at P8 for all ovariole classes ranged from 1.3 to 3.3 $\mu A/cm^2$ with standard errors ranging from 0.3 to 1.0 (Fig. 24). At P8a the means ranged from 1.6 to 2.9 $\mu A/cM^2$ with standard errors from 0.4 to 1.1 (Fig. 25). At P8b the means were slightly less, ranging from 0.7 to 2.6 $\mu A/cM^2$ with standard errors from 0.3 to 1.1 (Fig. 26). Parallel measurements were made only at P8. Two-thirds of the ovarioles (12) examined had current directed towards the tropharium tip, while the remainder (7) had current moving towards the tropharium base. The means were quite similar, 2.5 ±1.9 S.D. and 2.0 ±0.8 S.D. $\mu A/cM^2$ for anterior and posterior respectively. The net current movement ie., all measurements combined with anterior as the negative values, was 0.7 ±2.4 S.D $\mu A/cM^2$ towards the tropharium.

The anterior tip of the tropharium, P8c, exhibited only small current fluxes which did not follow any particular pattern with respect to direction during the oogenesis cycle (see Fig. 27).

Dynamics of Extracellular Current During Oogenesis

The current flux measured at the majority of positions did not appreciably change during the oogenesis cycle. At P1 there is a trend of increasing current density as the T follicle enters the later stages of vitellogenesis (Fig. 12).

Analysis of variance and the Bayes Rule multiple comparison test could not demonstrate any significant differences between the means, however.

Likewise, no significant changes were observed for the means at P1a, P2, P2a and P2b (Figs. 13, 14, 15 and 16 respectively). At P2 however, the current influx appears to be more consistent during ovariole classes 7, 8 and 9 (Fig. 14). Position P2b shows the same trend as does P1 ie., increasing efflux as the T oocyte increases in size.

At P2c and P3, where the largest current effluxes are observed, the greatest changes in current density also occur. Initially at the follicle apex, P2c, the current density is small (4-5 $\mu A/cM^2$, Fig. 17) and gradually increases except for a small decrease at ovariole class 5, until reaching a maximum (18.6 $\pm$3.7 S.E. $\mu A/cM^2$) at class 6, just prior to trophic cord loss (Fig. 17). Current density at P2c was maintained at a lesser intensity during the later stages 7, 8 and 9. The mean current densities during ovariole classes 6, 7 and 8 were all significantly larger (k=100) than the means of classes 1, 2 and 5. Means from classes 6 and 8 were larger (k=100) than means from 3 and 4.

At P3 the efflux current density increased from 3.7 $\pm$0.9 S.E. during previtellogenesis to 18.4 $\pm$4.3 S.E. $\mu A/cM^2$ during early vitellogenesis (class 3, Fig. 18), a significant increase (k=100). This high current was maintained throughout vitellogenesis until the last stage, when the oocyte nears maturation (class 9), where it decreases significantly from the means at classes 7 and 8 (Fig. 18).

These changes at P2c and P3 can also be seen in Figs. 28 and 29 which are continuous data plots of current versus T oocyte size. The regression correlation coefficients for the predicted line of the P2c plot is r= 0.62, while

for the P3 plot r= 0.53. Although the correlations are not large, they do provide some indication to the changes that occur at these two positions during oogenesis.

Position P4 did not exhibit any significant changes in current density during oogenesis, except for class 3 (Fig. 19) which has a mean skewed by one anomalously high value. Statistical analysis without this value results in no differences between any means.

The large variability of current direction and magnitude seen at P5 during the cycle is evident in Fig. 20. Only during the final stage of T oocyte vitellogenesis (class 9) does the position produce a consistent current efflux with a mean of 4.9 $\pm$1.0 S.E. $\mu A/cM^2$. The same situation exists at P6, except a small influx is observed (0.4 $\pm$0.3 S.E. $\mu A/cM^2$) during ovariole class 9.

The positions P7, P7a, P8, P8a, P8b and P8c did not exhibit any statistically significant differences between means during the oogenesis cycle (Figs. 22-27).

Variable Current Properties at Positions P5, P6 and P7

The variable direction of current flux observed at the previtellogenic region of the ovariole made interpretation of the data difficult. Therefore the frequency of current efflux at each of the three positions, P5, P6 and P7 were plotted for each ovariole class (Figs. 30-32). It is immediately obvious that during ovariole classes 4, 5 and 6, almost all current at P5 is leaving; that the frequency of efflux decreases during class 7 and then increases so that all current detected during class 9 leaves this region (Fig. 30). At P6 a similar pattern exists except that during previtellogenesis all current is efflux and this

proportion drops dramatically as vitellogenesis begins (classes 2 and 3, Fig. 31). The frequency of efflux then rises to 60-70% during the earlier vitellogenic stages and then drops precipitously during later stages indicating a predominant current influx (Fig. 31). P7 is remarkably consistent, with about a third to a half of the direction frequency being efflux (Fig. 32).

TABLE I. Ovariole classification based on T oocyte size and the accompanying stage of vitellogenesis.

Ovariole Class	T Oocyte Size (μM)	Characteristics
1	300-400	Previtellogenesis
2	400-500	Late previtellogenesis to very early vitellogenesis
3	500-600	Early vitellogenesis
4	600-700	Vitellogenesis
5	700-800	"
6	800-900	"
7	900-1000	Mid-vitellogenesis, Trophic cord loss to T oocyte
8	1000-1500	Mid- to late vitellogenesis
9	1500-2000	Late vitellogenesis, chorion formation

Figure 1. The numeric positions along the ovariole surface corresponding to the locations of extracellular current measurement. Positions will be designated as P1, P2 etc. etc. in the text, although the "P" has been omitted in this diagram. P1, the posterior end of the terminal follicle, near the pedicel. P1a, just anterior to P1, near the beginning of the patent follicular epithelium. P2, the mid-lateral surface of the tropharium. In larger follicles, P2 was located about a third of the total follicle length from the anterior end of the follicle. P2a was located just posterior to the start of the apical follicle cells. P2b, was placed right at the boundary between the lateral and apical follicle cells. P2c, was located at the apical follicle cells. P3, the interfollicular connective. P4, the mid-lateral surface of the T-1 follicle. P5, the region destined to become the interfollicular connective for the T-1 follicle, when the T follicle has been ovulated. P6, a region equidistant between P5 and P7; the previtellogenic region. P7, the tropharium base. P7a, the basal portion of the tropharium proper. P8, the mid-lateral position, approximately a third of the total tropharium length from the tropharium base. P8a, anterior to P8, about two-thirds the way up the tropharium. P8c, the tropharium apex near the terminal filamant. Diagram in modified from Huebner (1984a).

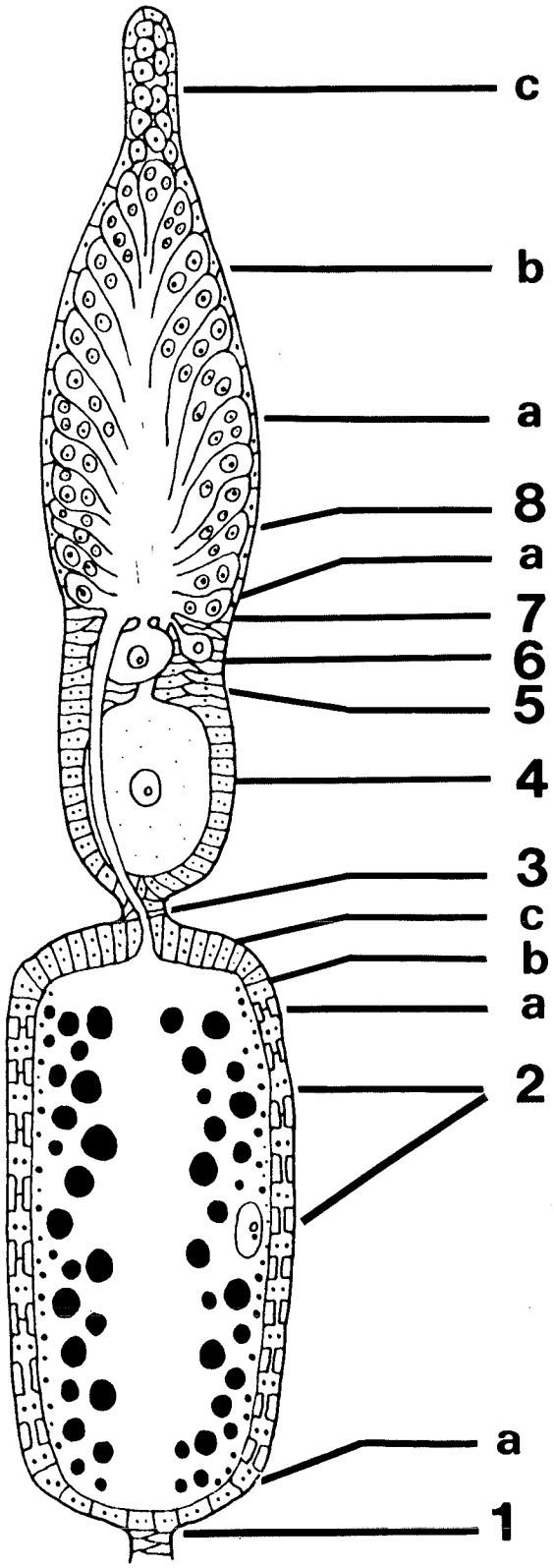
c
b
a
8
a
7
6
5
4
3
c
b
a
2
a
1

Figure 2. The movement of tangential extracellular current along the ovariole surface. Arrows indicate current direction and average magnitude (length proportional to current density; ordinate, current density in $\mu A/cM^2$, abscissa in μM). Each position from Fig. 1 except, P8a, P8b and P8c are represented. At certain positions, two arrows are used to indicated current was found moving in both directions. Diagram modified from Huebner (1984).

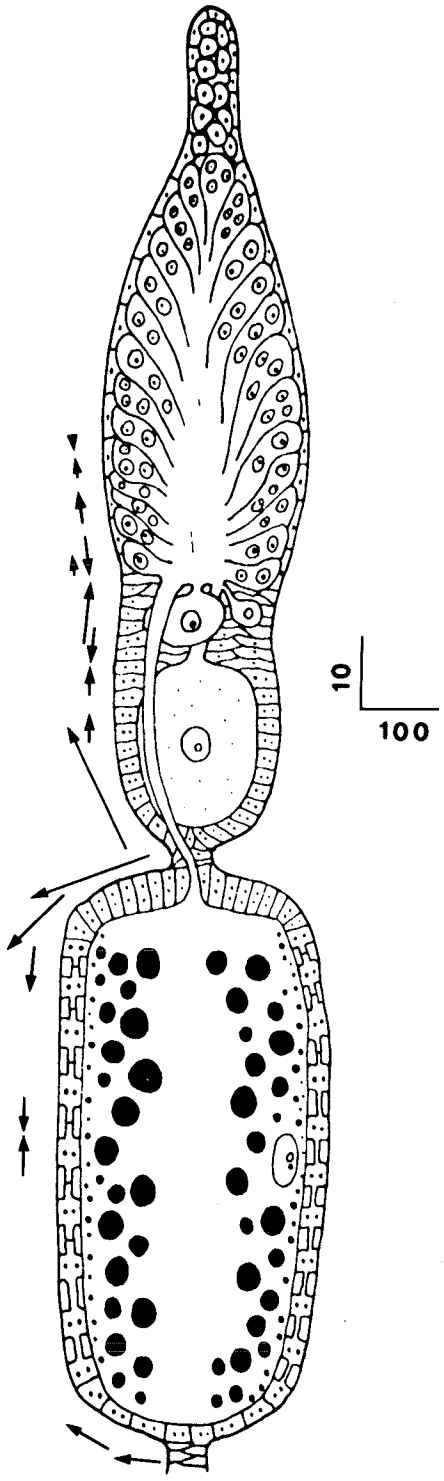
10
100

Figure 3. Extracellular current measurements along the ovariole surface from ovariole class 1. By convention, all current is considered positive. The typical pattern of current efflux at P1, P2b, P2c and P3, influx over the tropharium at P7a, P8, P8a and P8b is evident from the earliest stage of oogenesis examined. P2b is the result of one value.

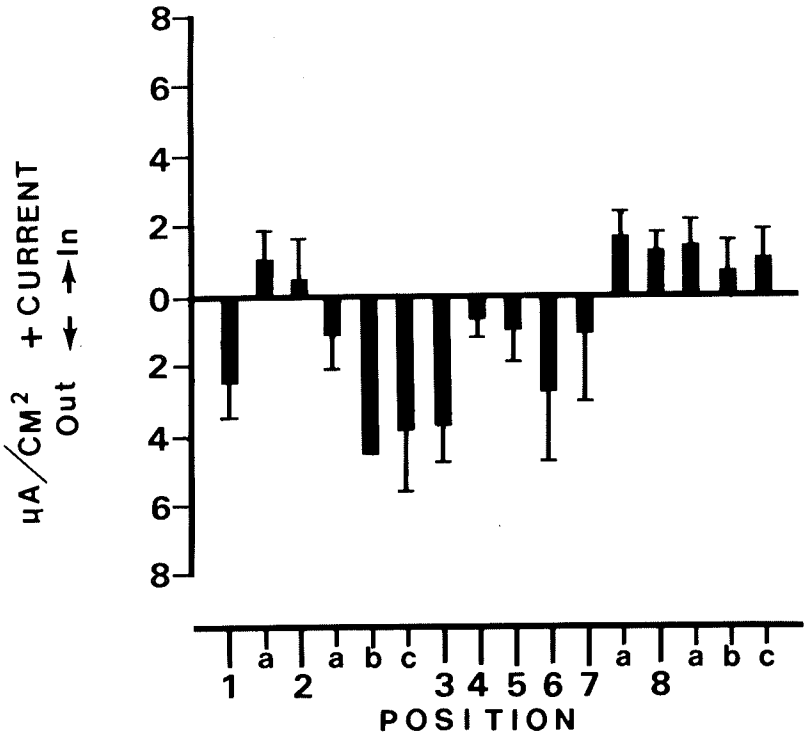
8
6
4
2
0
2
4
6
8
μA/CM² + CURRENT
Out → In
a
a b c
a
a b c
1 2 3 4 5 6 7 8
POSITION

Figure 4. Extracellular current measurements along the ovariole surface from ovariole class 2. The efflux at P2c and P3 has begun to increase during this stage of "activation" of the terminal follicle. The previtellogenic region has predominantly current influx at this stage.

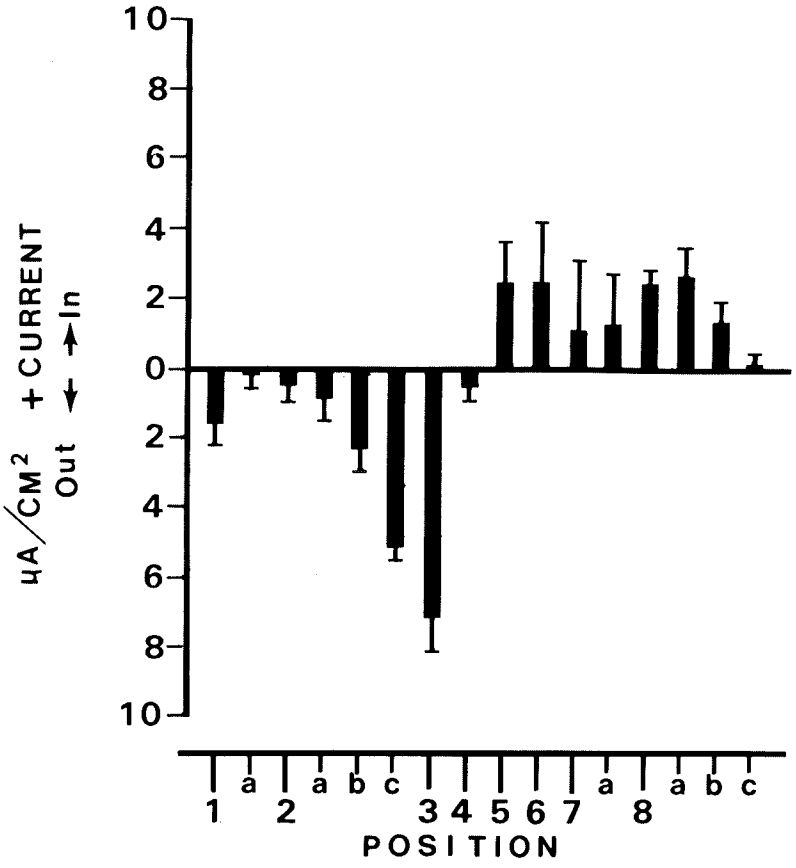
10
8
6
4
2
0
2
4
6
8
10
μA/CM² + CURRENT
Out → In
1 a 2 a b c 3 4 5 6 7 a 8 a b c
POSITION

Figure 5. Extracellular current measurements along the ovariole surface during ovariole class 3. Current efflux at P2c and P3 has increased again as the terminal oocyte begins vitellogenesis. The previtellogenic region now begins to show a great deal of varibility in magnitude and direction of current flow.

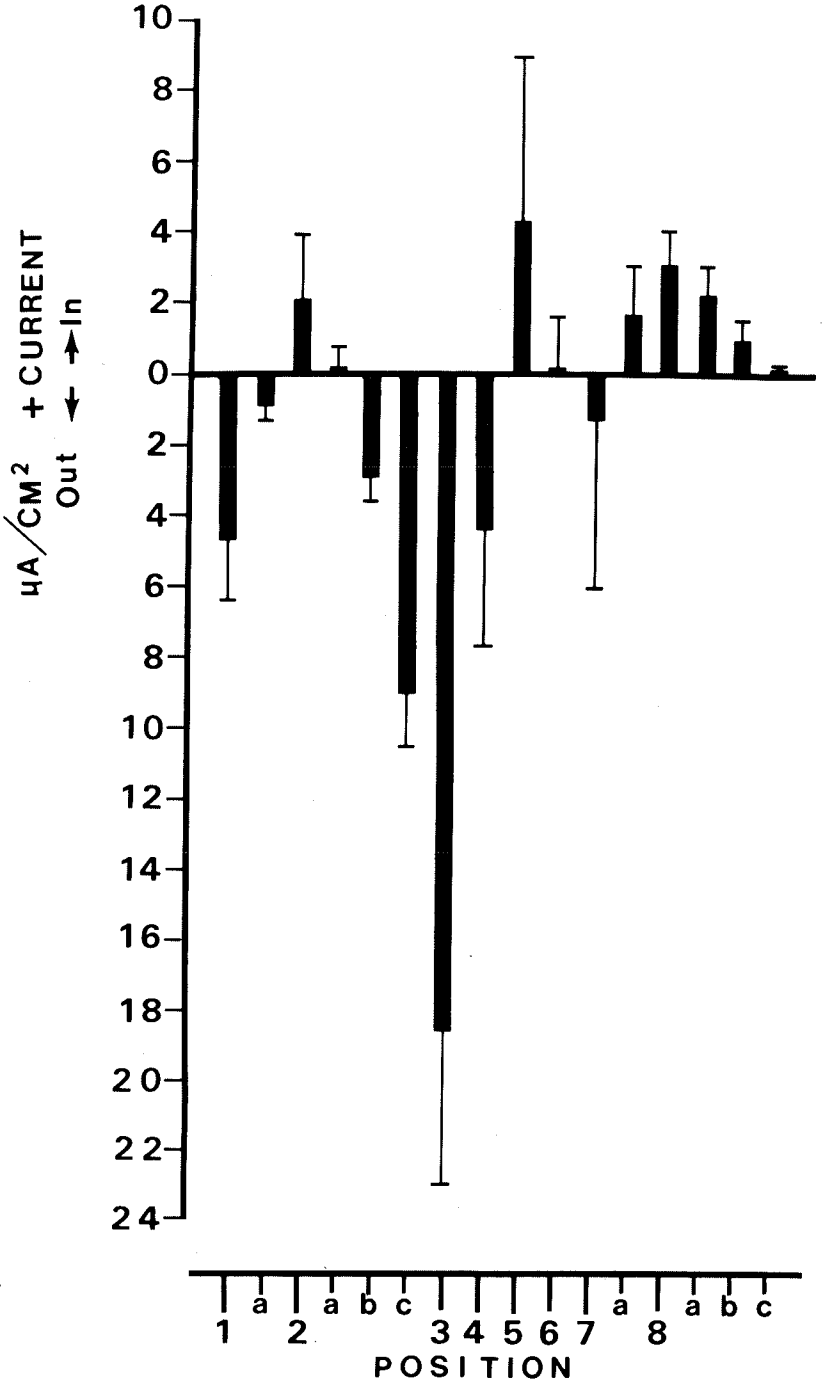
10
8
6
4
2
0
2
4
6
8
10
12
14
16
18
20
22
24
μA/CM²
+ CURRENT
Out → ← In
1
a
2
a
b
c
3
4
5
6
7
a
8
a
b
c
POSITION

Figure 6. Extracellular current measurements along the ovariole surface from ovariole class 4. The pattern of current influx over the tropharium and efflux at the posterior and anterior ends of the T follicle remains unchanged now that the terminal oocyte is vitellogenic.

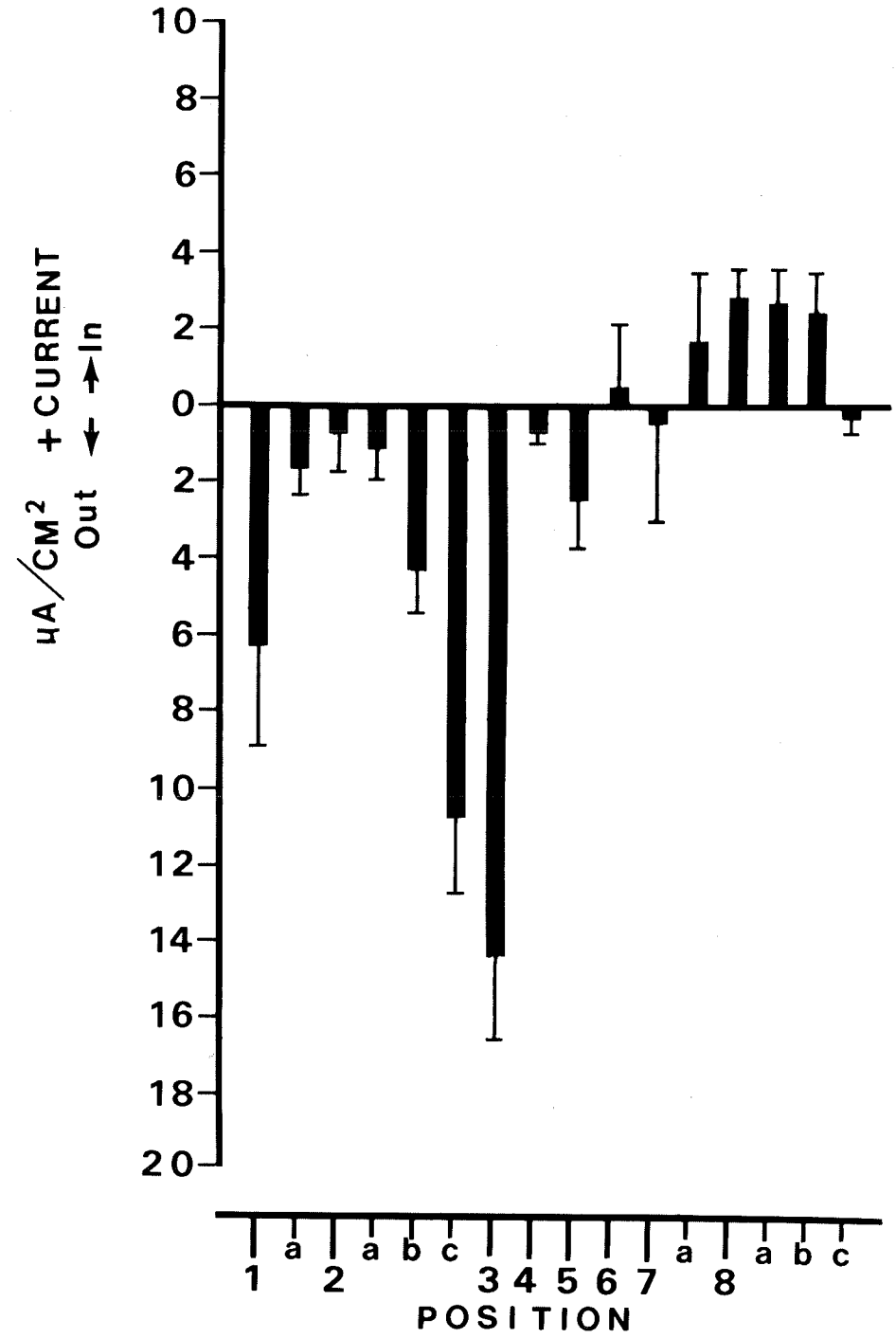
10
8
6
4
2
0
2
4
6
8
10
12
14
16
18
20
μA/CM²
+ CURRENT
Out ↑ ↓ In
a
a b c
a
a b c
1 2 3 4 5 6 7 8
POSITION

Figure 7. Extracellular current measurements along the ovariole surface from ovariole class 5.

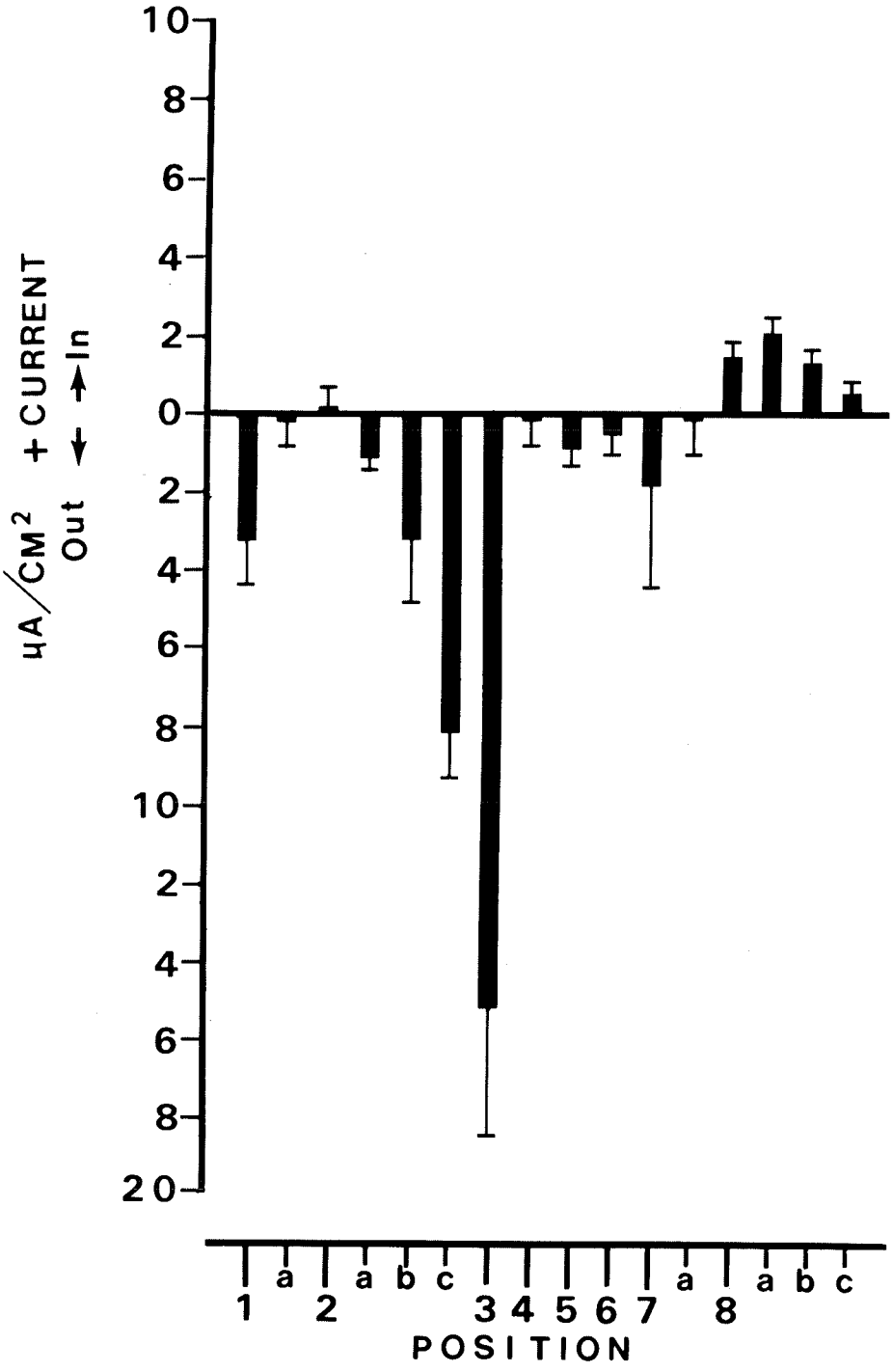
10
8
6
4
2
0
2
4
6
8
10
2
4
6
8
20
μA/CM² + CURRENT
Out → ← In
1
a
2
a
b
c
3
4
5
6
7
a
8
a
b
c
POSITION

Figure 8. Extracellular current measurements along the ovariole surface from ovariole class 6.

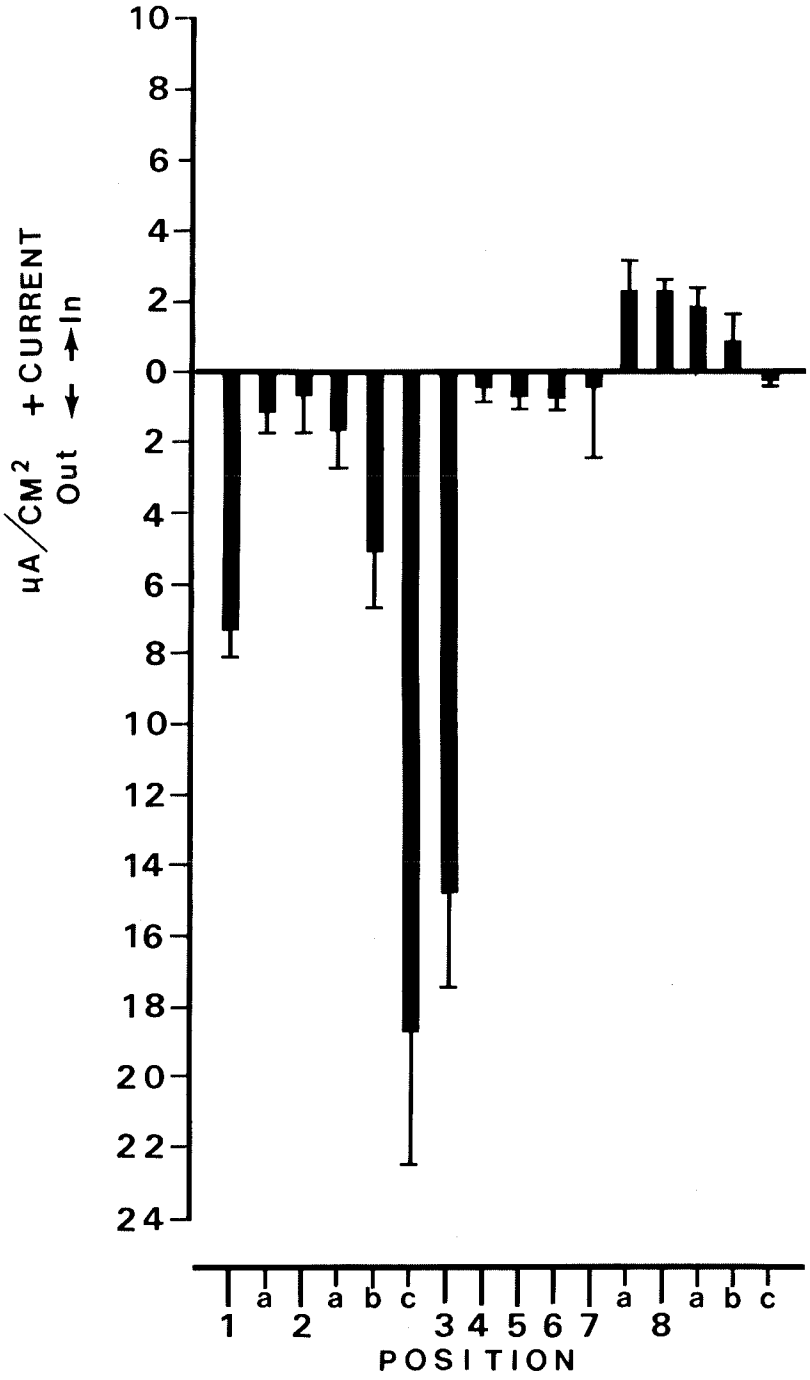
10
8
6
4
2
0
2
4
6
8
10
12
14
16
18
20
22
24
μA/CM² + CURRENT
Out → ← In
1
a
2
a
b
c
3
4
5
6
7
a
8
a
b
c
POSITION

Figure 9. Extracellular current measurements along the ovariole surface from ovariole class 7. The initiation of trophic cord severance to the vitellogenic oocyte.

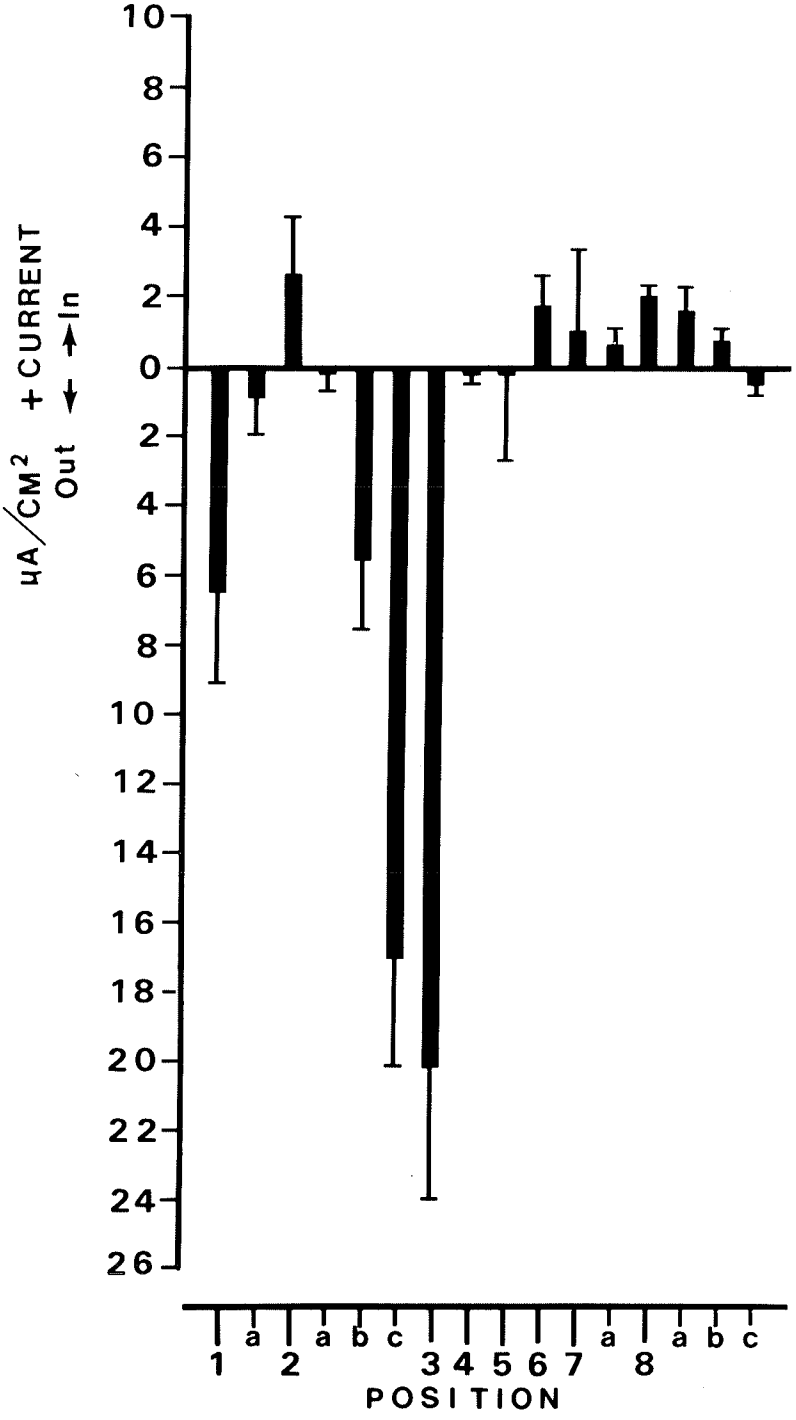
10
8
6
4
2
0
2
4
6
8
10
12
14
16
18
20
22
24
26
μA/CM²
+ CURRENT
Out → In
1
a
2
a
b
c
3
4
5
6
7
a
8
a
b
c
POSITION

Figure 10. Extracellular current measurements along the ovariole surface from ovariole class 8. By this stage the terminal oocyte has severed its connection with its trophic cord. This coincides with near maximum current fluxes at the posterior, lateral and anterior ends of the T follicle and current influxes over the tropharium.

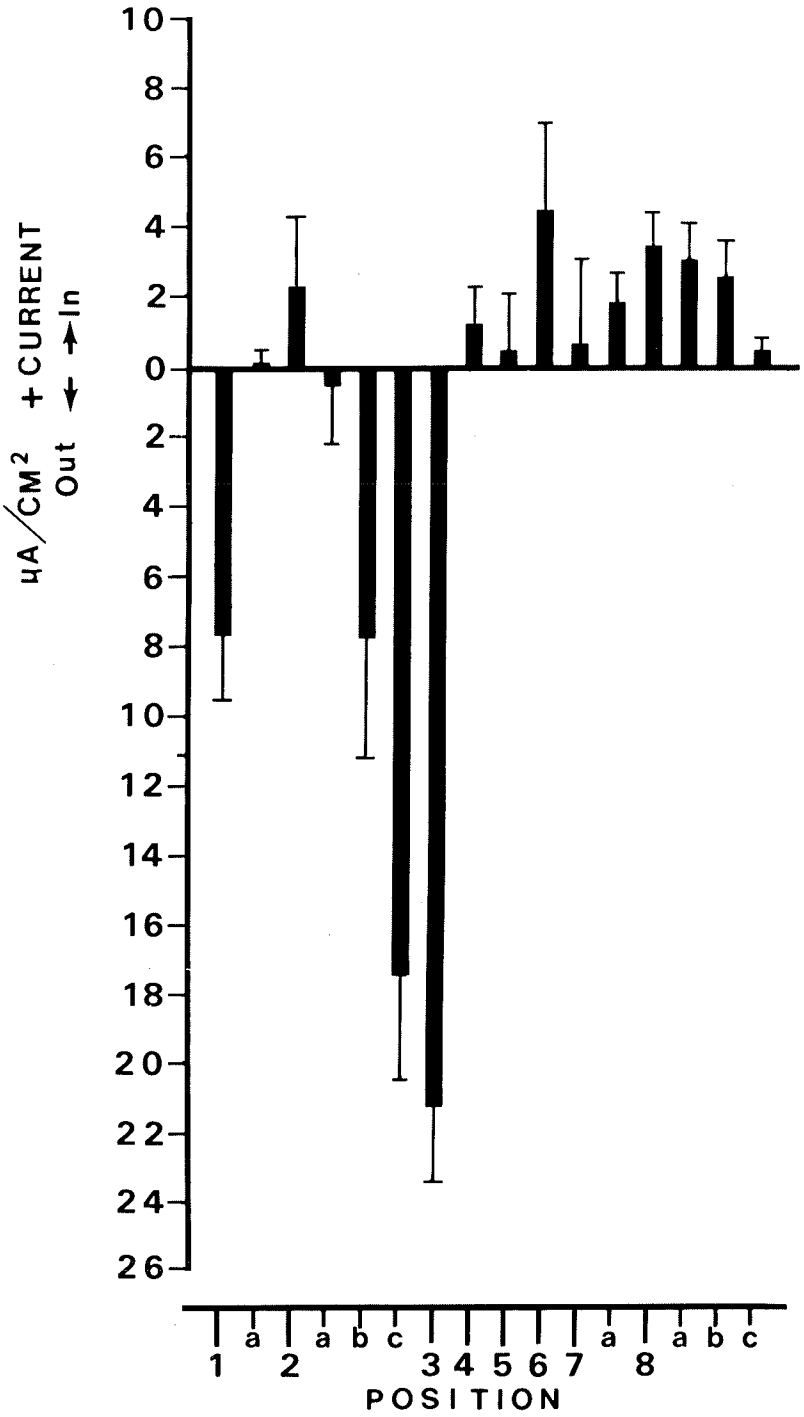
10
8
6
4
2
0
2
4
6
8
10
12
14
16
18
20
22
24
26
μA/CM²
+ CURRENT
Out → ← In
a
a b c
a
a b c
1 2 3 4 5 6 7 8
POSITION

Figure 11. Extracellular current measurements along the ovariole surface from ovariole class 9. The efflux at P3 starts to subside while efflux at P5 begins to increase as the terminal oocyte nears the end of vitellogenesis and begins chorionation.

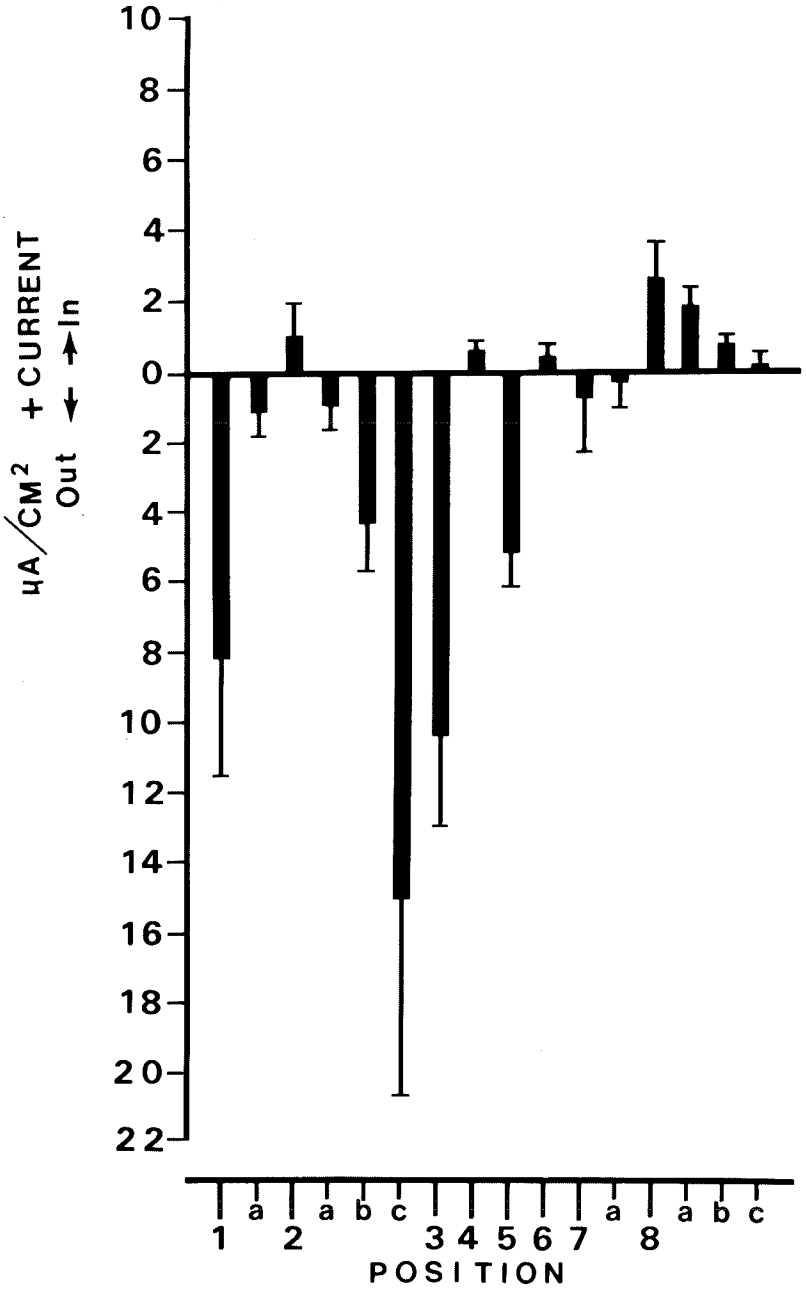
10
8
6
4
2
0
2
4
6
8
10
12
14
16
18
20
22
μA/CM² +CURRENT
Out → ← In
1 a 2 a b c 3 4 5 6 7 a 8 a b c
POSITION

Figure 12. Changes in extracellular current direction and density during oogenesis at position P1. Although there appears to be a gradual increase in current efflux as the terminal oocyte grows, significant differences could not be demonstrated.

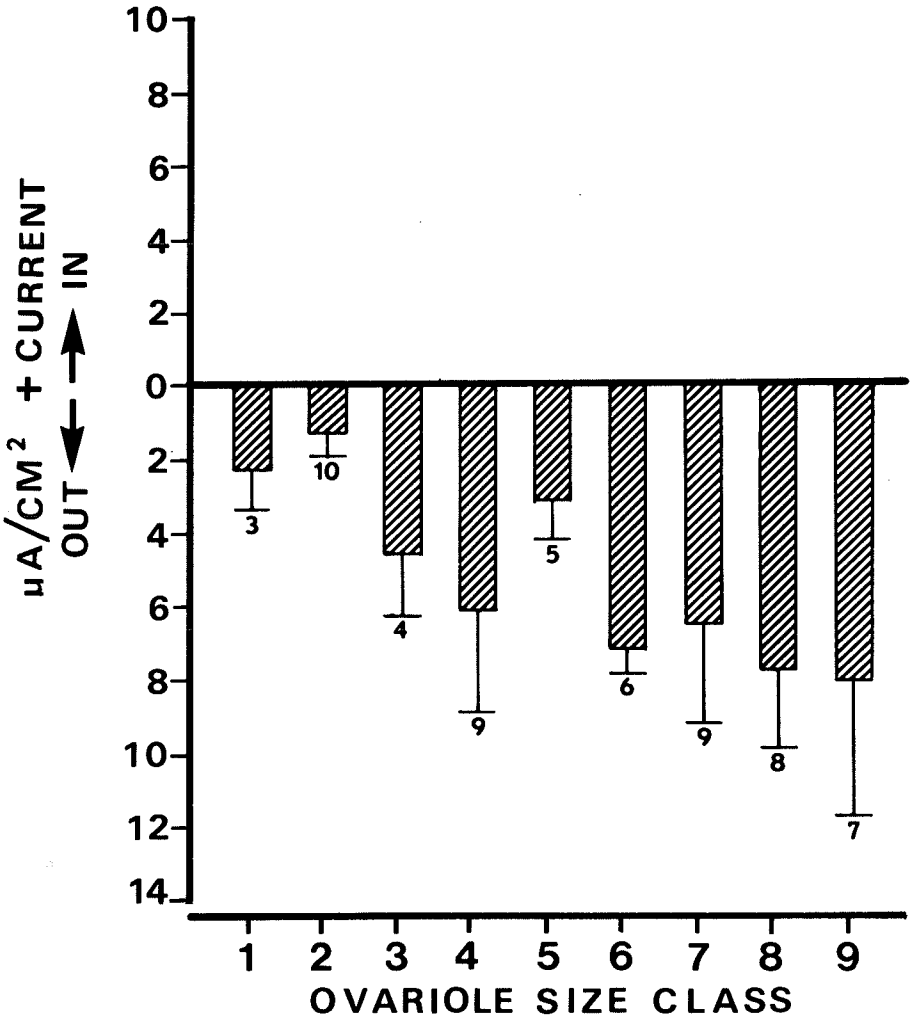
10
8
6
4
2
0
2
4
6
8
10
12
14
μA/CM² + CURRENT
OUT ← → IN
3
10
4
9
5
6
9
8
7
1 2 3 4 5 6 7 8 9
OVARIOLE SIZE CLASS

Figure 13. Changes in extracellular current direction and density during oogenesis at position P1a. The pattern and density of extracellular current did not change during oogenesis.

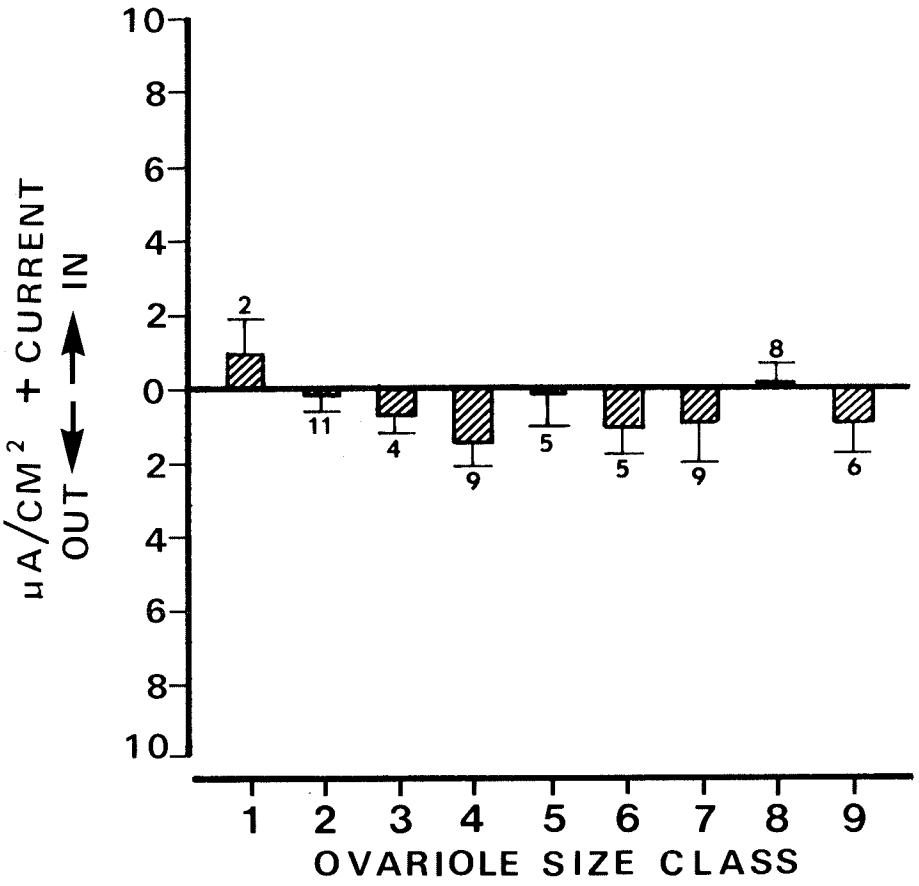
10
8
6
4
2
0
2
4
6
8
10
μA/CM² + CURRENT
OUT ↓ ↑ IN
2
11
4
9
5
5
9
8
6
1 2 3 4 5 6 7 8 9
OVARIOLE SIZE CLASS

Figure 14. Changes in extracellular current direction and density during oogenesis at position P2. Although variable in terms of direction during previtellogenesis and vitellogenesis, current influx tends to become more consistant during the latter stages of vitellogenesis. Statistically, differences were not detected.

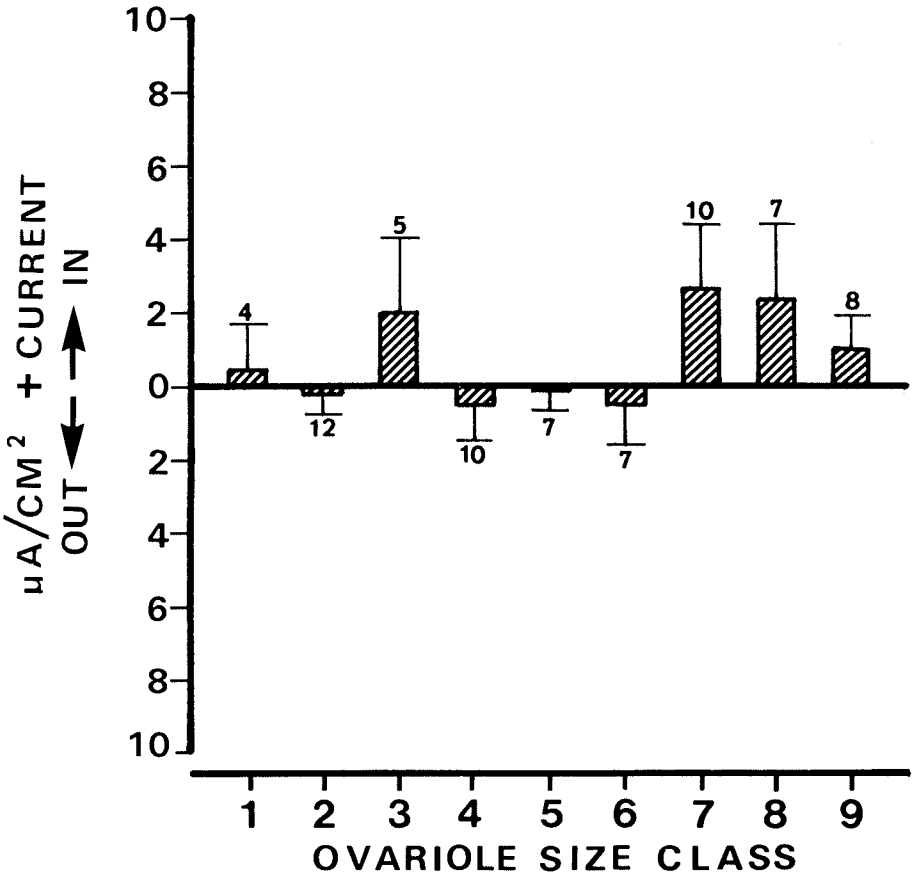
10
8
6
4
2
0
2
4
6
8
10
μA/CM² + CURRENT
OUT ← → IN
4
12
5
10
7
7
10
7
8
1 2 3 4 5 6 7 8 9
OVARIOLE SIZE CLASS

Figure 15. Changes in extracellular current direction and density during oogenesis at position P2a. The pattern and density of current do not change during oogenesis.

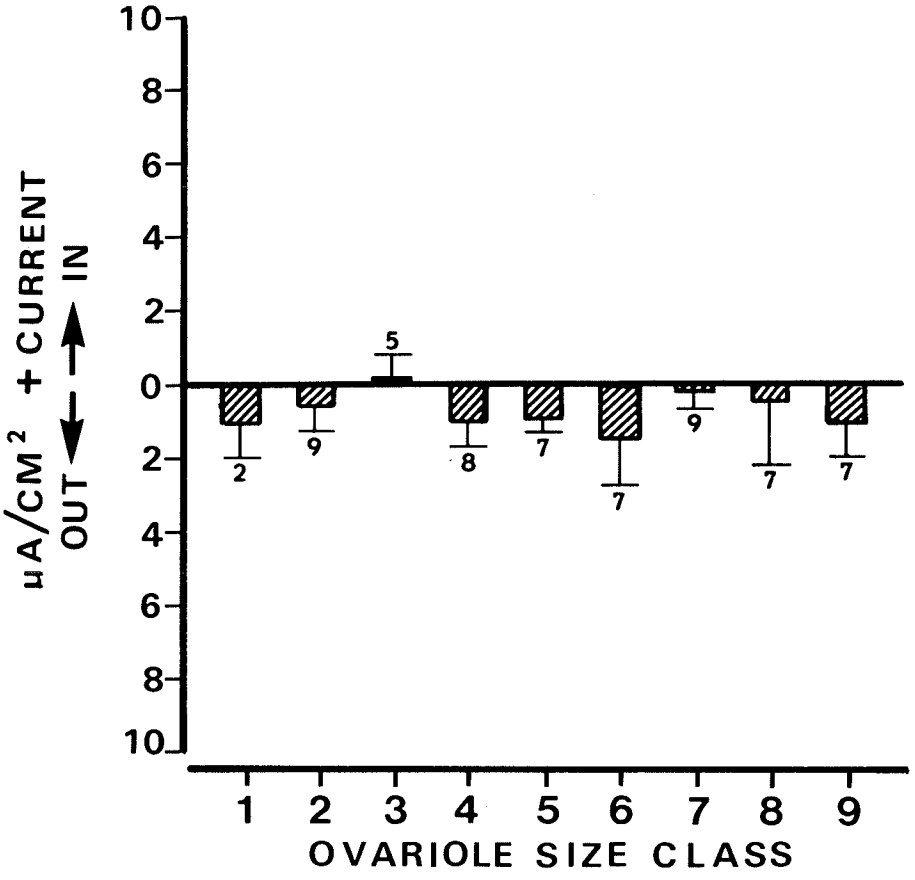
10
8
6
4
2
0
2
4
6
8
10
μA/CM² + CURRENT
OUT ↓ ↑ IN
5
2
9
8
7
7
9
7
7
1 2 3 4 5 6 7 8 9
OVARIOLE SIZE CLASS

Figure 16. Changes in extracellular current direction and density during oogenesis at position P2b. The current efflux appears to increase as the oocyte grows and then subside at completion of vitellogenesis, but this trend was not statistically significant.

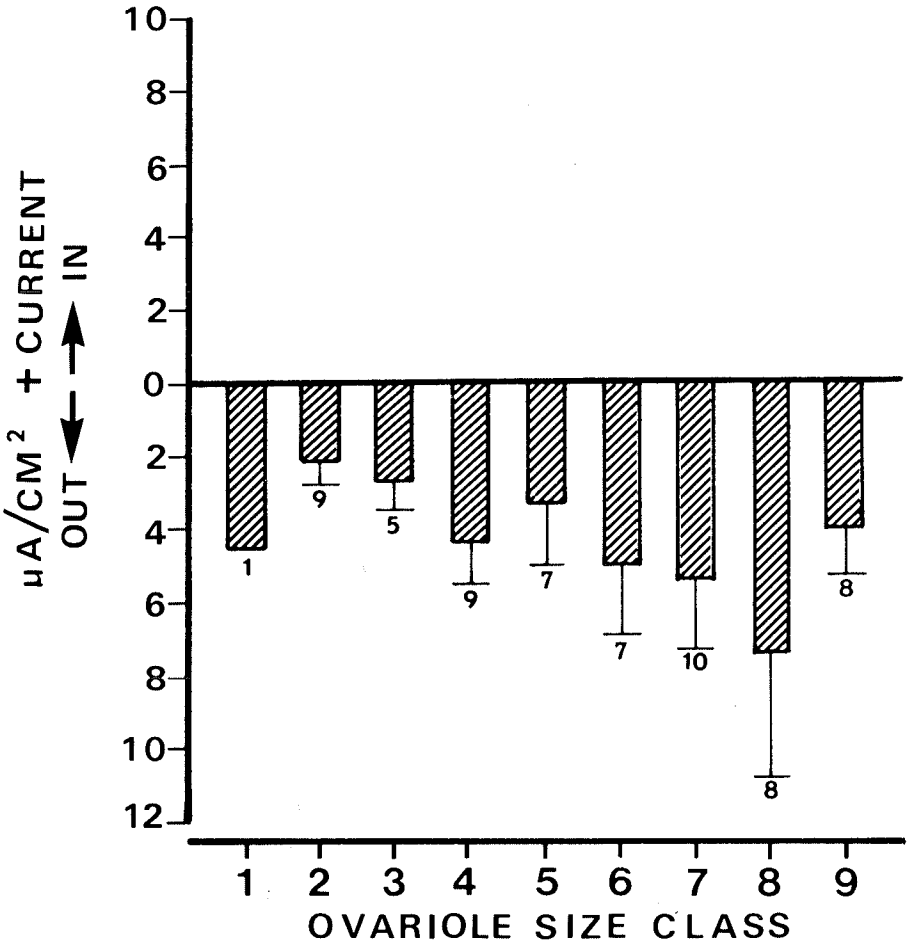
10
8
6
4
2
0
2
4
6
8
10
12
μA/CM² + CURRENT
OUT ← → IN
1
9
5
9
7
7
10
8
8
1 2 3 4 5 6 7 8 9
OVARIOLE SIZE CLASS

Figure 17. Changes in extracellular current direction and density during oogenesis at position P2c. Current efflux increases as vitellogenesis proceeds and then levels off at ovariole class 6.

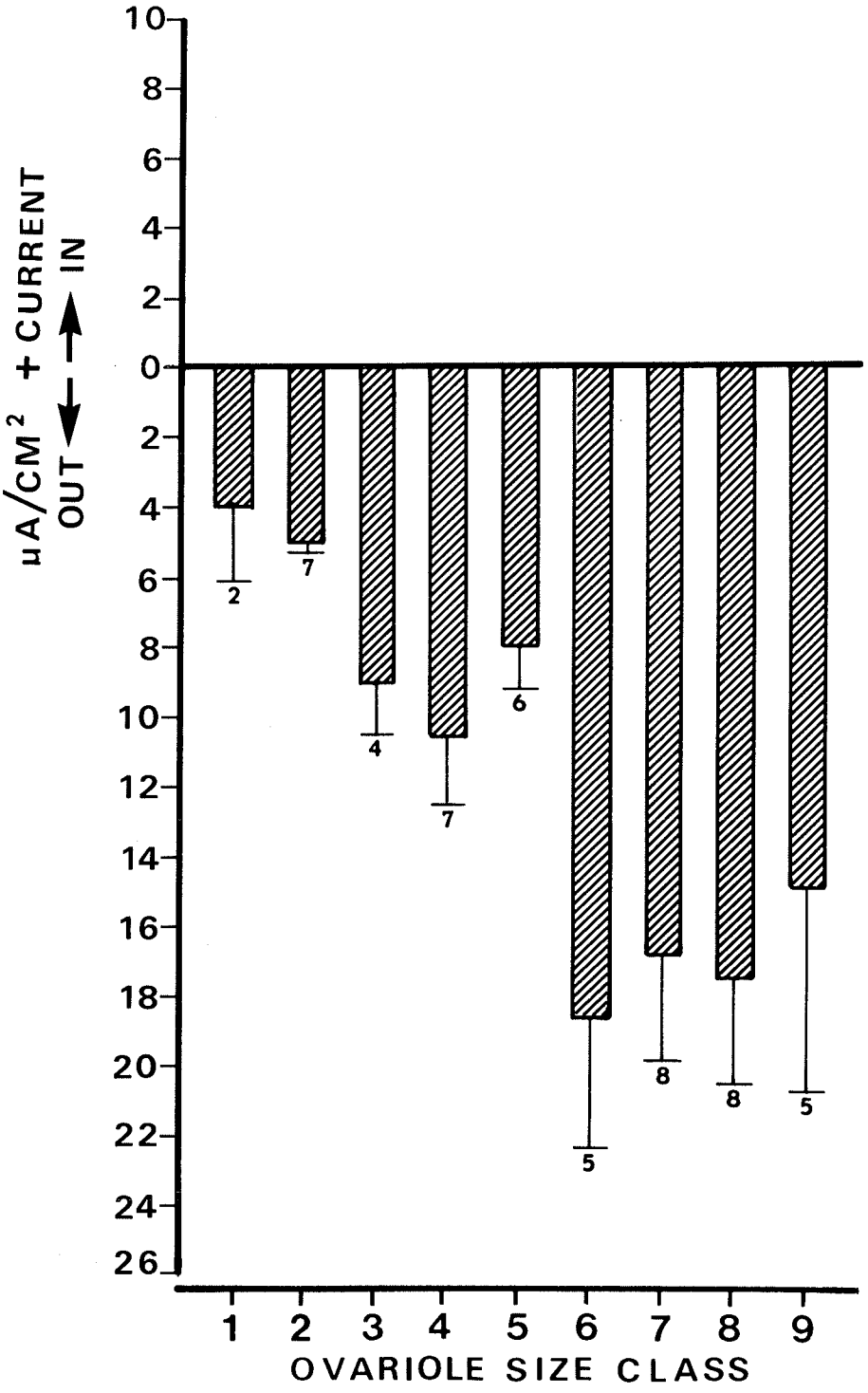
10
8
6
4
2
0
2
4
6
8
10
12
14
16
18
20
22
24
26
μA/CM² + CURRENT
OUT ↓ ↑ IN
2
7
4
7
6
5
8
8
5
1 2 3 4 5 6 7 8 9
OVARIOLE SIZE CLASS

Figure 18. Changes in extracellular current direction and density during oogenesis at position P3. As the oocyte enters vitellogenesis there is a sudden efflux current increase, which is maintained until ovariole class 9, where it decreases significantly.

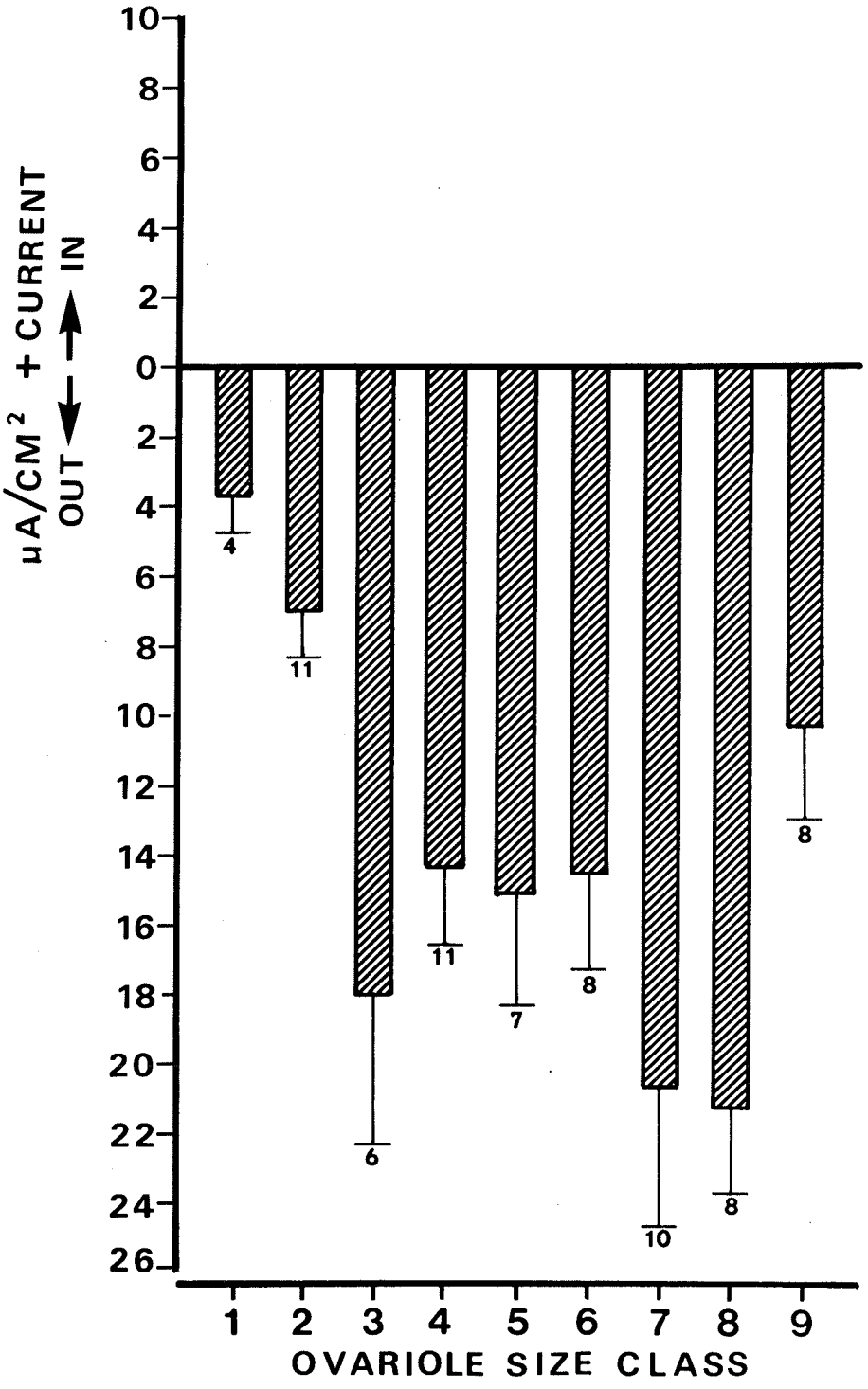
10
8
6
4
2
0
2
4
6
8
10
12
14
16
18
20
22
24
26
μA/CM² + CURRENT
OUT ↓ ↑ IN
4
11
6
11
7
8
10
8
8
1 2 3 4 5 6 7 8 9
OVARIOLE SIZE CLASS

Figure 19. Changes in extracellular current direction and density during oogenesis at position P4. The current appears to leave at this position until the end of vitellogenesis when it begins to enter the T-1 follicle, but statistically no differences were dectected.

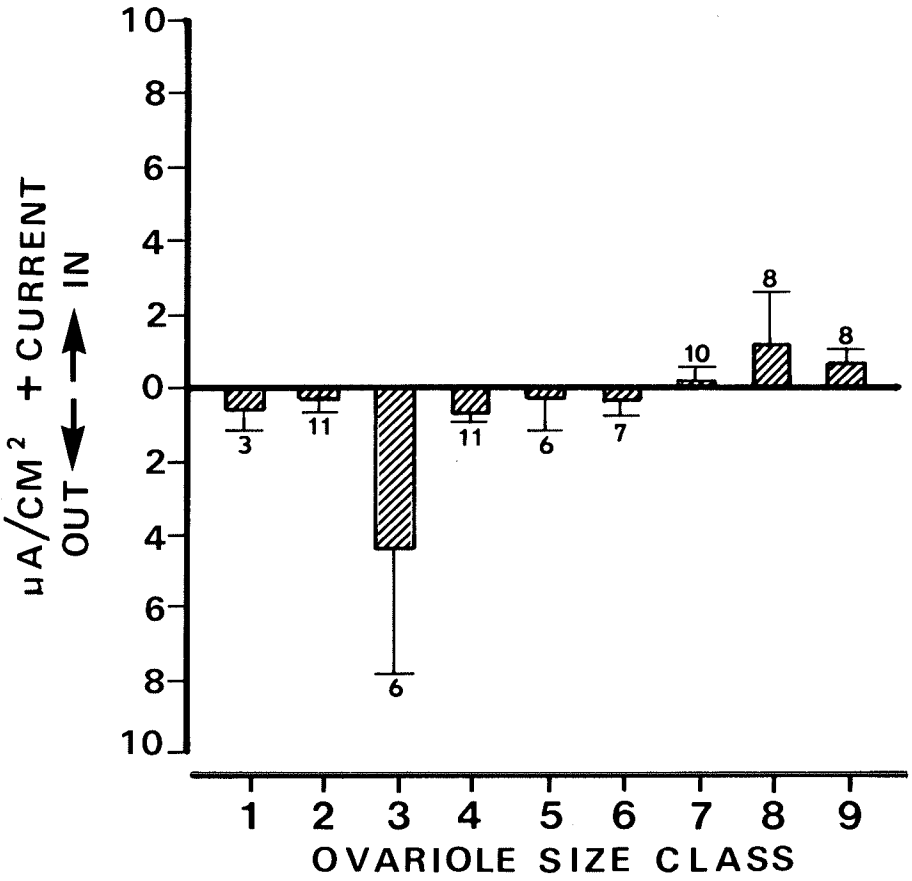
10
8
6
4
2
0
2
4
6
8
10
μA/CM² + CURRENT
OUT ↓ ↑ IN
3
11
6
11
6
7
10
8
8
1 2 3 4 5 6 7 8 9
OVARIOLE SIZE CLASS

Figure 20. Changes in extracellular current direction and density during oogenesis at position P5. During the majority of oogenesis, current direction and flux are variable. Only during ovariole classes 4, 5, 6 and 7 is there consistent current efflux. The mean current efflulx during class 9 is significantly different from the other means.

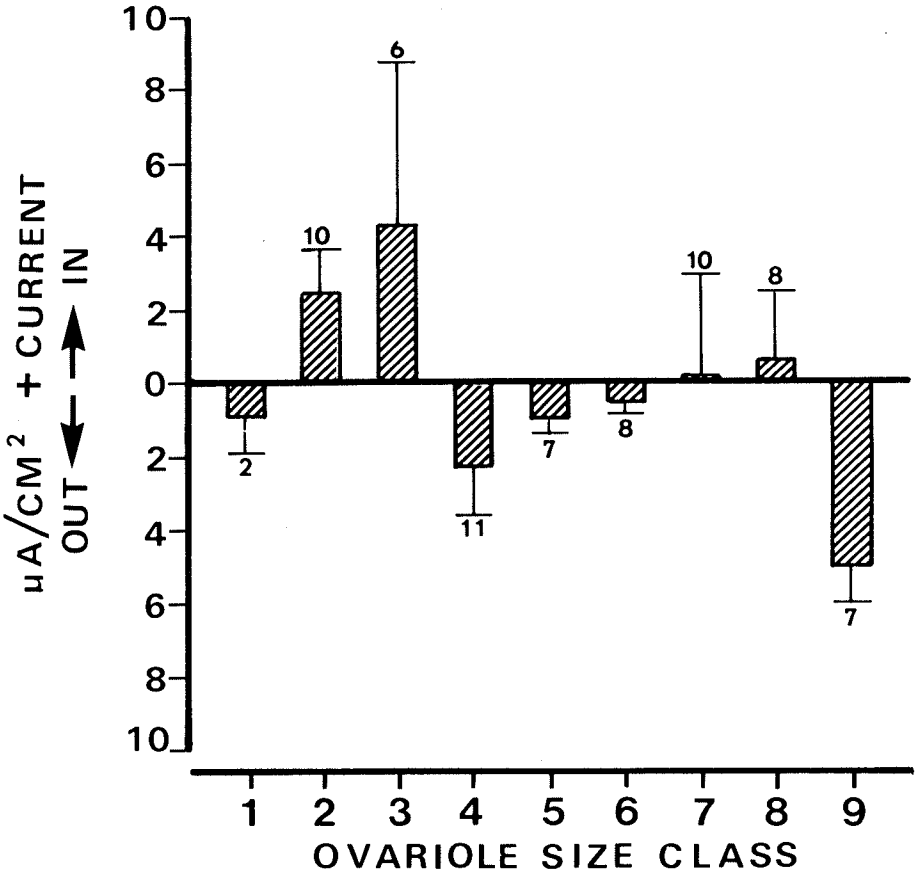
10
8
6
4
2
0
2
4
6
8
10
μA/CM² + CURRENT
OUT ← → IN
2
10
6
11
7
8
10
8
7
1 2 3 4 5 6 7 8 9
OVARIOLE SIZE CLASS

Figure 21. Changes in extracellular current direction and density during oogenesis at position P6. Current direction and density are variable throughout oogenesis at this position. No differences between these means were found.

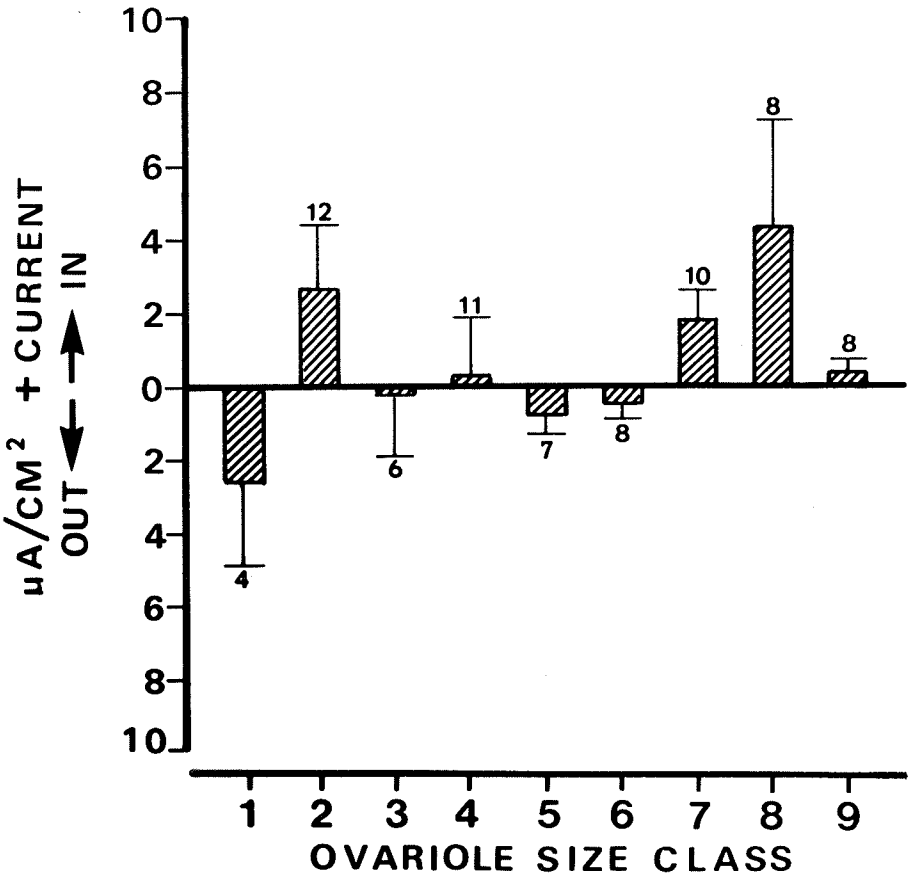
10
8
6
4
2
0
2
4
6
8
10
µA/CM² + CURRENT
OUT ← → IN
12
11
10
8
8
6
7
8
4
1 2 3 4 5 6 7 8 9
OVARIOLE SIZE CLASS

Figure 22. Changes in extracellular current direction and density during oogenesis at position P7. This position was very variable in terms of current direction and density throughout oogenesis.

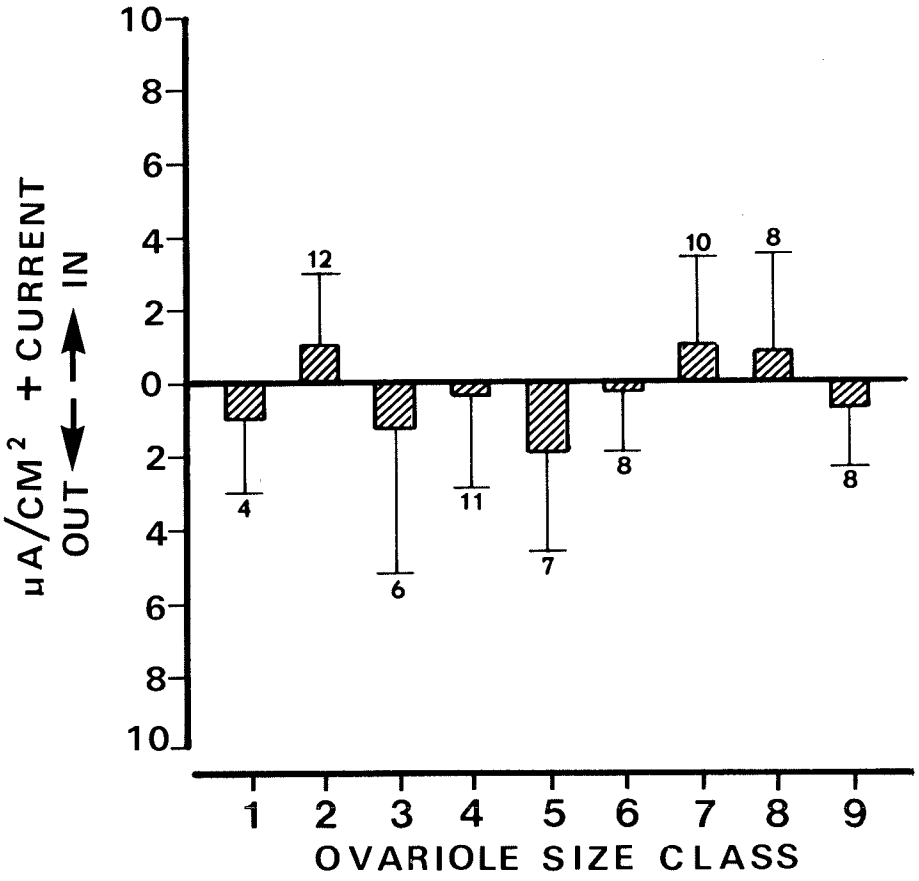
10
8
6
4
2
0
2
4
6
8
10
μA/CM² + CURRENT
OUT ← → IN
12
4
6
11
7
8
10
8
8
1 2 3 4 5 6 7 8 9
OVARIOLE SIZE CLASS

Figure 23. Changes in extracellular current direction and density during oogenesis at position P7a. There were no changes in current magnitude or direction which could be shown to be statistically significant.

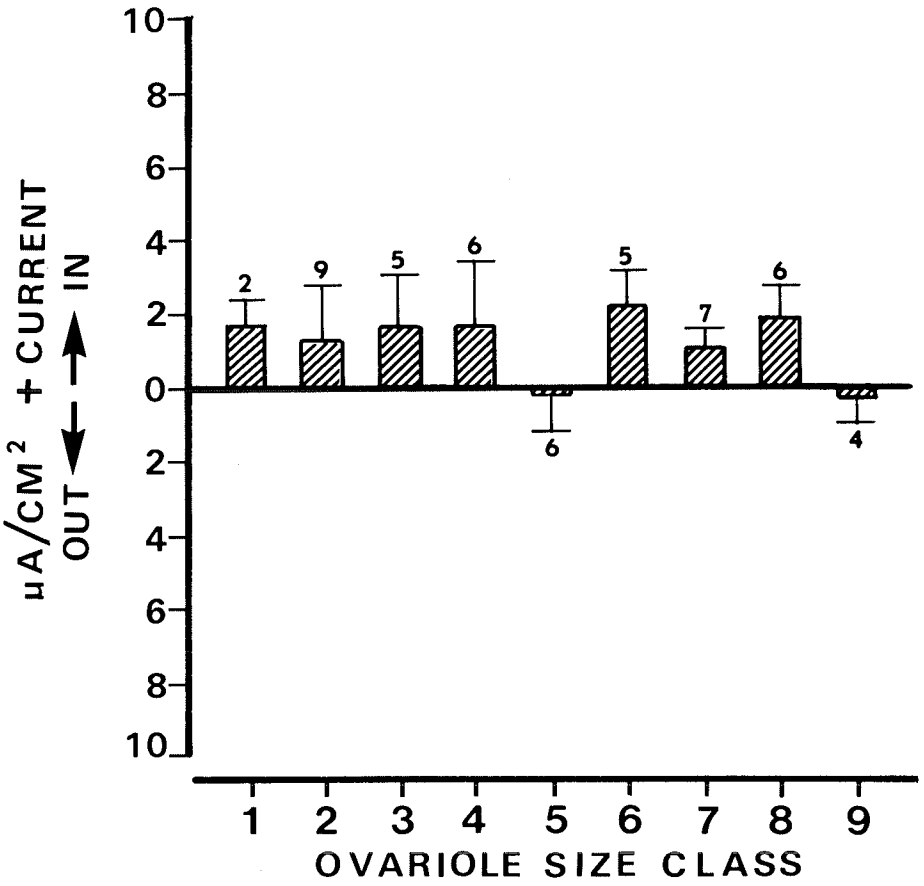
10
8
6
4
2
0
2
4
6
8
10
2
9
5
6
6
5
7
6
4
μA/CM² + CURRENT
OUT ← → IN
1 2 3 4 5 6 7 8 9
OVARIOLE SIZE CLASS

Figure 24. Changes in extracellular current direction and density during oogenesis at position P8. There were no detectable changes in extracellular current during oogenesis at this position.

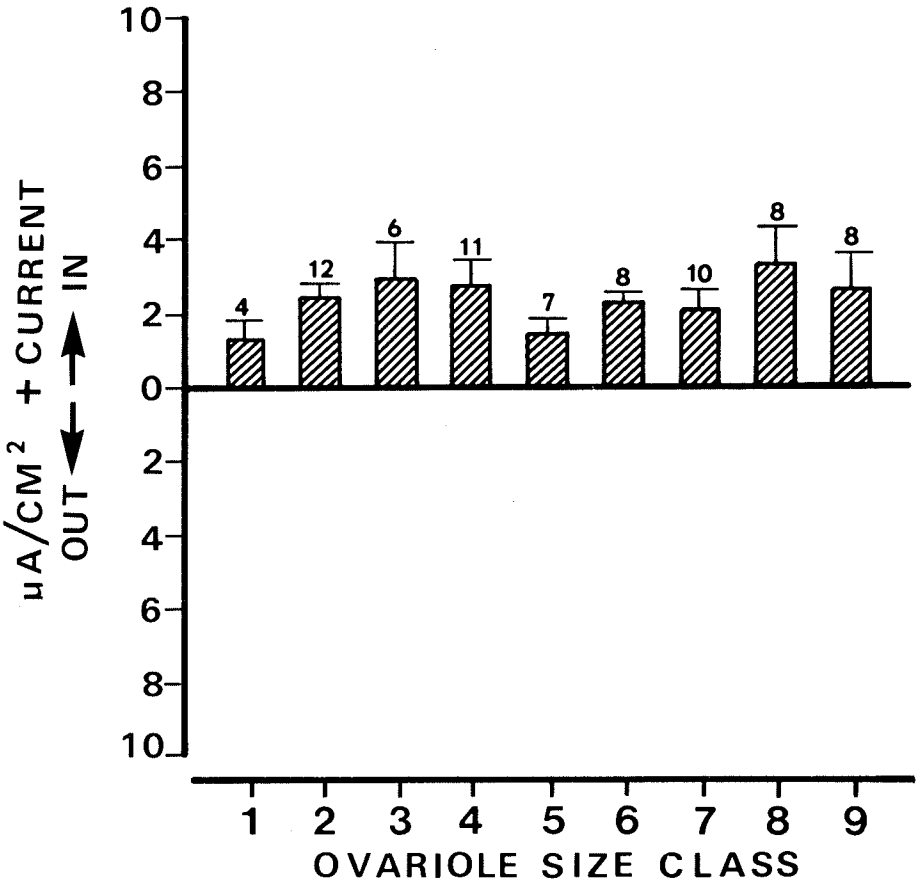
10
8
6
4
2
0
2
4
6
8
10
μA/CM² + CURRENT
OUT ↓ ↑ IN
4
12
6
11
7
8
10
8
8
1 2 3 4 5 6 7 8 9
OVARIOLE SIZE CLASS

Figure 25. Changes in extracellular current direction and density during oogenesis at position P8a. There were no detectable changes in extracellular current during oogenesis at this position.

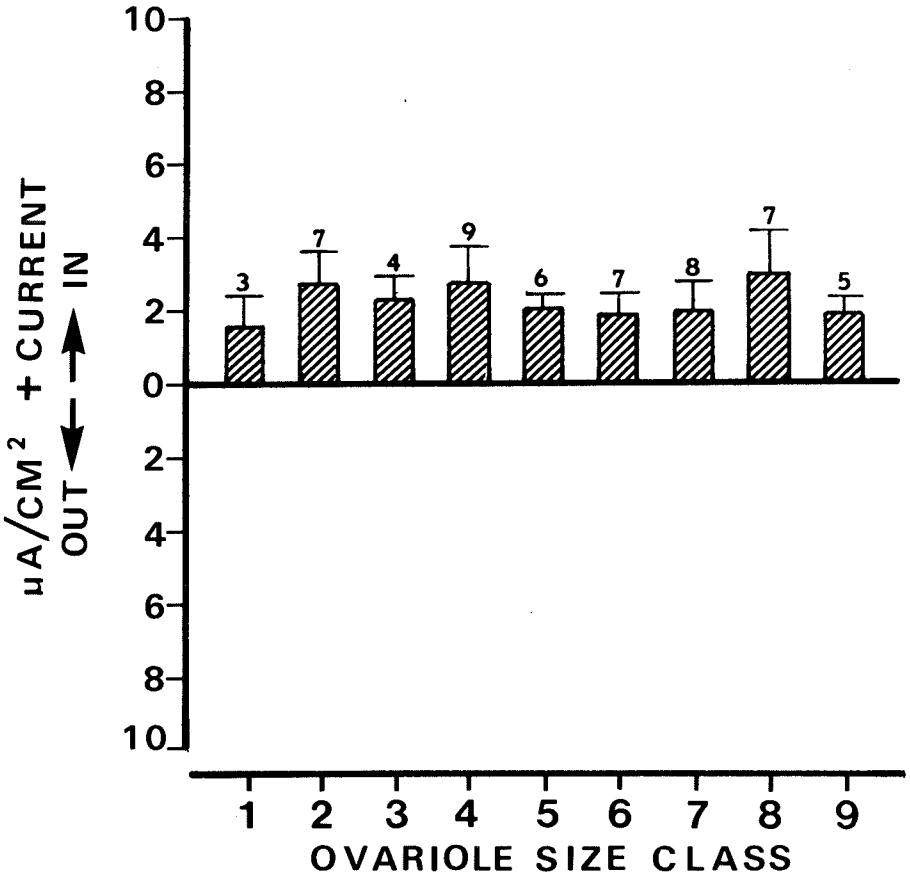
10
8
6
4
2
0
2
4
6
8
10
3
7
4
9
6
7
8
7
5
μA/CM² + CURRENT
OUT ↓ ↑ IN
1 2 3 4 5 6 7 8 9
OVARIOLE SIZE CLASS

Figure 26. Changes in extracellular current direction and density during oogenesis at position P8b. There were no detectable changes in extracellular current during oogenesis at this position.

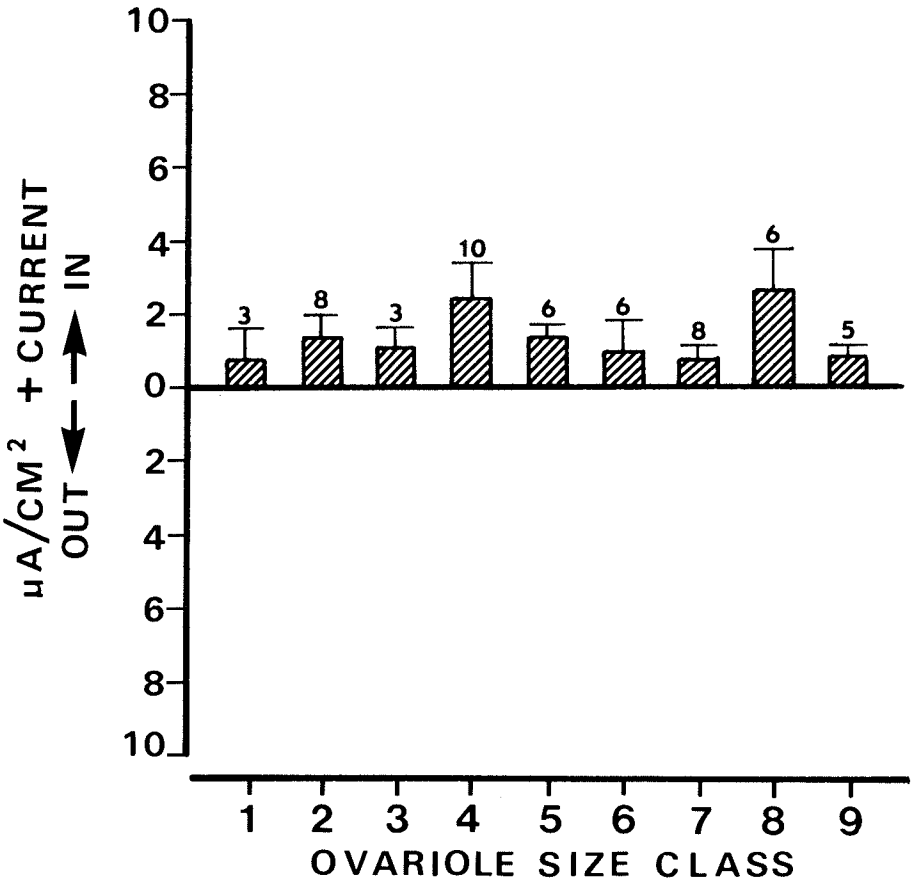
10
8
6
4
2
0
2
4
6
8
10
μA/CM² + CURRENT
OUT ← → IN
3
8
3
10
6
6
8
6
5
1 2 3 4 5 6 7 8 9
OVARIOLE SIZE CLASS

Figure 27. Changes in extracellular current direction and density during oogenesis at position P8c. There were no detectable changes in extracellular current during oogenesis at this position.

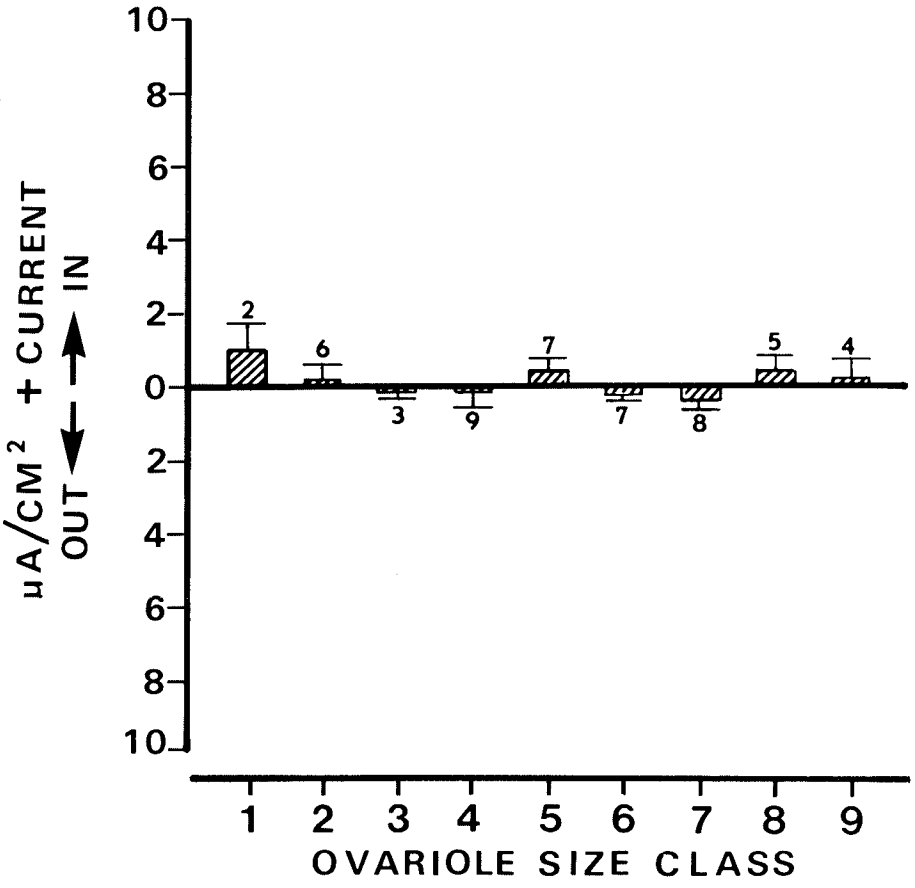
10
8
6
4
2
0
2
4
6
8
10
µA/CM² + CURRENT
OUT ← → IN
2
6
3
9
7
7
8
5
4
1 2 3 4 5 6 7 8 9
OVARIOLE SIZE CLASS

Figure 28. Continuous data plot of individual current values at P2c versus T follicle size. The scatter suggests an initial increase, peaking with oocyte sizes of 1000-1500 μM and then decreasing as vitellogenesis ends. The correlation coefficient for the predicted line (solid triangles) is, r= 0.62. and was derived from a SAS statistical analysis package run on a large main frame computer.

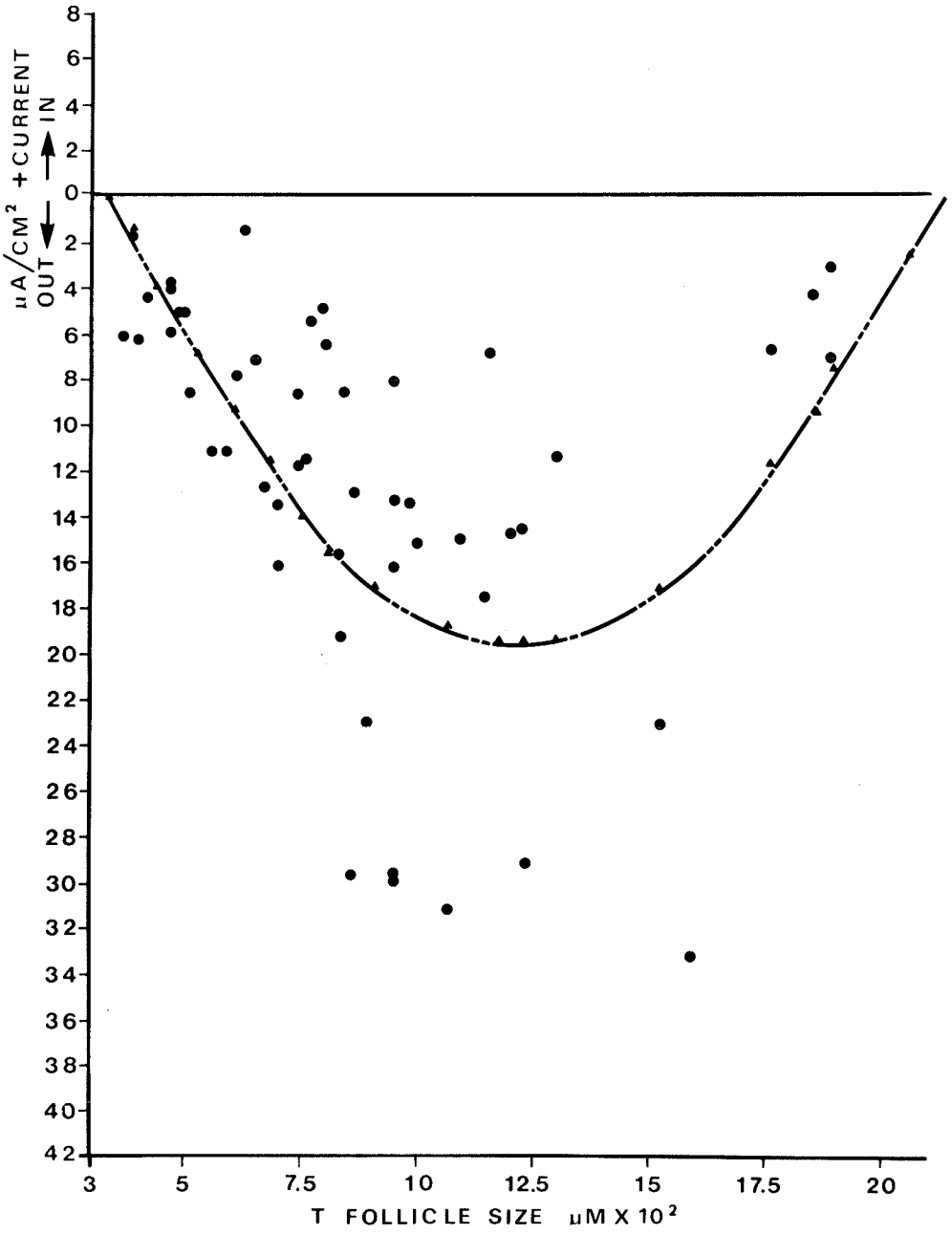
8
6
4
2
0
2
4
6
8
10
12
14
16
18
20
22
24
26
28
30
32
34
36
38
40
42
μA/CM² +CURRENT
OUT ← → IN
3
5
7.5
10
12.5
15
17.5
20
T FOLLICLE SIZE μM X 10²

Figure 29. Continuous data plot of individual current values at P3 versus T follicle size. The scatter of data points is greater than found at P2c, but the same trend is apparent. The correlation coefficient, r= 0.53.

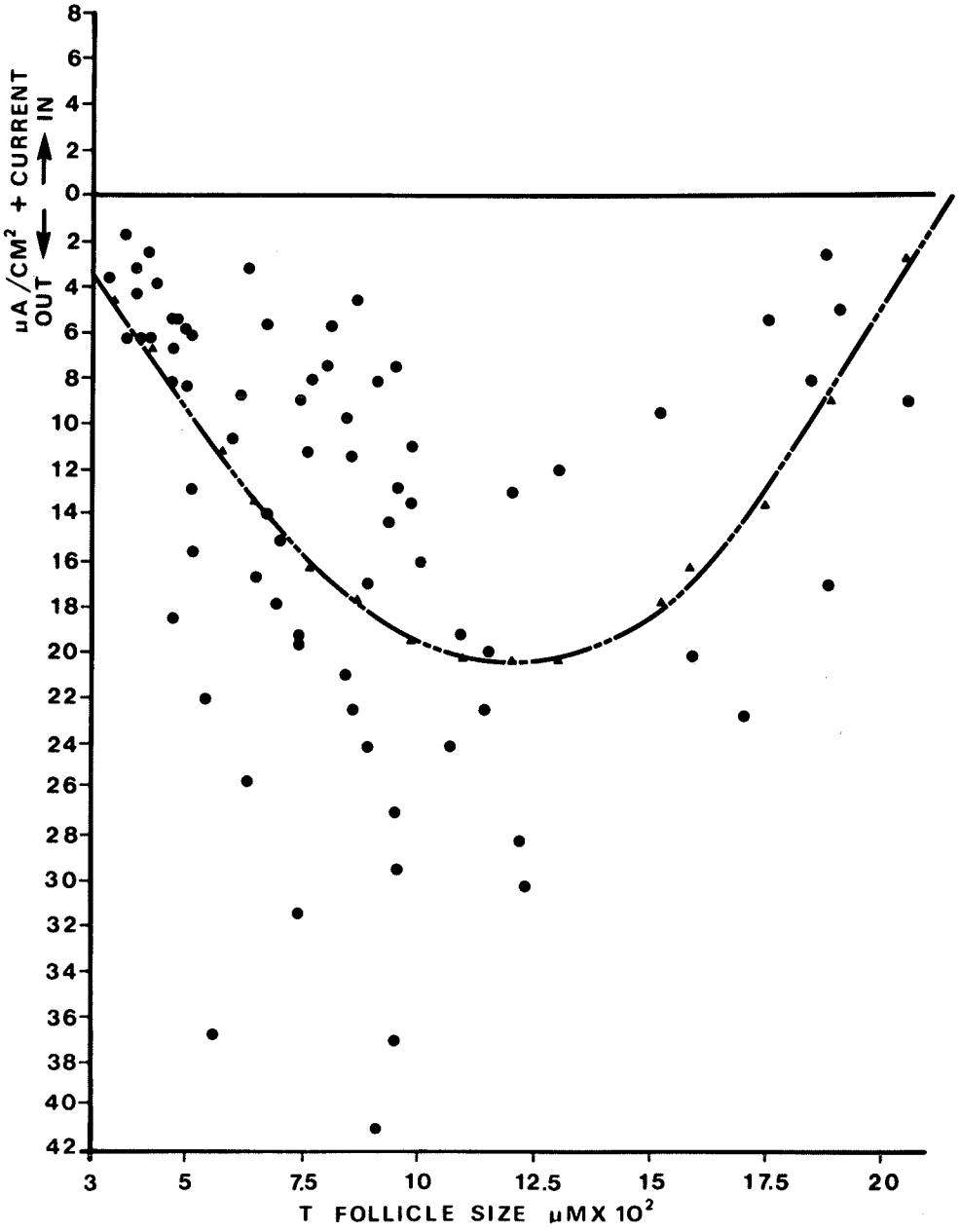
8
6
4
2
0
2
4
6
8
10
12
14
16
18
20
22
24
26
28
30
32
34
36
38
40
42
μA/CM² + CURRENT
OUT
IN
3
5
7.5
10
12.5
15
17.5
20
T FOLLICLE SIZE μMX 10²

Figure 30. The frequency of current efflux at P5 during oogenesis. Except for ovariole class 7 and previtellogenesis and early vitellogenesis, efflux current predominatly the ovariole. Only one measurement during ovariole class 1 detected current, while other measurements did not detect any current flux.

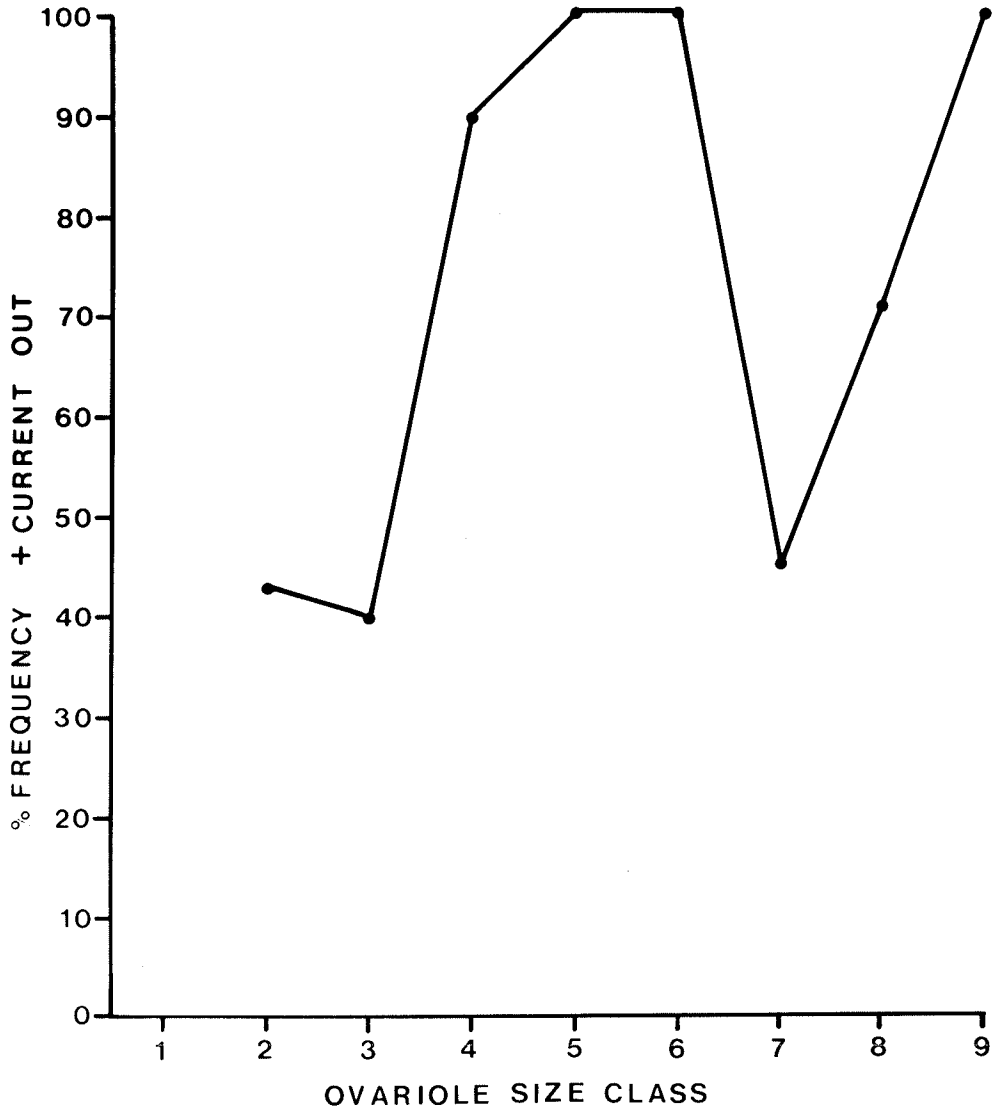
100
90
80
70
60
50
40
30
20
10
0
% FREQUENCY + CURRENT OUT
1
2
3
4
5
6
7
8
9
OVARIOLE SIZE CLASS

Figure 31. The frequency of current efflux at P6 during oogenesis. The extracellular current direction fluctuates between efflux, during previtellogenesis, changing to influx as vitellogenesis begins and then becoming predominatly efflux as vitellogenesis proceeds. When trophic cord loss is imminent, current direction moves back into the ovariole and continues to be influx for the rest of oogenesis.

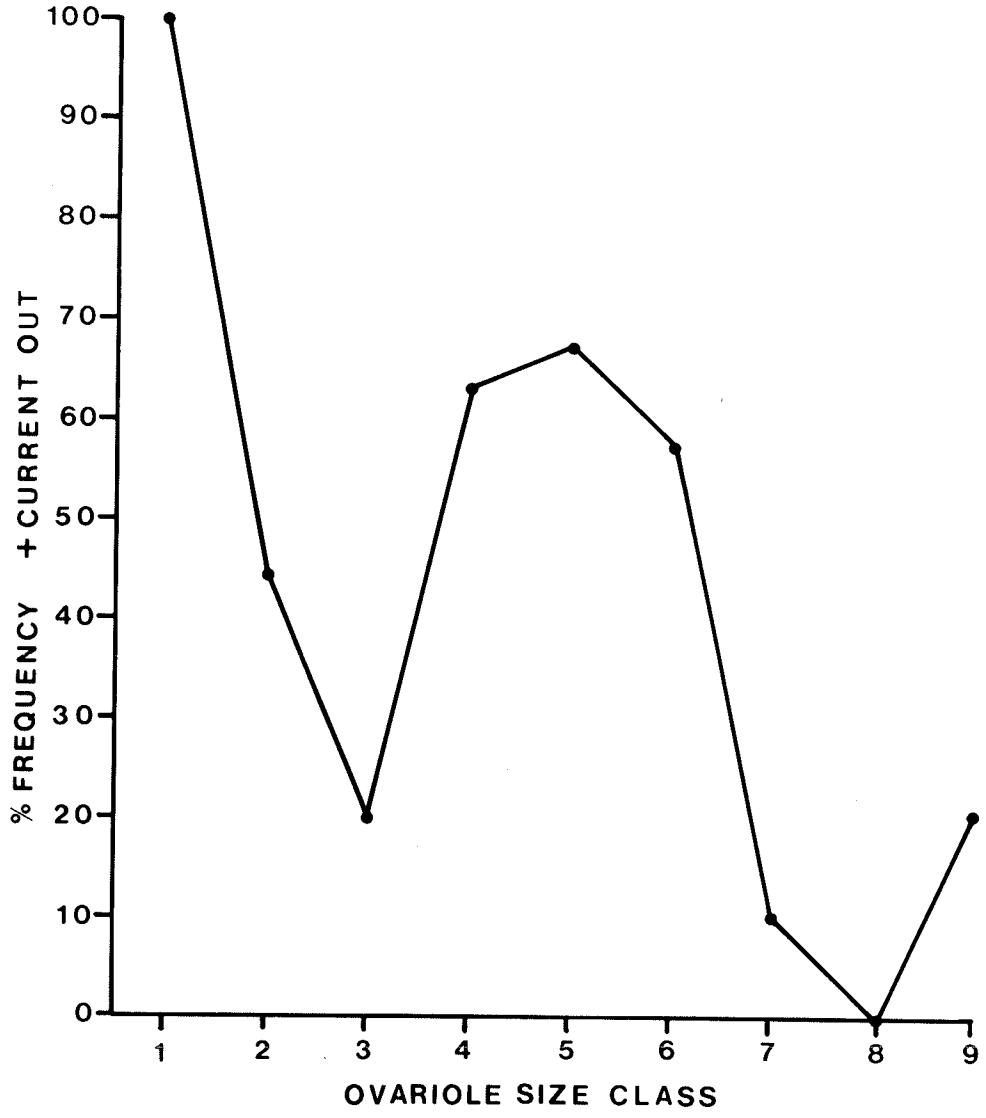
100
90
80
70
60
50
40
30
20
10
0
% FREQUENCY +CURRENT OUT
1
2
3
4
5
6
7
8
9
OVARIOLE SIZE CLASS

Figure 32. The frequency of current efflux at P7 during oogenesis.The base of the tropharium was the most variable in terms of magnitude and as this plot indicated, in direction as well. Current efflux occurred in about 30-50% of the measurements made during oogenesis.

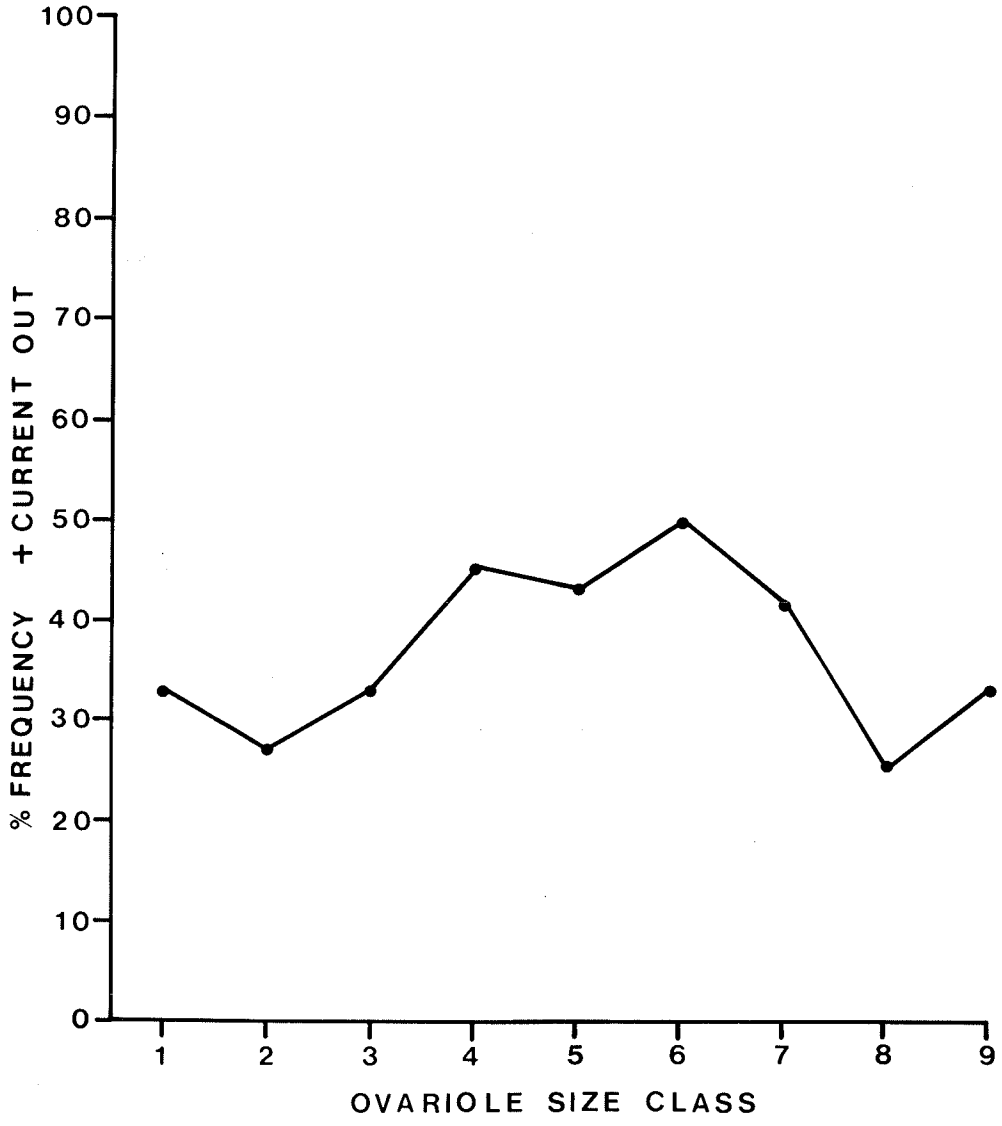
100
90
80
70
60
50
40
30
20
10
0
% FREQUENCY +CURRENT OUT
1
2
3
4
5
6
7
8
9
OVARIOLE SIZE CLASS

Discussion

The underlying concept involved in the elucidation of steady electric fields around animal cells and tissues, is that these fields represent certain physiological processes involved in the normal development of these cells and tissues. How these electrophysiological processes may effect development have been recently reviewed (Jaffe, 1981; Telfer et al., 1981; De Loof et al., 1982). One hypothesis is quite speculative and suggests a universal mechanism of gene expression is the result of electrophysiological processes (DeLoof et al., 1982). Other hypotheses such as electrophoretic intercellular transport, are based on substantial experimental evidence and will be considered here in relation to results presented in this study.

The presence of steady electric fields flowing in a consistent pattern around the Rhodnius ovariole is the primary finding of this study. The efflux of strong positive current from the anterior end of the terminal follicle and interfollicular connective region plus the smaller but less concentrated influx over the tropharium are features observed in all ovarioles at all stages of the oogenesis cycle. These currents therefore must be related to important electrophysiological processes occurring during oogenesis. The current efflux observed at the posterior end of the T follicle is not as large as at P2c or P3 but is nearly as consistent. These three observations indicate at least two extracellular current circuits within the ovariole. The first surrounds the terminal follicle and consists of efflux current leaving the apical follicle cells and follicle posterior and moving toward the lateral follicle surface where the current enters (Fig. 2, Figs. 3-11). The second circuit consists of efflux from

the interfollicular connective which moves towards the trophariun and the influx of current over the trophariun.

The first circuit resembles that found in Dysdercus follicles (Dittmann et al., 1981) except current densities are 4 to 10 times less in the Rhodnius ovarioles. The vitellogenic oocytes in Dysdercus are not connected to the trophariun and therefore appear much like the follicles from panoistic ovarioles (Dittmann et al., 1981; DeLoof, 1983). Extracellular currents around the panoistic Periplaneta follicles have been found to leave interfollicular connectives and enter the lateral surface of follicles just entering vitellogenesis (Huebner, 1984a; Huebner and Sigurdson, 1984). Preliminary experiments in the coleopteran telotrophic ovariole from Ips perturbatus are inconclusive as to the current pattern around vitellogenic follicles, but may be reversed from that observed in the hemipterans (Huebner, 1984a; Huebner and Sigurdson, 1984). Very small or no currents at all have been detected around the follicles from the megalopteran Sialis velata (Huebner, 1984a; Huebner and Sigurdson, 1984). Polytrophic ovarioles from Drosophila (Bohrmann et al., 1984) and Hyalophora cecropia (Jaffe and Woodruff, 1979) have shown current efflux from all regions of the oocyte. The second circuit is not as clearly defined as the first due to the variable current fluxes in the previtellogenic region, but consistent anteriorly directed current at P3, P4 and P7a (Fig. 2) indicates current moving from the interfollicular plug to the trophariun. In Dysdercus the efflux current from the prefollicular region moves to and enters the trophariun and forms the second extracellular current system (Dittmann et al., 1981). At this time data are insufficient to determine the current circuits in Ips ovarioles. Jaffe and

Woodruff (1979) detected strong influx of current at anterior end of the nurse cell cap in cecropia follicles, thus completing the single circuit of current flow.

This is the first study to examine in detail the extracellular current properties of a telotrophic ovariole through a complete cycle of oogenesis. Jaffe and Woodruff (1979) have examined the extracellular currents around polytrophic follicles during oogenesis, although changes in current density were not related to follicle size.

As the terminal oocyte enters vitellogenesis, the current efflux at the anterior end rises gradually until ovariole class 6 (Fig. 17). Thus the current increase appears to anticipate the trophic cord loss which will occur primarily during the next size class and therefore signals the forthcoming independence of the terminal follicle. The rise in efflux density at the interfollicular plug occurs earlier in vitellogenesis and is significantly larger than that observed at P2c. The strong efflux is maintained throughout vitellogenesis, peaks during the time of trophic cord loss, and then decreases so that at the end of vitellogenesis the efflux from P3 is less than from the now independent P2c region (Figs. 17 and 18). Therefore at the end of vitellogenesis, the T connective (P3) which becomes the pedicel of the T-1 follicle experiences a decreased current efflux.

The rest of the positions do not show any significant changes throughout oogenesis, except P5 during the final stages of oogenesis (Fig. 11). When the T oocyte has been ovulated the position at P5 becomes equivalent to P3 and as expected a consistent efflux of current begins to leave the presumptive interfollicular connective. At the same time, P4 will becomes equivalent to P2 and thus begins to show current influx (Fig. 19). At ovariole class 9, the T-1 oocyte is about the same size as the T oocyte was during early vitellogenesis

(see Appendix 2, Fig. 2) and as was observed during class 2, current again begins to enter at P6 (Fig. 21). Therefore, as the terminal oocyte nears completetion of vitellogenesis, another current circuit is being set up around the T-1 follicle, signalling the start of another round of vitellogenesis. These changes in current magnitudes and directions, notably at P5, also provide an indication that the inhibition preventing the T-1 from entering vitellogenesis has been lifted. This prediction of future morphological and physiological changes based on extracellular currents has been observed in fucoid eggs (Nuccitelli and Jaffe, 1974), amebas (Nuccitelli et al., 1977) and water mold (Stump et al., 1980; Kropf et al., 1983). In cecropia follicles a current reversal occurs at the posterior end of the follicle during nurse cell collapse (Jaffe and Woodruff, 1979). This study did not indicate if this reversal preceeded the nurse cell collapse or was coincident with it. Therefore the results presented here are the first to show extracellular currents patterns changing, coincident with changes in the regulation of an insect ovarian tissue.

The variability in current direction and magnitude observed in the previtellogenic region represented by positions P5, P6 and P7, is surprising (Figs. 20, 21, 22). The barrier artefact may introduce errors in current density (Jaffe and Nuccitell, 1974; Dorn and Weienseel, 1982). This error routinely produced no more than 0.1 $\mu A/cM^2$ current of either polarity. The consistency of probe operation is evident in the measurements of influx current over the tropharium (see Figs. 24-26).

The largest source of damage that may occur to the ovariole is during desheathing. Visibly damaged ovarioles produced very large injury currents over the damaged area. Damaged ovarioles were discarded.

The variability must be due to either individual variation between ovarioles and between animals or represents a region of the ovariole which is very dynamic in terms of its electrophysiological properties. Variation of hormonal levels or other factors between animals may have influenced the results, except that the T follicle development is not synchronized between ovarioles of the same ovary (Huebner and Injeyan, 1980). Therefore to some extent, each ovariole responds independently to the control factors present, thus reducing the effect of variation between animals. The variation in direction and magnitude can result in a net current flux of zero (see Fig. 20, class 7). Current direction may be more important than density, since this determines the electrical polarity of the cells. If current density is ignored and direction frequency examined, patterns do emerge at P5 and P6 during oogenesis (Figs. 29-30). This indicates the changing membrane properties of the cells in these area. How these patterns relate to the observed events of oogenesis is not clear. The clarification of this problem requires further detailed work, perhaps by subdividing the ovariole classes even further, enabling a consistent sequence of events to be observed. Extended monitering of this region may detect current pulses, which would have contributed to the observed variability. Nuccitelli and Jaffe (1974, 1975; 1976) described spontaneous current pulses in developing fucoid eggs.

The nurse cell products which are transported via the trophic cord to the oocyte include, ribosomal RNA (Davenport, 1974, 1976; Telfer, 1975), ribosomes (Huebner and Anderson, 1970; Hyams and Stebbings, 1977), messenger RNA (Telfer, 1975, Capco and Jeffrey, 1979), proteins (Vanderburg, 1963; Telfer et al., 1981) and possibly mitochondria (Telfer, 1975; Hyams and Stebbings, 1977).

The specific types of proteins that appear to be transported have not been identified although there is speculation that regulatory proteins and/or histones may be prefrentially transported to the oocyte or restricted to the nurse cells (Telfer et al., 1981). These regulatory proteins would maintain the differentiated states of the nurse cell-oocyte syncytium (Telfer et al., 1981). The mechanism of transport may be the generation of electrophysiological polarity within cells or syncytia causing the electrophoretic movement of charged species, thus partitioning the soluble cytoplasmic or plasma membrane bound components (Jaffe, 1977, 1981; Telfer et al., 1981).

Only two examples of cytoplasmic electrophoretic transport of charged proteins exist, both in insect ovaries. Woodruff and Telfer (1973, 1974, 1980) demonstrated unidirectional movement of charged proteins microinjected into the oocyte and nurse cells of cecropia follicles, coinciding with a 10 mV potential difference between the germ cells (nurse cells more electronegative). The acidic proteins, fluorescein labelled serum globulin (FSG) and methycarboxylated lysozyme (McFLy) were able to move only from the injected nurse cell into the oocyte and never diffused to other nurse cells despite the presence of intercellular bridges (Woodruff and Telfer, 1980; Telfer et al., 1981). When injected into the oocyte, FSG and McFLy were never seen crossing the intercellular bridge to the nurse cell cap (Woodruff and Telfer, 1980). The basic FLy was able to freely move to other nurse cells, but never entered the oocyte. If FLy was injected into the oocyte, it was observed to move into the nurse cell cap (Woodruff and Telfer, 1980; Telfer et al., 1981). Clearly there is preferential transport of proteins based upon their charge and an implied possible mechanism for the transport of charged species between the oocyte and

nurse cells (Telfer et al., 1981). This has lead to similar work on the Rhodnius ovariole. In the presence of JH a 10 mV potential difference existed between the tropharium and oocytes (Telfer et al., 1981; Huebner et al., in preparation). JH omission caused oocyte hyperpolarization reducing the difference to 3 mV, with the tropharium still more negative (Telfer et al., 1981; Huebner et al., in preparation). FLy and McFLy exhibited different mobilities when injected into the tropharium. The acidic McFLy freely diffused throughout the tropharium, while the basic FLy was restricted to the injection site. It was proposed that the nurse cell lobes were more electronegative than the trophic core, thus causing the partitioning of charged species within the tropharium (Telfer et al., 1981). When injected into the oocyte both tracers freely diffused throughout the ooplasm (Telfer et al., 1981). It was estimated a 100 mV potential difference between the tropharium and oocyte would have to exist to produce a gradient as steep as found in cecropia, and this may explain the lack of electrophoretic parititioning in the oocyte (Telfer et al., 1981). The oocyte may act as a receptacle for nurse cell products maintaining an electropositive cytoplasm to restrict back diffusion up the trophic cords. A large electropotential gradient along the trophic cord would cause electrophoretic transport through the cord. Because the cords are long (0.5 to 1.0 mM), cytoplasmic resistances within the cords would be very high enabling large electrical gradients to exist. Although speculative, Kinosita (1963) has presented a similar theory to explain pigment migration within fish melanophores.

The establishment of regions of plasma membrane heterogeneity may be attributed to electrophoresis of charged proteins along cell membranes (Jaffe, 1977; McLaughlin and Poo, 1981; Poo, 1981). Jaffe (1977) calculated a 10

mV/cM potential difference along a cell surface is sufficient to transport a charged membrane protein. Externally applied electric fields can affect the distribution of cytoplasmic and membrane components (Poo and Robinson, 1977; Brower and Giddings, 1980), DNA synthesis (Rodan et al., 1978) and the cell shape and movement (Luther et al., 1983; Erickson and Nuccitelli, 1984). Therefore, endogenous steady electric fields could also influence the physiology of the tissue in similar ways. The mapping of steady electrical currents around the ovariole has provided clues as to where these processes may be occurring. The strong efflux at P1, P2c and P3 indicates that these are likely regions of the terminal follicle where the oocyte plasma membrane may be influenced by these fields. Determining the electric field strength at the oocyte surface is difficult due to the intervening follicular epithelium. Preliminary denuding experiments involving follicle cell dissociation have shown electric currents are still found around the oocyte, but the data is insufficient to draw conclusions on the comparative strengths of the fields.

The electronegativity of the nurse cells appears contradictory to the influx of positive extracellular current observed in this study. A similar situation exists in the cecropia follicle (see Woodruff and Telfer, 1973, 1974; Jaffe and Woodruff, 1979), which prompted Jaffe and Woodruff (1979) to propose that electrogenic pumps in the nurse cell membrane were located in the cleft between the nurse cell cap and oocyte. This would produce a loop of current across the cleft into the oocyte and then back through the intercellular bridge to the nurse cells. This model is not applicable to telotrophic ovarioles. A modified hypothesis based on new experimental, morphgological and comparative data has been proposed which is applicable to both ovariole types (Woodruff et

al., 1984; submitted). The hypothesis states that inner sheath cells act as an insulating layer preventing the escape of positive charge being pumped out by the nurse cells. The cations are forced to to flow through the peri-nurse cell space until reaching the cleft or the tropharium base where it may exit or continue to pass through the follicular epithelium. This hypothesis is supported by different McFLy and FLy mobilities in the peri-nurse space and the observation of current efflux from denuded cecropia nurse cells (see Woodruff et al., 1984; Woodruff et al., submitted). Current efflux from the Ips tropharium coincides with the morphological observation of spaces between the inner sheath cells exposing the nurse cell surface (Huebner, 1984a). Observing extracellular currents around denuded Rhodnius ovarioles may provide further supporting evidence for this hypothesis.

There are many questions concerning the extracellular currents around insect ovarian tissues which remain to be answered. The ionic composition of the currents, location of the electrogenic pumps and the modulating effect of hormones known to control oogenesis are of immediate interest. The problem of relating the electrophysiological properties to the processes involved in oogenesis will stimulate further research in this area and hopefully will provide answers to long standing questions of intercellular transport and cellular differentiation. The insect ovariole has provided the basis for much of our present understanding of these processes and will undoubtedly continue to serve as excellent model systems for further investigations.

Chapter 3

Hormonal Modulation of Extracellular Currents

Introduction

From the preceding chapter it is evident that electrical polarity within insect syncytia may have a profound influence on the cellular physiology. Therefore, modulation of the electrophysiological properties by hormones could regulate the functioning of the ovariole.

Although there is no direct evidence that extracellular currents are the consequence of the observed potential differences in the cecropia follicle, Woodruff and Telfer (1973, 1974) and Jaffe and Woodruff (1979) have shown that both of these phenomena require energy expenditures. Application of 2,4-dinitrophenol (DNP) significantly reduced the potential difference between oocyte and nurse cells (Woodruff and Telfer, 1973). Anoxia and DNP also reduced transfollicular potentials (Woodruff and Telfer, 1974). DNP caused a dramatic reversal of extracellular current flow at the nurse cell cap region, which because of the rapidity of the response led Jaffe and Woodruff (1979) to conclude that oocyte-nurse cell membrane potential is generated by electrogenic pumps.

It is therefore reasonable to assume that, in the insect systems so far examined, useful work is being done by the generation of these gradients of charge. The question which then arises is; can the extracellular current patterns and intracellular potential differences be modulated by external control factors, such as hormones, thus influencing the course and rate of oogenesis?

Hormones can have fast or delayed effects on the electrophysiological properties of the target tissue. Rapid changes in membrane resistance occur in insect epithelia exposed to 5-hydroxytryptamine (Berridge et al., 1975) or diuretic hormone (Farmer et al., 1981). The site of action is likely the cell membrane in these cases.

A much slower response occurred in Rana oocytes which were depolarized in response to progesterone (Weinstein et al., 1982), while the extracellular currents around Xenopus oocytes were greatly reduced after progesterone exposure (Robinson, 1979). In these examples the maximum response occurred after several hours and is likely due to changes at the translational level of regulation (Weinstein et al., 1982).

Juvenile hormone is required for oogenesis in Rhodnius, directing the synthesis and release of yolk protein in the fat body (Engelmann, 1979) and influencing vitellogenesis in the ovariole (Pratt and Davey, 1972a; Huebner and Davey, 1973). The follicle cells of the terminal oocyte form large spaces between each other, permitting yolk protein from the hemolymph to reach the oolemma for subsequent incorporation (Huebner and Anderson, 1972a; Huebner, 1981b; Telfer et al., 1980). The degree of patency is increased by JH under in vitro conditions (Huebner and Davey, 1973; Huebner and Injeyan, 1980) implying its site of action is the follicle cells. A less defined action of JH is the "activation" of previtellogenic follicles rendering these competent to undergo patency (Pratt and Davey, 1972a). Recently a JH sensitive Na^+-K^+ ATPase derived from vitellogenic follicle cells was demonstrated (Abu-Hakima and Davey, 1979; Ilenchuk and Davey, 1982, 1983). Given this information, plus the previously mentioned JH induced oocyte depolarization (Telfer et al., 1981;

Huebner et al., in preparation), it is of considerable interest to investigate the effect of JH or JH analogues on the extracellular currents surrounding the Rhodnius ovariole, in relation to the site of action and speed of the effect. Huebner and Injeyan (1980) determined that the increase in patency index produced by the JH analogue Altosid (ZR515) was greater than C18 JH at the same dosage. Although the depolarizing effect of Altosid on the oocyte equilibrium membrane potential is unknown, the greater degree of patency induction was seen to have greater significance in light of the proposed mechanism of patency (see Abu-Hakima and Davey, 1979; Ilenchuk and Davey, 1982). For this reason Altosid was used in this study.

Pratt and Davey (1972c) suggested the presence of an antigonadotropin which retards oogenesis in virgin females. Subsequent research showed the antigonadotropin antagonized the JH induced patency response of vitellogenic follicle cells (Huebner and Davey, 1973; Davey and Huebner, 1974). Although the antigonadotropin effects on oocyte-nurse cell potential differences have not been examined, it was felt that the extracellular current patterns surrounding ovarioles from virgin females, may shed some light on the mechanism of this important form of ovarian regulation (Huebner, 1983). Measurement of the extracellular currents around "virgin" ovarioles in the presence of Altosid could also provide an indication of the site of the antigonadotropin inhibition, by the comparision to any Altosid produced increase in current seen in ovarioles not under antigonadotropin influence ie., from mated females.

The results of these experiments have shown that Altosid can modulate the magnitude of extracellular currents at certain positions around the ovarioles from mated and virgin females.

Materials and Methods

The reference for care and feeding of insects, and the dissection of ovaries is indicated in Chapter 2.

The positions examined with the vibrating probe are the same as Fig. 1, Chapter 2, although it was not always possible to measure at every postion for all ovarioles used in this study.

Altosid (ZR515) (Zoecon Corp., Palo Alto, CA) was serially diluted to a concentration of 10^{-4} µl/ml (10^{-7}M) in Rhodnius Ringers (Maddrell, 1969), with a resistivity of 60 Ω-cm. The dilutions were vigorously mixed for 2 minutes each, to ensure an even distribution of the hormone suspension. The dilutions were protected from light, refridgerated and replaced after 2 days.

The number of ovarioles examined did not permit classification based the T follicle size. Data from all size classes have been combined. Fifth instar insects were sexed and the females kept separate during the feeding and handling of the insects. After moulting into adults, the virgins were fed, and the ovaries removed at 3, 6, 7 and 10 days post-feed. Ovaries from mated females were removed 2 to 10 days post-feed. All ovarioles had vitellogenic T follicles (>500µM in length).

Extracellular Current Measurements

The vibrating probe used to detect small steady extracellular electric fields is described in Chapter 2 and Appendix 1.

Desheathed ovarioles were placed in chambers filled with fresh Rhodnius Ringers permitting control measurements to be made. During these measurements

and those with Altosid Ringers, fresh saline was drawn into the chamber replacing the old Ringers, without disturbing the ovariole or the level of saline in the chamber. This was repeated every 10-15 minutes and ensured the ovariole did not encounter anoxic conditions. After control measurements were made, the Ringers was quickly replaced with the Altosid Ringers by 3 complete washes of the ovariole and chamber. Recordings could usually resume within 2 minutes of the last control measurement. This allowed the detection of transient responses to the Altosid occurring within 5 minutes of exposure to the JH analogue.

For the control measurements, ovarioles were examined either immediately after dissection or after 1-2 hours. In all cases Altosid was not applied until at least 1 hour post-dissection. Due to time constraints, only measurements perpendicular to the ovariole surface were made, thus indicating the current magnitude of influx or efflux.

A paired difference t test (Mendenhall, 1975) was used to detect statistically significant changes from the control values. This test uses the differences between individual control and treated values at one position, thus eliminating any variation in current magnitudes between ovarioles. The mean of these differences is then tested to determine if it differs significantly from zero. The significant mean differences therefore represent the average increase or decrease in current flux caused by the treatment.

Results

Altosid Effects on Extracellular Current Patterns

The large current efflux at P2c and P3, and the less localized influx at the tropharium described in Chapter 2 was not disturbed in regard to current direction by application of Altosid. In general this was true for all positions along the "mated" ovariole. In the 17 ovarioles examined, only 9 reversals of current direction were detected out of a total of 158 measurements (6%). These reversals were clustered around the posterior end of the T follicle, primarily at P1a, where after application of the hormone, 3 of 7 measurements detected a changed from efflux to influx. It is this change in direction which accounts for the average current increase seen in Table 1. Only 1 reversal each was seen at positions P1 and P2, both changing from efflux to influx. The region represented by P4, P5 and P6 produced 4 reversals, 3 of which occurred at P4, P5 and P6 and were changes from efflux to influx.

The extracellular current patterns around ovarioles from virgin females did not differ from those observed in mated animals. Altosid treatment caused 8 reversals in current direction, out of 121 measurements (7%). As in the "mated" ovarioles, half of these were observed at the posterior end of the T follicle and all consisted of changes from efflux to influx. The remaining reversal occurred at P2, P2a, P4 and P7 and all except one (P4) consisted of changes from efflux to influx.

Altosid Effects on Current Magnitude

These results are summarized in Table 1.

Altosid treatment did not cause any significant changes in current magnitudes, compared to controls, at positions P1, P2a, P6, P8a and P8c, for ovarioles from both mated and virgin females (Table 1).

The observed responses to Altosid occurred within the 2 to 5 minute period after changing to the Altosid medium. There were no graded responses in current increase or decrease observed during the first 5 minutes after adding the Altosid Ringers. Ocasionally a change to fresh Altosid Ringers would cause a small increase in current at certain positions after initial addition of the hormone analogue.

Differences between control and treated values were made by subtracting the treated from the control. To distinguish current direction, efflux values were made negative. Therefore positions which experienced a large proportion of reversals (see above), relative to the total number of measurements, produce differences large enough to be statistically significant, but do not reflect changes in magnitude. This is evident in the changes observed at P1a. All reversals observed at P1a consisted of efflux to influx, and this difference has been arbitrarily placed in the d increase column of Table 1.

Along the lateral surface of the vitellogenic follicle (P2), Altosid produced an average 0.8 $\mu A/cM^2$ increase in "mated" ovarioles. There was no change in "virgin" ovarioles.

At the junction between the lateral and apical follicle cells, P2b, "virgin" ovarioles showed a mean decrease of 0.7 $\mu A/cM^2$ ($P<0.1$). At P2c this decrease

had become larger (2.5 $\mu A/cM^2$) and highly significant. "Mated" ovarioles showed no changes at these two positions.

In mated females the interfollicular connective region, P3, produced a large efflux increase of 4.5 $\mu A/cM^2$ during treatment. In contrast, "virgin" ovarioles demonstrated a tendency to decrease current efflux.

On the lateral surface of the T-1 follicle (P4), Altosid produced a significant decrease of 0.5 $\mu A/cM^2$ in "mated" ovarioles. Ovarioles from virgins were not affected. Anterior to P4, at P5, "mated" ovarioles again showed a tendency to reduce the current flux, while "virgin" ovarioles remain unaffected.

At the tropharium base (P7), the average increase in current flux was a significant 2.4 $\mu A/cM^2$ in "virgin" ovarioles. At P7a, this effect continues although the average has dropped to 1.7 $\mu A/cM^2$. "Mated" ovarioles also became stimulated at P7a and P8 with average increases of 1.1 and 0.8 $\mu A/cM^2$ respectively. Ovarioles from virgins were not affected by Altosid treatment along the mid-lateral tropharium surface (P8).

TABLE I. Summary of Altosid effects on the extracellular current around the Rhodnius ovariole. For each position the data consists of mated, virgin and combined mated and virgin ovarioles from all size classes. The significant increases or decreases are given by the mean difference, d, between the control and treated current values.

Position		n	d increase ($\mu A/cM^2$)	d decrease ($\mu A/cM^2$)	P<
P1	combined	18	nil	nil	—
	mated	10	nil	nil	—
	virgins	8	nil	nil	—
P1a	combined	15	0.5	—	0.05
	mated	7	1.1	—	0.1
	virgins	8	0.7	—	0.1
P2	combined	20	0.7	—	0.01
	mated	12	0.8	—	0.05
	virgins	8	nil	nil	—
P2a	combined	13	nil	nil	—
	mated	5	nil	nil	—
	virgins	8	nil	nil	—
P2b	combined	14	nil	nil	—
	mated	6	nil	nil	—
	virgins	8	—	0.7	0.1

TABLE I. continued.

Position		n	d increase ($\mu A/cM^2$)	d decrease ($\mu A/cM^2$)	P<
	combined	12	—	2.0	0.025
P2c	mated	4	nil	nil	—
	virgins	8	—	2.5	0.025
	combined	25	2.7	—	0.1
P3	mated	17	4.5	—	0.05
	virgins	8	—	1.0	0.1
	combined	20	—	0.4	0.05
P4	mated	13	—	0.5	0.05
	virgins	7	nil	nil	—
	combined	22	nil	nil	—
P5	mated	14	—	0.8	0.1
	virgins	8	nil	nil	—
	combined	20	nil	nil	—
P6	mated	12	nil	nil	—
	virgins	8	nil	nil	—

TABLE I. continued.

Position		n	d increase ($\mu A/cM^2$)	d decrease ($\mu A/cM^2$)	P<
	combined	23	0.8	—	0.1
P7	mated	15	nil	nil	—
	virgins	8	2.4	—	0.025
	combined	15	1.4	—	0.005
P7a	mated	8	1.1	—	0.025
	virgins	7	1.7	—	0.01
	combined	25	0.5	—	0.01
P8	mated	17	0.6	—	0.025
	virgins	8	nil	nil	—
	combined	14	nil	nil	—
P8a	mated	7	nil	nil	—
	virgins	7	nil	nil	—
	combined	12	0.5	—	0.1
P8b	mated	6	nil	nil	—
	virgins	6	nil	nil	—
	combined	11	nil	nil	—
P8c	mated	5	nil	nil	—
	virgins	6	nil	nil	—

Discussion

The primary effect of the juvenile hormone analogue, Altosid, on the extracellular currents surrounding the Rhodnius ovariole, is the modulation of current density, rather than changes in current pattern or direction. These changes were observed at specific locations along the ovariole surface, and include the lateral vitellogenic follicle surface, the anterior end of this follicle, the interfollicular connective, the lateral surface of the penultimate previtellogenic follicle and the basal region of the tropharium. Only one position demonstrated current direction reversal, the posterior end of the T follicle ie., at P1a.

The changes in current density were determined in such a way that variations between ovarioles due to the vitellogenic stage of the terminal follicle (see Chapter 2) were eliminated, which means that stage specific effects of the JH analogue will be not be observed. Huebner and Injeyan (1980) identified a stage specific response to Altosid in the patency index of follicles, where the larger vitellogenic follicles tended to be more sensitive to Altosid. Thus the current increases observed at P2 and P3 in mated females may be underestimated in this study, since all size classes were combined. The current influx observed along the tropharium does not change significantly during an oogenesis cycle (see Chapter 2). Therefore the current increases observed in both "mated" and "virgin" ovarioles reflect more accurately the maximum response to Altosid.

The paucity of information on the effects of juvenile hormone or its analogues on ovarian electrophysiological properties, makes interpretation of the

data difficult and speculative. The current increase observed on the lateral surface of the vitellogenic follicle may be related to the oocyte membrane depolarization found after JH exposure (Telfer et al., 1981; Huebner et al., in preparation). The mechanism of follicle cell patency proposed by Abu-Hakima and Davey (1977) (see Davey, 1981) involves follicle cell volume reduction due to a Na^+-K^+ ATPase. The activity of this ATPase can be increased in the presence of JH (Abu-Hakima and Davey, 1979; Ilenchuk and Davey, 1982). Therefore the increase in current flux observed may be due to membrane associated events in either or both the oocyte and follicle cells. The function of those processes which produce the large current efflux found at P2c and P3 is not known, but its presence throughout oogenesis (see Chapter 2) presumably points to its importance during oogenesis. The sensitivity to Altosid at P3 indicates this region may respond to in vivo hormonal fluctuations and act in some regulatory manner. The lack of sensitivity at P2a, P2b and P2c, correlates with the changing morphology of the follicle cells. In vivo the apical follicle cells do not become patent (Huebner and Anderson, 1972a) and presumably do not respond to JH in the same manner as the lateral follicle cells.

The small decrease in current flux found at the lateral surface of the T-1 follicle is difficult to explain. Ilenchuk and Davey (1982, 1983) showed a small, but nonsignificant increase in Na^+-K^+ ATPase activity in previtellogenic follicles in the presence of JH. Why Altosid should cause a small, but significant decrease in current flux is not known, and it could be argued that it represents a reduced state of health of the ovariole. Although a plausible explanation, it cannot explain the stability of current flux at other positions of the ovariole.

If the ovariole were suffering from the length of time in vitro, all positions not sensitive to Altosid should have shown a general decrease in current flux.

The basal and mid-lateral tropharium surface is a region of unchanging current influx during oogenesis (see Chapter 2). The ability of Altosid to cause an increase of influx indicates this area may also be a site for ovariole regulation. The absence of JH in allatectomized females reduced the number of nurse cell mitoses (Pratt and Davey, 1972a), although it was thought this was due to the reduced demand for nurse cell products. The results presented here indicate that Altosid may exert a more direct effect on the tropharium.

The maximum response to Altosid in both "mated" and "virgin" ovarioles occurs within 2 to 5 minutes of adding the analogue. Therefore the site of action is likely the plasma membrane. This is similar to the findings of membrane resistance changes in insect epithelia exposed to 5-hydroxytryptamine and diuretic hormone (Berridge et al., 1975; Farmer et al., 1981). Exogenous JH also affects follicle cell volume within 10 minutes of exposure (Abu-Hakima and Davey, 1977).

Oogenesis in virgin females is characterized by a reduction in the number of eggs laid and produced, and the insensitivity to JH induction of patency (Pratt and Davey, 1972c; Huebner and Davey, 1973; Davey and Heubner, 1974; Huebner, 1983). Therefore antigonadotropin appears to act directly on the follicles by the reduction in the rate of oogenesis. This correlates well with the observation that Altosid did not stimulate an increase in extracellular current flux on the lateral surface of the vitellogenic follicle. The oocyte membrane potential in ovarioles from virgin females is not known, so it is not possible to differentiate between an insensitivity at the oocyte or follicle cell membrane.

It is tempting to speculate however, that JH or its hormone analogues are inhibited from stimulating the Na^+-K^+ ATPase found in the follicle cell membrane by an antigonadotropin. The reduction of patency in virgin female ovarioles and the prevention of JH induced patency by antigonadotropin (Pratt and Davey, 1972c; Huebner and Davey, 1973; Davey and Huebner, 1974), both correlate with this hypothesis. This inhibition of vitellogenesis is also characterized by the decrease in current efflux at the anterior end of the terminal follicle in response to Altosid. How this observation relates to the process of oogenesis is not known, but it is clear that substantial changes in the physiology of the oocyte and/or apical follicles cells have occurred. Altosid did not induce changes in current density along the T-1 follicle (P4) from virgin females, again demonstrating a possible site for antigonadotropin action. Altosid produced similar responses in current density at the tropharium base (P7, P7a) in both "mated" and "virgin" ovarioles, thus indicating that the antigonadotropin acts primarily on the follicles.

The action of the antigonadotropin appears long lasting, exceeding the time required to make control and treated extracellular measurements. This is similar to the effects of progesterone on a Na^+-K^+ ATPase in Rana oocytes (Weinstein et al., 1982) and the extracellular currents around Xenopus oocytes (Robinson, 1979). Therefore as suggested for progesterone (Weinstein et al., 1982), the antigonadotropin may be acting at the transcriptional or translational level of regulation. Ilenchuk and Davey (1983) proposed that two populations of Na^+-K^+ ATPase exist in the follicle cells from vitellogenic follicles and that "activation" of previtellogenic follicles by pre-exposure to JH results in the appearance of the second population of JH sensitive sites. The results presented

here permit tentative extension of this hypothesis; the presence of an antigonadotropin prevents the appearance of this second population of JH sensitive sites, presumably a Na^+-K^+ ATPase, thus inhibiting the volume changes of the follicle cells and ultimately vitellogenesis. Although this hypothesis is simplistic, considering the many effects juvenile hormone has on insect physiology, it is clear that the role of JH and antigonadotropin in regulating oogenesis in the Rhodnius ovariole, may be approached by the examination of its electrophysiological properties.

Chapter 4

Membrane Charge Distribution of Germ-Cell Syncytia and Somatic Cells

Introduction

The fluid mosaic model of cell membrane structure predicts that through cooperative effects, aggregations of membrane proteins may occur (Singer and Nicolson, 1972). These microdomains of differentiated membrane surface composition have been demonstrated by the distribution of membrane surface charge (Nicolson, 1973; Grinnel et al., 1975; Burry and Wood, 1979; Simionescu et al., 1981; many others). This involves the technique of binding charged electron-dense tracers to the surfaces of cells and observing the distribution of tracer in the electron microscope (Gasic et al., 1968; Danon et al., 1972; De Bruyn et al., 1978; Burry and Wood, 1979). The bound distributions of tracers such as positive colloidal iron hydroxide and cationized ferritin have been observed in a large variety of cell types and tissues; primarily of vertebrate origin (Gasic et al., 1968; Grinnel et al., 1975; Anderson and Hein, 1977; De Bruyn et al., 1978; Jakoi et al., 1982; others).

The microdomains tend to range in size from the tips of cilia (Anderson and Hein, 1977), coated pits (De Bruyn et al., 1978) and endothelial fenestral diaphrams (Simionescu et al., 1981), to large regions of cell contact (Jakoi et al., 1982). Recent examples of membrane specialization over a larger areas are the fusomal membrane of guinea pig sperm (Bearer and Friend, 1981) and the retinal glial cell membrane (Newman, 1984).

The best studied examples of insect membrane specializations are the various forms of cell junctions, found in insect epithelia (see Lane's review, 1982). In Rhodnius, gap junctions have been found between nurse cells, follicle cells and follicle cells and oocytes (Huebner, 1981b; Huebner and Injeyan, 1981). Recently, the surface charge distributions of Calpodes fat body cell membranes demonstrated a possible function for anionic charges, in the charge sieving of hemolymph proteins (Locke and Huie, 1983; Brac, 1983).

The Rhodnius ovariole is a complex intergrated tissue, and differentiated regions in somatic and germ-cell plasma membranes are expected. The plasma membrane of the germ-cell syncytium in Rhodnius is continuous as shown by fluorescent dye microinjection (Huebner, 1981a) and ultrastructural observations (Huebner and Anderson, 1972b, 1972c; Huebner, 1981a). The high degree of structural polarity leads one to speculate on the heterogeneity of plasma membrane composition throughout the syncytium. This differential topography would be a reflection not only of the polarized nature of the germ-cell syncytia, but also of the somatic cell interactions, which occur in the epithelial covering and between germ cells. Therefore, the binding distribution of the charged tracers, positive colloidal iron, native (anionic) and cationic ferritin were observed on the somatic and germ cells of the Rhodnius ovariole.

The use of charged tracers has also been used in the elucidation of the charge on subcellular structures, such as endothelial cell fenestrae (Simionescu et al., 1981; Thürauf et al., 1983) and basement membranes (Rennke et al., 1975; Dermietzel et al., 1983; Locke and Huie, 1983; Brac, 1983). These subcellular structures are presumed to act as charged sieves permitting protein separation based on their charge (Rennke et al., 1975; Brac, 1983).

The recent findings of Brac (1983), and Locke and Huie (1983) have shown that charge sieving of proteins may occur in insect basement membranes. This was based on cationic ferritin binding to the basal lamina of Calpodes fat body cells. The exchange of hemolymph proteins during secretion and uptake by the fat body cells may be influenced by the anionic sites found in the basal lamina.

The passage of hemolymph proteins (vitellogenins) also occurs across the basement membrane of vitellogenic follicles in Rhodnius (Huebner, 1984b). The large spaces between follicle cells during vitellogenesis, prevent selective absorption of unwanted hemolymph proteins and therefore the basement membranes may act as a sieve excluding proteins with the wrong charge. The sign and distribution of charged sites in the basement membrane of the Rhodnius ovariole was therefore determined using native and cationic ferritin.

Materials and Methods

Insects were reared as referred to in Chapter 2.

The cell surface must be accessible to the tracers, therefore enzymatic digestion and cell dissociation procedures were employed to produce a basement membrane free, denuded trophariumoocyte complex (see Huebner, 1984a). Once this denuding procedure was complete, the ovariole was exposed to the charged tracers and then processed for electron-microscopy.

Ovariole Dissection and Preparation

Ovaries were dissected from animals 3-4 days post-feed to obtain vitellogenic follicles.

The ovariole sheathes were removed under Rhodnius Ringers (Maddrell, 1969) and placed in 1% trypsin Ca^{2+}-Mg^{2+} free, 1 mM EGTA Rhodnius Ringers. Basal lamina removal proceeded for 5 minutes, 10 minutes or 1 hour. The basal lamina "expanded" or lost contact with the ovariole after 10 minutes at which time it was either removed by grasping with fine forceps (in the case of the 5 minute digestion) or allowed to further digest until it fragmented.

The ovariole was then washed and further cell dissociation allowed to continue for 1 hour in Ca^{2+}-Mg^{2+} free Ringers. To denude the ovariole, a fine stream of Ca^{2+}-Mg^{2+} free Ringers was forced from a finely drawn pipette and directed at the follicular epithelium. When approximately 50% of the epithelial cells were washed from the oocyte and nurse cell lobes clearly separated, the denuded ovariole was placed in complete Rhodnius Ringers for 5-10 minutes.

Colloidal Iron Binding

Ovarioles were denuded as above and then prefixed for 1-1½ hours in modified Karnovsky's fixative (see below), rinsed with 0.1 M cacodylate buffer and then immersed in a colloidal iron solution (pH 1.1-1.3) prepared according to Mowry (1958) for a 3 hour incubation. The ovarioles were then placed in 12% acetic acid for 10 minutes, rinsed with cacodylate buffer and then osmicated in 1% OsO_4 in 0.1 M phosphate buffer. Tissue was then processed for electron microscopy.

All digestions and incubations were done at room temperature (22°C) except for prefixation which was carried out at 4°C.

Cationic and Native Ferritin Binding

Denuded ovarioles were incubated in either native ferritin (2X recrystallized, cadmium free) or cationic ferritin (Miles Yeda Lab.) at a concentration of 0.1 mg/ml in Rhodnius Ringers for 5, 10 or 30 mintues, followed by three washes of Ringers. Intact desheathed ovarioles were dissected from the insect at the same time as ovarioles which were denuded, and allowed to wait in Ringers until denuded ovarioles were ready. Therefore any physiological changes in the denuded ovarioles during the time in vitro would be partially mimicked in the intact ovarioles. Intact ovarioles were incubated in 0.1 mg/ml of tracer for 30 minutes, washed, and processed for electron microscopy.

All digestions and incubations were done at room temperature (22°C).

Light and Electron Microscopy

Denuded and intact ovarioles were fixed in a modified Karnovsky's fixative (Huebner and Anderson, 1972a) containing 1% paraformaldehyde, 3% glutaraldehyde, 0.15% $CaCl_2$ in 0.1 M sodium cacodylate pH 7.2-7.4. Ovarioles were fixed for 1½-2 hours at 4°C, washed in buffer, and then osmicated for ½ hour in 0.5% or 1% OsO_4 in phosphate buffer pH 7.2. Rapid dehydration in ice cold ethanol preceded infiltration with proplylene oxide and Epon-Araldite and embedding in Epon-Araldite (Huebner and Anderson, 1972a).

Semi-thin sections (1 μM) were cut using glass knives on a Sorval MT-2B ultramicrotome, stained in 1% toluidine blue in 1% borax and examined with a Zeiss Photo II microscope. Ultrathin sections (silver interference colours) were cut with glass knives and examined unstained in an AEI EM 6-B or 801 electron microscope. Subsequent to examining some sections unstained, other sections from the same series were briefly stained in uranyl acetate and lead citrate to enhance cytological detail.

Results

Colloidal Iron Binding

The colloidal iron (CI) was precipitated as dense particles which bound to all surfaces of the denuded ovariole. The distribution of CI was uniform on the oocyte surface, covering microvilli, the oolemma and pinocytotic pits (Fig. 1 and 2). During the process of denuding, follicle cells become separated and lose contact with each other and the oocyte. The CI bound uniformly to all exposed regions of the follicle cell surfaces (Fig. 1). Prefollicular cells also separate and become uniformly coated with the CI, but in some cases contact between cells was retained and the tracer was excluded in these areas (Fig. 3).

The process of "blowing" the saline during the denuding procedure not only removes follicle cells but also separates the lobes of nurse cells which comprise the tropharium. The degree of separation limited the extent of the CI binding to exposed surfaces of the nurse cells (Fig. 4). Again, the CI iron was bound uniformly on the surface of the nurse cells, except where contact between lobes prevented its penetration (Fig. 5). The inner sheath cells which form the epithelial covering of the tropharium also bound CI on exposed surfaces and excluded it from regions of contact with nurse cells (Fig. 6).

Native and Cationic Ferritin Binding

Native ferritin (NF) used at the physiological pH of 6.9 will be anionic and presumably will bind to cationic sites (Danon et al., 1972). Native ferritin did not bind to the plasma membrane of the denuded ovariole in a consistent manner. Scattered ferritin particles were rarely present on or near the

microvilli of the oocyte (Fig. 7). Follicle cells, nurse cells or inner sheath cells did not bind NF (Figs. 8, 9 and 10).

Cationic ferritin (CF) has a positive charge at physiological pH and presumably binds to anionic sites on the plasma membrane (Danon et al., 1972). The amount of CF bound was small with large areas free of CF binding (Fig. 11). The oocyte bound CF only in regions where microvilli contact other microvilli or the surface of the adjacent follicle cell (Fig. 12). The separated follicle cells (Fig. 13) often formed small blebs or projections, some of which made direct contact with other cells, although reduced from that in intact patent follicles (Huebner and Anderson, 1972a; Huebner, 1981). CF bound in these regions of contact between follicle cells, either between projections or in areas of larger contact (Figs. 15 and 16). CF was less often found adhereing to the surface of the follicle cell (Fig. 17) and generally the exposed surface did not exhibit any CF binding (Fig. 14). The prefollicular cells found at the base of the tropharium also become separated during the denuding procedure and form numerous blebs or small projections (Fig. 18). CF was not observed binding to any surfaces of the prefollicular cells (Fig. 19 and 20) or on follicle cells near small previtellogenic oocytes (Fig. 21).

The denuded tropharium has exposed nurse cell lobes which form large blunt projections (Fig. 22). CF binding to exposed nurse cell lobes was restricted to small clusters near pinocytoic pits and/or vesicles (Fig. 23). Ocasionally CF was seen between two nurse cell lobes in close proximity (Fig. 24). CF was never observed in the trophic core region of the tropharium (Fig. 25). The inner sheath cells, which form a complete sheet covering the nurse cells, retract their peripheries but, retain cytoplasmic projections which contact

neighbouring inner sheath cells (Figs. 22 and 26). The inner sheath cells retain regions of contact with nurse cells, but these are less extensive compared to the intact state (see Figs. 22 and 30). Typically CF never bound in regions of contact between nurse cells and inner sheath cells (Fig. 22).

The cytoplasmic projections which extend between inner sheath cells as well as more direct areas of contact, are very convoluted and interdigitating (Fig. 27). The CF bound primarily in the intercellular spaces where inner sheath cells made contact (Figs. 27 and 28), but was also observed on the basal surface, superimposed on flocculent material adhering to the cell membrane (Fig. 29). The CF bound in regular linear arrays when seen in en face sections (Fig. 29, inset), but also appeared in a more random arrangement (Fig. 27, inset).

Native and Cationic Ferritin Binding to the Basal Lamina

Native ferritin did not bind to the ovariole basal lamina as seen in Fig. 30.

In preliminary experiments, CF binds extensively to the basal lamina surrounding the follicles (Figs. 31, 33-35) and tropharium (Figs. 36-38). Particle counts have not been made, but it appears there are more CF molecules bound to the basal lamina surrounding the follicle cells from previtellogenic and vitellogenic follicles (Figs. 33 and 34) than interfollicular cells (Fig. 31) and post-vitellogenic follicles (Fig. 35). CF particles bound to the interfollicular region between the terminal and penultimate follicle, where it is limited to small clusters on the exterior of the basal lamina (Fig. 31) with very few ferritin molecules actually within the basal lamina itself. CF binding to basal

lamina from previtellogenic and vitellogenic follicles (Figs. 33 and 34) extends from the surface and into the basal lamina, while CF binds primarily to the surface of post-vitellogenic follicles (Fig. 35). CF binding was not reduced by the action of trypsin, when used for basal lamina removal during the denuding procedure. The remnants of the basal lamina are sometimes preserved in denuded follicles and here CF has bound densely (Fig. 32).

CF bound densely throughout the basal lamina surrounding the tropharium (Fig. 36), and when seen in en face sections, appears to be bound as small clusters (Figs. 37 and 38).

Plate Abbreviations

Follicle Cells ..... F

Oocyte ..... O

Prefollicular Cells ..... PF

Nurse Cell ..... NC

Inner Sheath Cells ..... IS

Pre-vitellogenic Oocyte ..... PO

Interfollicular Plug I

Basal Lamina ..... B

NOTICE/AVIS

PAGE(S) 98 - 106 ~~IS~~/ARE ~~EST~~/SONT black and white photos

PLEASE WRITE TO THE AUTHOR FOR INFORMATION, OR CONSULT THE ARCHIVAL COPY HELD IN THE DEPARTMENT OF ARCHIVES AND SPECIAL COLLECTIONS, ELIZABETH DAFOE LIBRARY, UNIVERSITY OF MANITOBA, WINNIPEG, MANITOBA, CANADA, R3T 2N2.

VEUILLEZ ECRIRE A L'AUTEUR POUR LES RENSEIGNEMENTS OU VEUILLEZ CONSULTER L'EXEMPLAIRE DONT POSSEDE LE DEPARTEMENT DES ARCHIVES ET DES COLLECTIONS SPECIALES, BIBLIOTHEQUE ELIZABETH DAFOE, UNIVERSITE DU MANITOBA, WINNIPEG, MANITOBA, CANADA, R3T 2N2.

Figures 1-6. Colloidal iron binding to the denuded ovariole. All sections were examined unstained.

Figure 1. Colloidal iron has bound to all accessible surfaces of the follicle cells (F) and oocyte (O). It is excluded from regions of contact between follicle cells (arrows). X8,000.

Figure 2. Colloidal iron bound to oocyte microvilli and pinocytotic pits and appears as dense particles of varying diameter. X40,000.

Figure 3. Prefollicular cells (PF) removed during the denuding procedure form small blebs on their surfaces, but still retain some contact with other cells (arrow), where the colloidal iron has not bound. X5,000.

Figure 4. The separated nurse cell (N) lobes, exposed during denuding have bound colloidal iron on their surfaces. X3,200.

Figure 5. At higher magnification the tracer is seen on all exposed nurse cell surfaces. X16,000.

Figure 6. Inner sheath cells (IS) also bound the tracer on their exposed surfaces. X10,000.

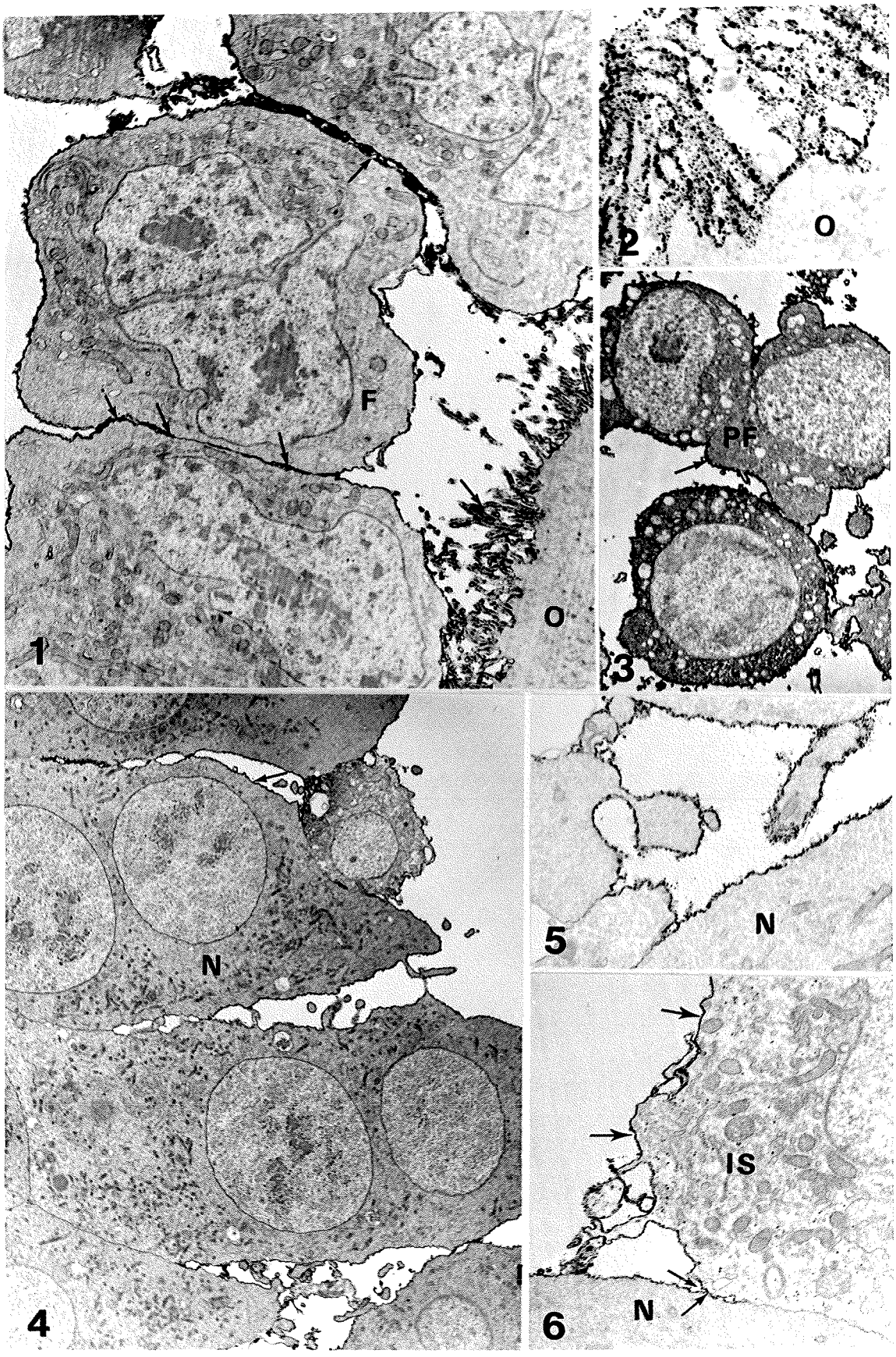
F
O
1
O
2
PF
3
N
4
N
5
IS
N
6

Figures 7-10. Native ferritin binding to the denuded ovariole. All sections briefly stained with uranyl acetate and lead citrate.

Figure 7. The oocyte (O) and follicle cells (F) did not bind the anionic native ferritin to any of their external surfaces, such as microvilli or pinocytotic pits. X6,800.

Figures 8, 9. The exposed surfaces of inner sheath cells (IS) and nurse cells (N) did not bind the tracer. Fig. 8. X28,000; Fig. 9. 64,000.

Figure 10. The tracer was not found in areas of inner sheath cell contact. X50,000.

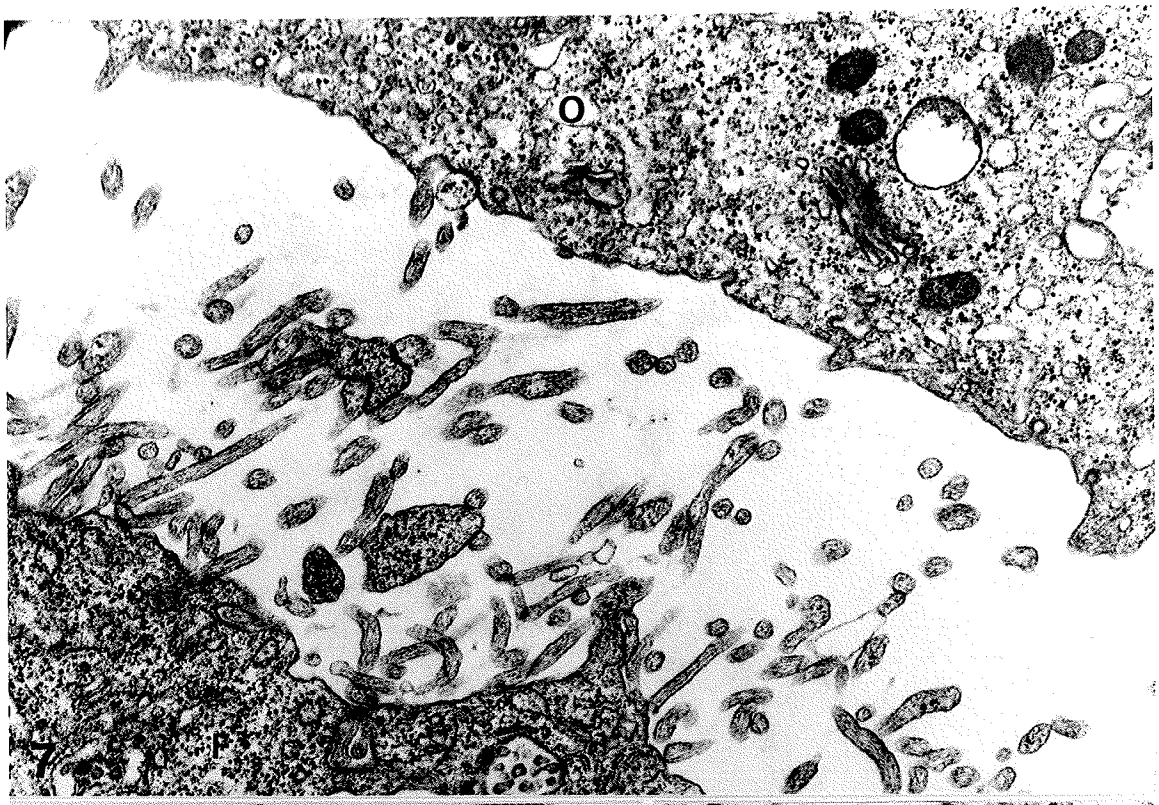

7

8

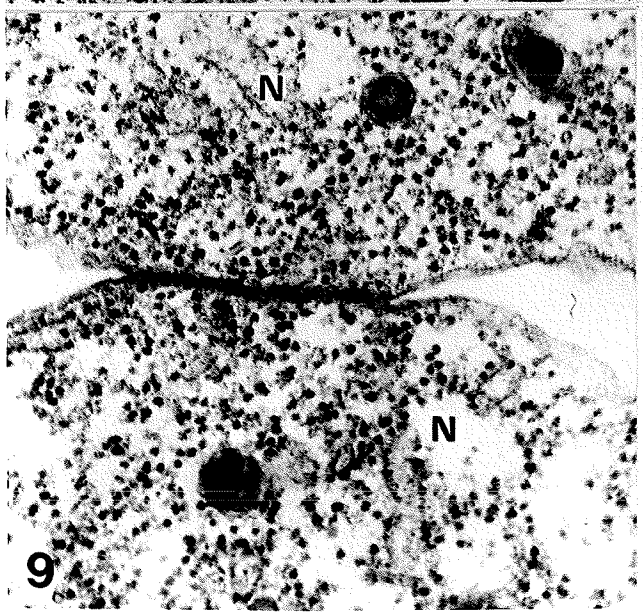

9

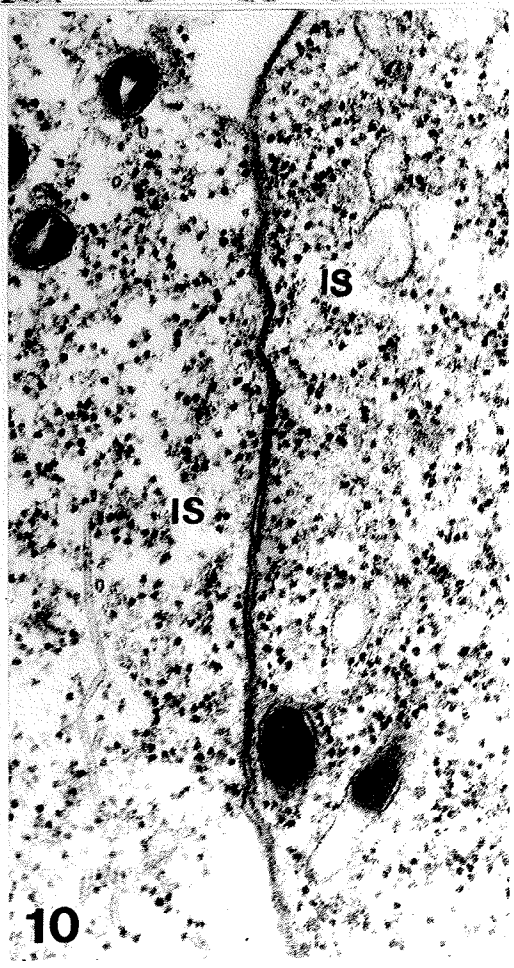

10

Figures 11-12. Cationic ferritin (CF) binding to the oocyte surface. Unstained sections.

Figure 11. Typically CF was not found binding to the microvilli, oolemma and coated pits of the oocyte (O) or to the follicle cell (F). X60,000.

Figure 12. Ocasionally CF particles were found adhering to areas where oocyte microvilli were in contact with other microvilli or with the follicle cell (arrows). The follicle cell is located near the top of this micrograph. X85,000.

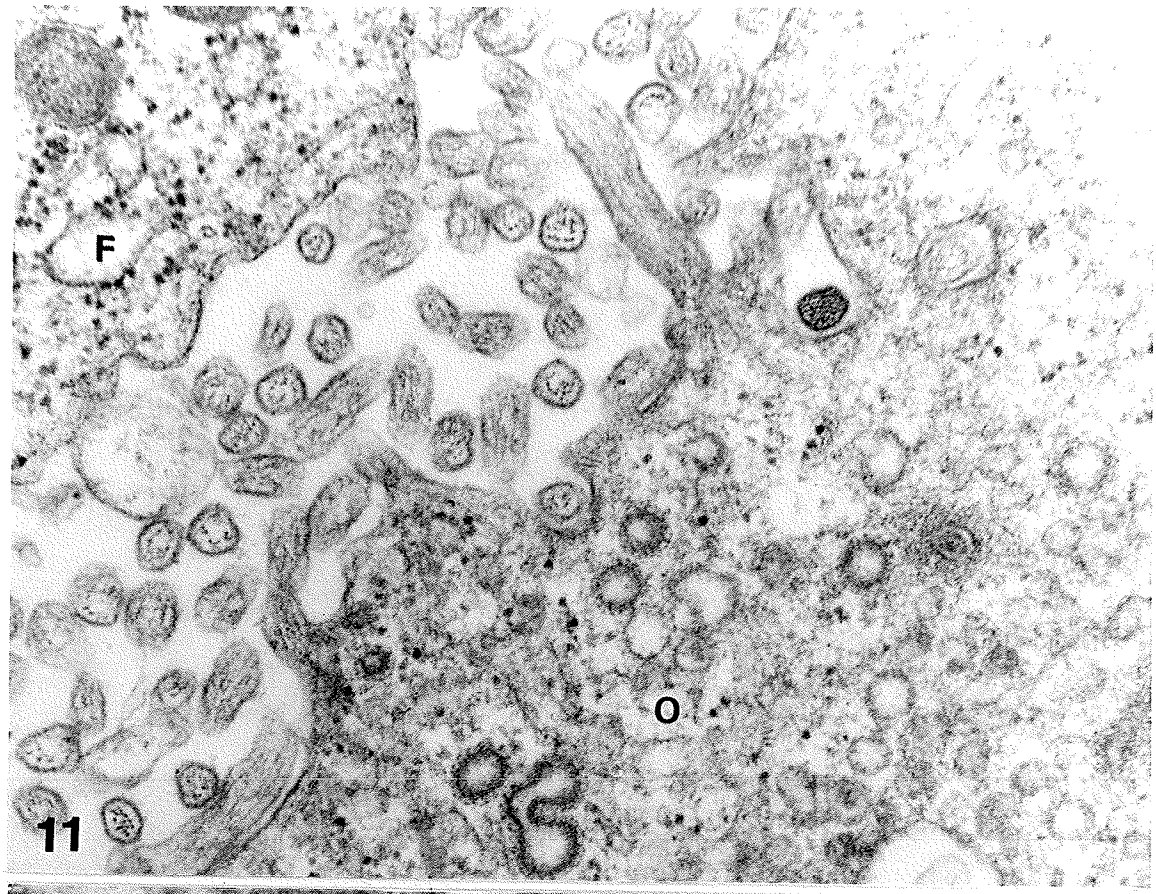
F
O
11

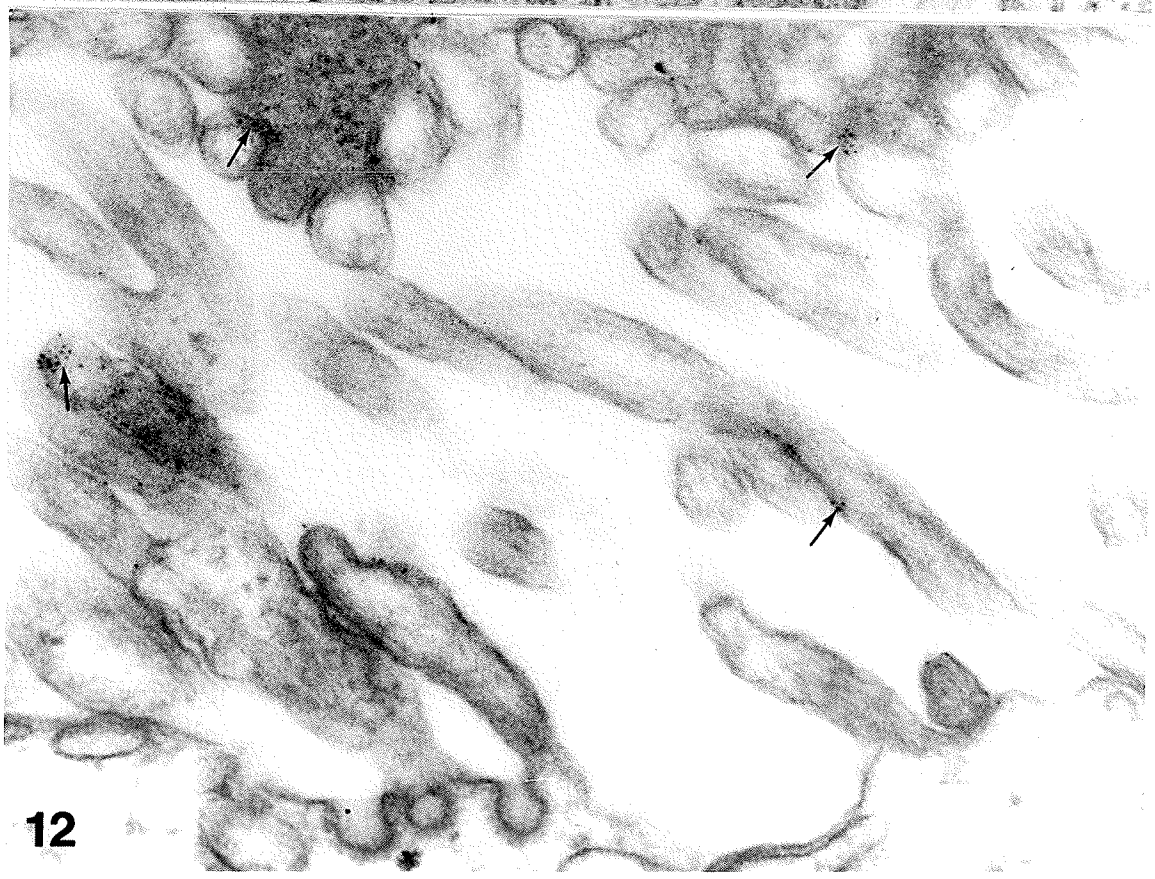
12

Figures 13-17. Cationic ferritin binding to follicle cells. Sections were briefly stained.

Figure 13. Follicle cells as they appear after the denuding procedure are generally well separated and have numerous blebs and projections. X7,000.

Figure 14. Typically the free follicle cell surface did not bind CF. X46,000.

Figure 15. CF did bind between regions where follicle cell projections were in contact (arrows). X76,000.

Figure 16. CF binding often was quite dense in the areas of contact depicted here. The intercellular spaces were narrow, but still accessible to CF (lower arrows). X68,000.

Figure 17. CF particles bound to exposed follicle cell surfaces were rarely seen and may represent former regions of contact. The small process to the right in the micrograph, may be a remnant of a larger process, now removed or out of the section plane. X95,000.

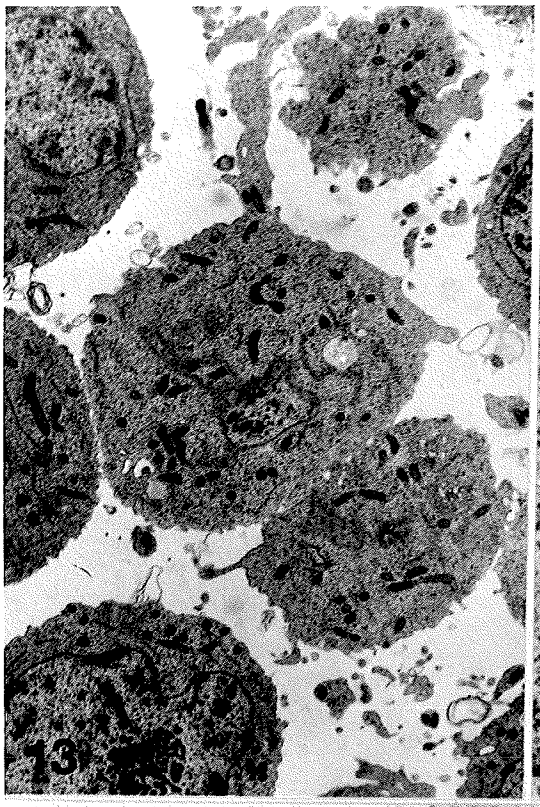
13

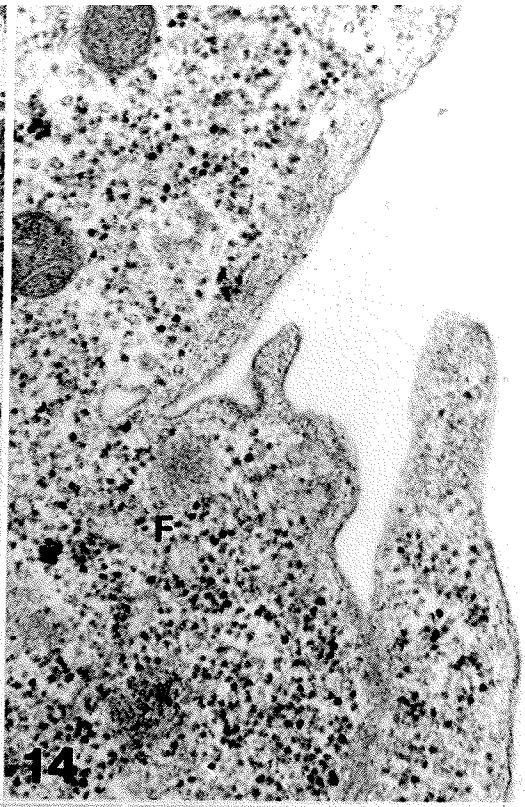
F
14


15

F

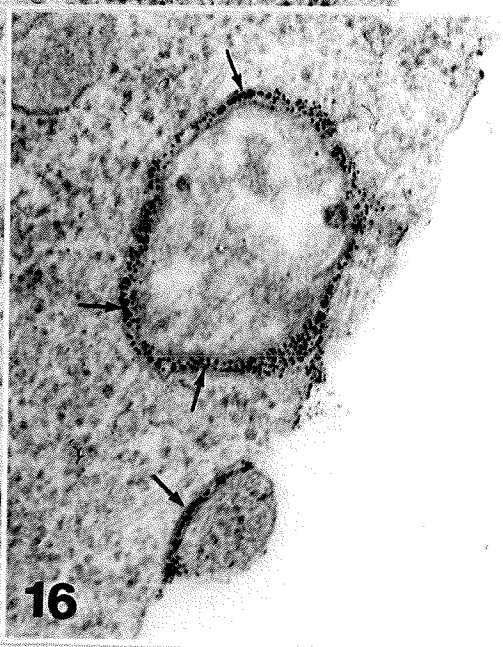
16

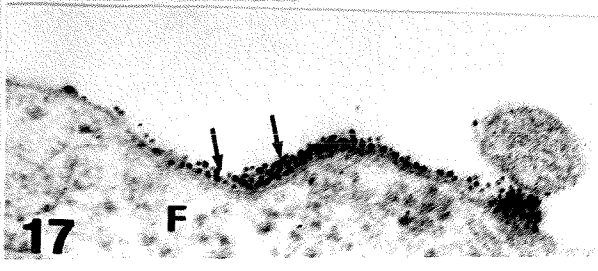
17
F

Figures 18-21. CF binding to prefollicular cells. Sections briefly stained.

Figure 18. This light micrograph reveals the separation of prefollicular cells (PF) that occurs during denuding. Note the numerous mitotic figures still present after several hours in vitro. X800.

Figure 19. Prefollicular cells located near the tropharium base come into close contact with nurse cells (N). CF did not bind to any of these cell surfaces. X60,000.

Figure 20. Prefollicular cells did not bind CF, even in areas of contact. X20,000.

Figure 21. Small previtellogenic oocytes and associated follicle cells do not bind CF, despite the presence of oocyte microvilli. X50,000.

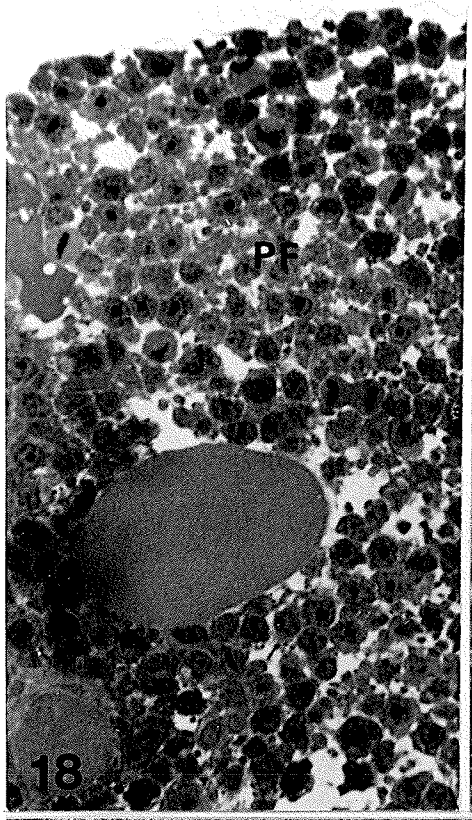
PF
18

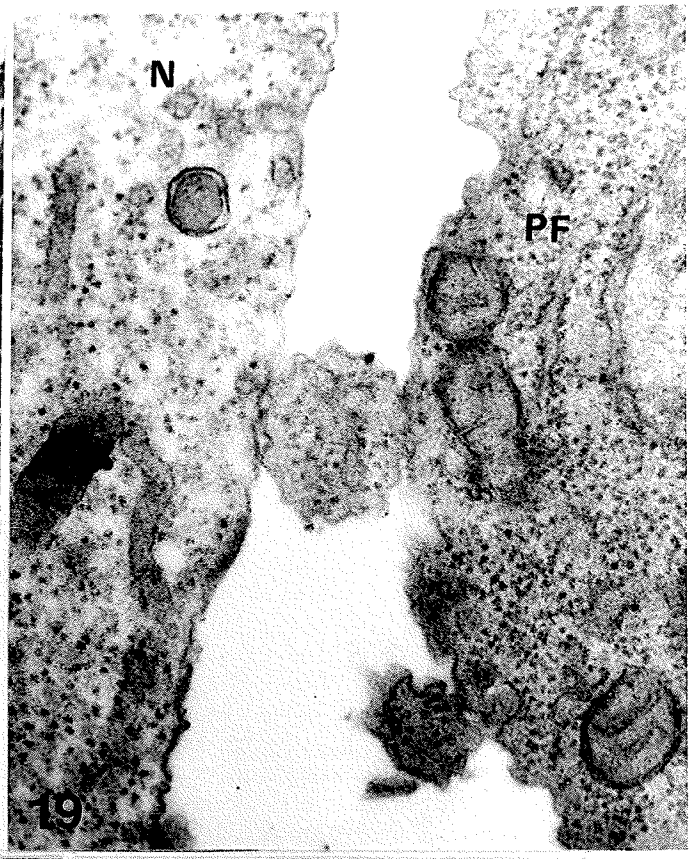
N
PF
19


PF
PF
PF
20

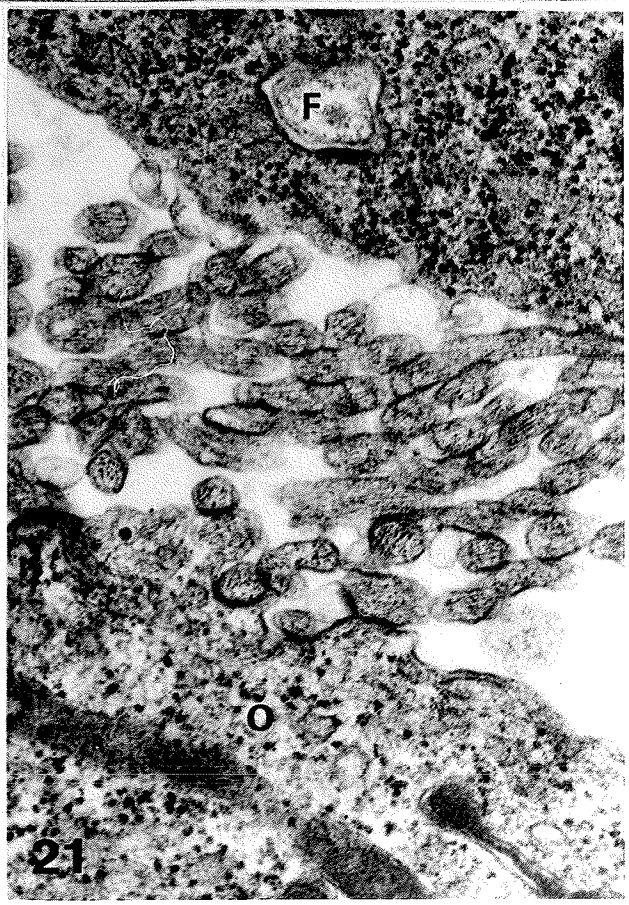
F
O
21

Figures 22-25. CF binding to the denuded tropharium. Sections were examined unstained except for Fig. 25.

Figure 22. The large exposed nurse cell lobe (N) was essentially free of CF binding when compared to inner sheath cells (arrows). X13,000.

Figure 23. CF was rarely found in small clumps (arrows) near small vesicles or pits in the nurse cell membrane. X45,000.

Figure 24. CF was rarely found between opposing nurse cell lobes (arrows) near the apex of the lobes. X43,000.

Figure 25. Down near the trophic core, CF was never observed binding to nurse cells. X54,000.

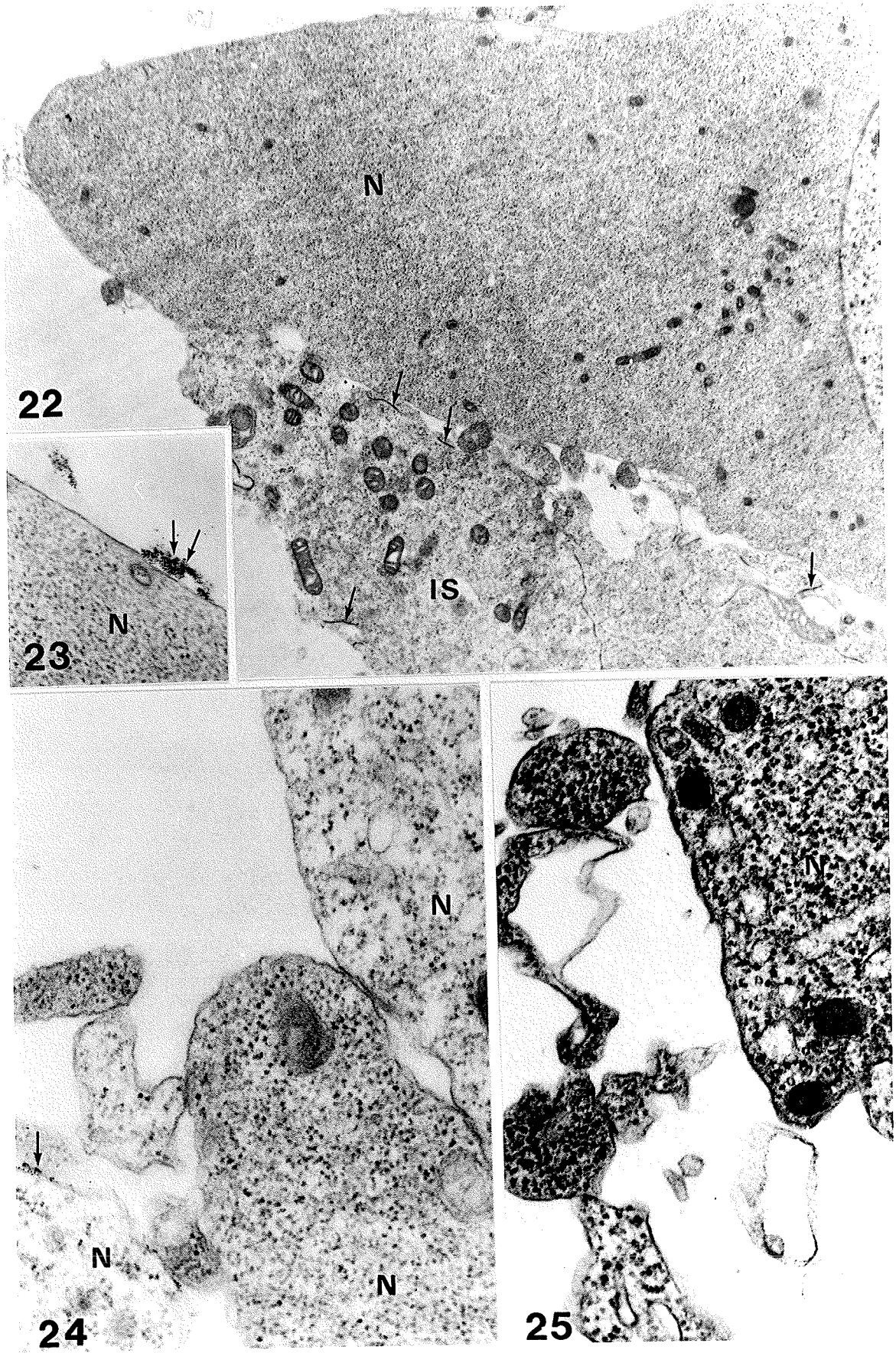
N
22
IS
N
23
N
N
N
24
N
25

Figures 26-29. CF binding distribution on inner sheath cells (IS). Sections were unstained.

Figure 26. CF bound extensively between the processes and interdigitations of the inner sheath cells (arrows) as seen in this survey electron micrograph. X12,600.

Figure 27. The convoluted nature of the inner sheath cell processes is evident, as well as the extensive CF binding (arrows). The number of CF particles found between the inner sheath cells is delimited by the width of the intercellular space (lower arrows), while en face views (upper arrows) show that CF bound throughout the intercellular space. X32,000.

Inset: The characteristic spacing of ferritin particles is evident here. Although the binding appears random, certain areas suggest a linear arrangement of particles (lower arrows). X50,000.

Figure 28. CF bound primarily between the inner sheath cells, often in single file (arrows) and is absent from the free surface. X40,000.

Figure 29. The random clustering of CF bound on flucculent material of the free surface of the inner sheath (upper arrow) is contrasted by the linear arrangement of particles seen in en face sections (lower arrows). X60,000.

Inset: The linear pattern of CF binding is clearly evident in this high magnification micrograph. X100,000.

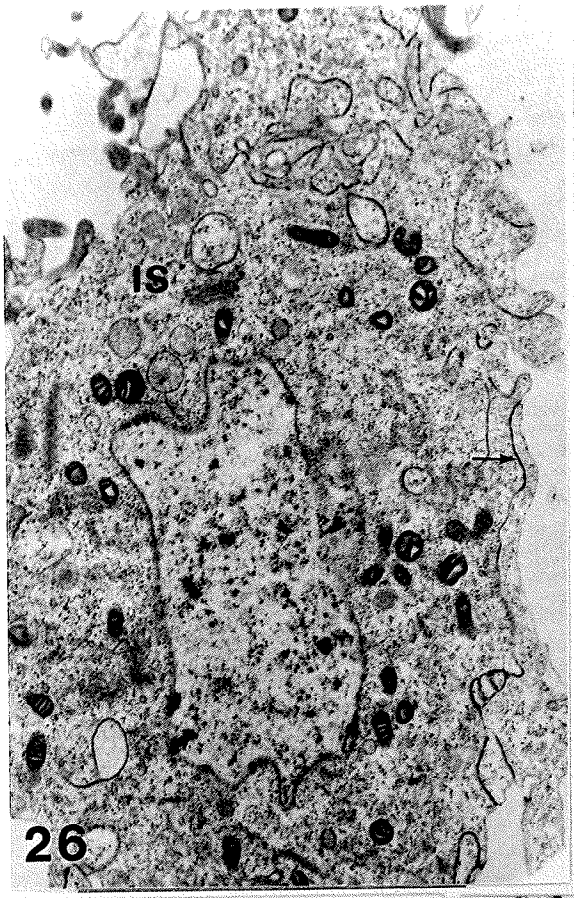

26

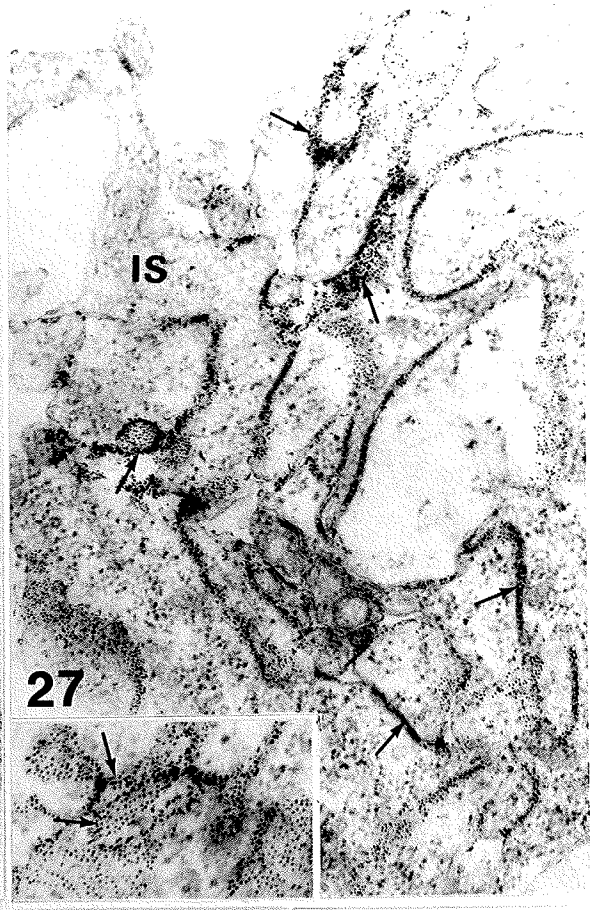

27

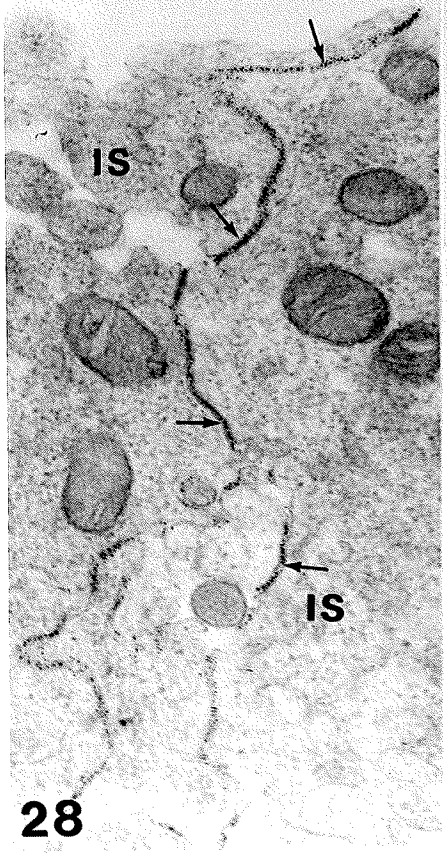

28

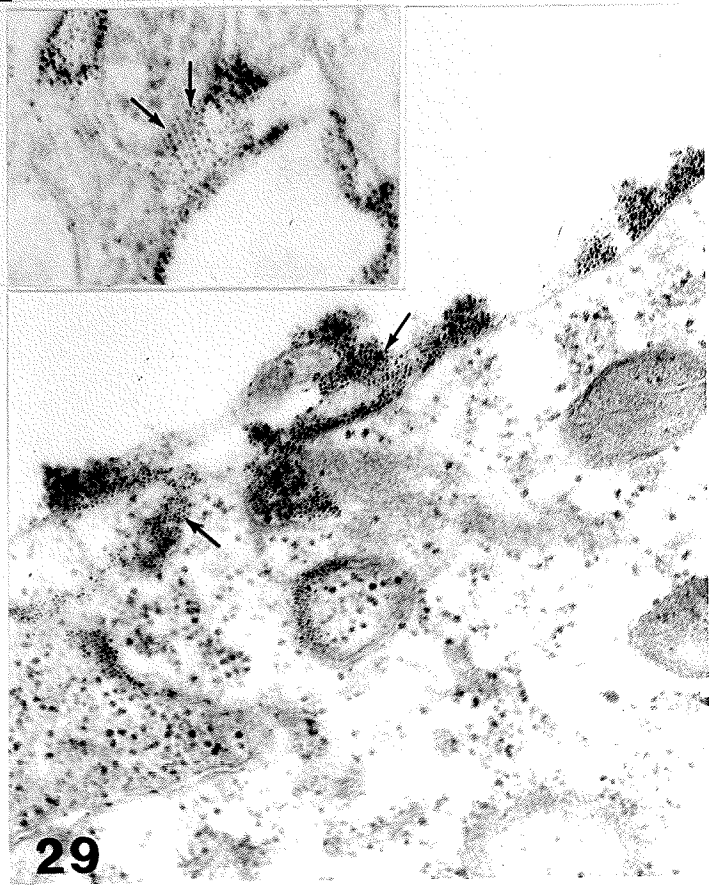

29

Figure 30. Native ferritin did not bind to the basal lamina; in this case around the tropharium. Section was briefly stained.

Figures 31-35. CF binding to the ovariole basal lamina (B).

Figure 31. This unstained section demonstrates the clustered binding of CF to the exterior of the basal lamina surrounding the interfollicular connective. X34,000.

Figure 32. After trypsin digestion basal lamina remnants still contained anionic sites accessible to CF. X25,000.

Figure 33. The basal lamina surrounding previtellogenic follicles is closely opposed to the follicles cells (F) and bound individual CF particles or small clusters (arrows). Unstained section. X80,000.

Figure 34. In patent, vitellogenic follicles the basal lamina loses contact with the follicle cells in large areas. CF bound densely in large clusters throughout the basal lamina, (arrows) but was not found on the follicle cells. Section briefly stained. X24,000.

Figure 35. In post-vitellogenic follicles CF binding has been restricted primarily to the exterior surface of the basal lamina. Section was briefly stained. X50,000.

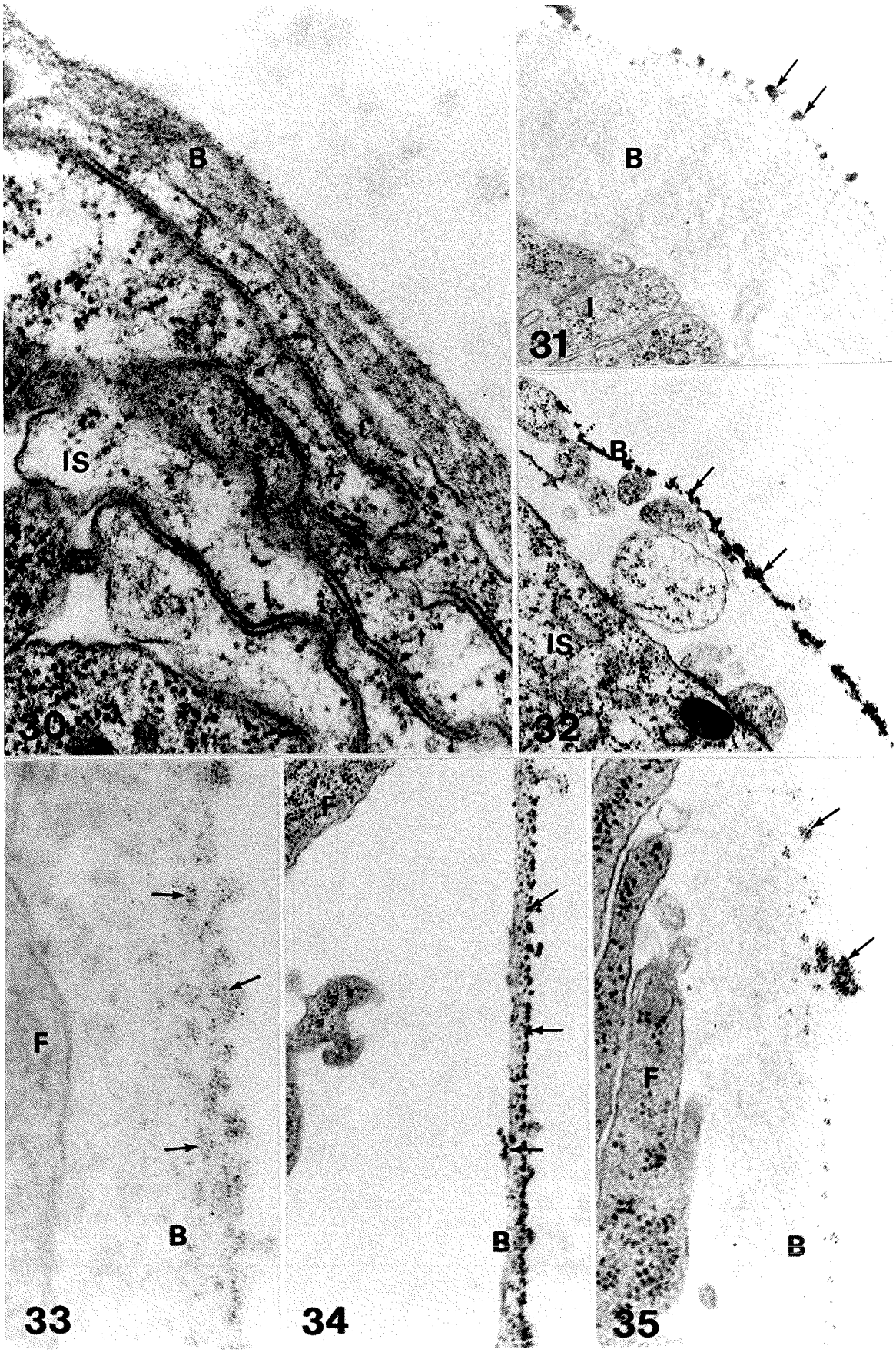
B
IS
30
B
I
31
B
IS
32
F
B
33
F
B
34
F
B
35

Figures 36-38. CF binding to the tropharium basal lamina (B). Sections briefly stained.

Figure 36. This survey electron micrograph demonstrates the close apposition of the inner sheath cells (IS) to the nurse cells (lower right hand area). The basal lamina has bound large amounts of CF. X22,000.

Figure 37. The areas of inner sheath cell (IS) interdigitation are noticably absent of CF particles, while the basal lamina has dense clusters throughout its thickness. X40,000.

Figure 38. An en face section of the basal lamina clearly shows the small clusters of bound CF (arrows). X80,000.

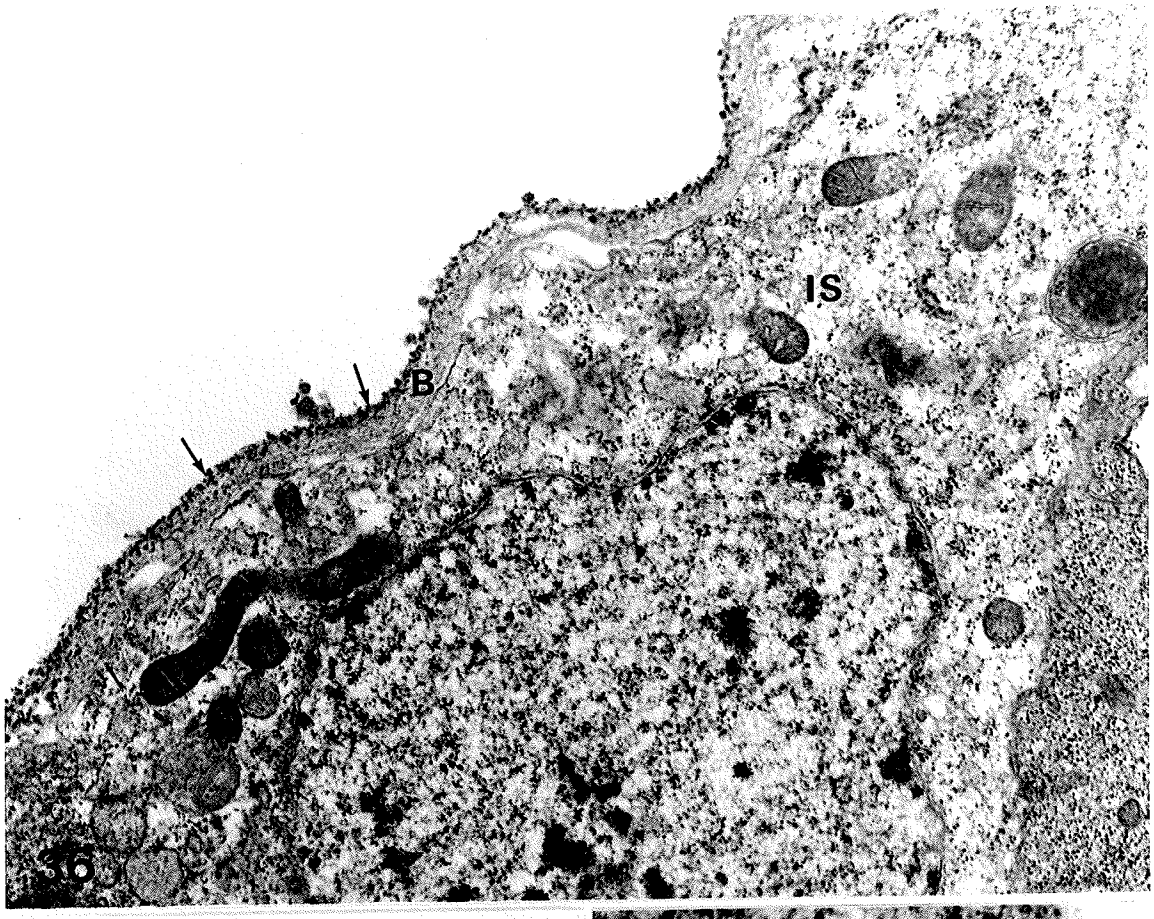

37

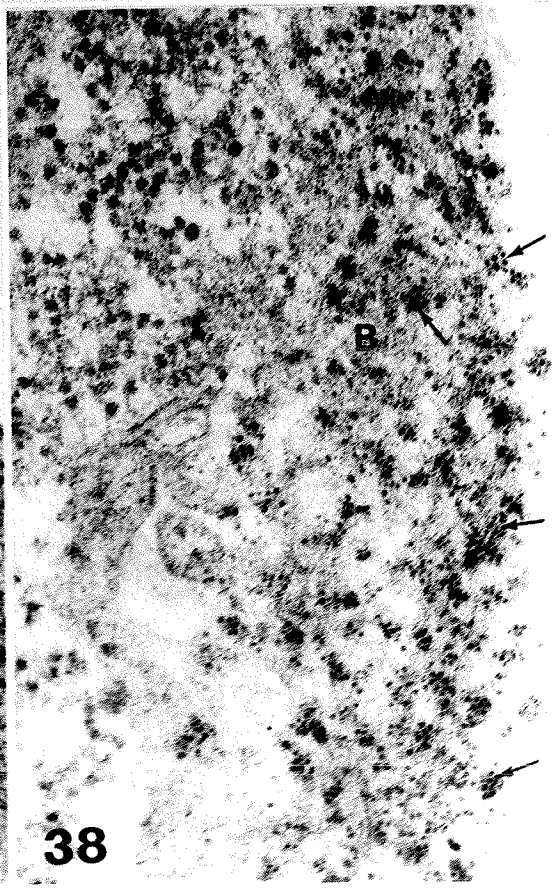

38

Discussion

The distribution of membrane surface charge permits the characterization of membrane heterogeneities on the germ and somatic cells in the Rhodnius ovariole, and may suggest functions for certain morphological features. The germ cell syncytium is bounded by a continuous plasma membrane (Huebner and Anderson, 1972b, 1972c; Huebner, 1981a, 1984a) which has structural differentiation present as microvilli, pinocytotic pits and gap junctions (Huebner and Anderson, 1972b; Huebner and Injeyan, 1981). It is therefore surprising that more surface charge heterogeneity was not observed.

The failure of colloidal iron to show selective binding distributions, indicates that the entire germ cell syncytium surface is negatively charged. This is in contrast to the paucity of cationic ferritin binding. A possible explanation for this discrepency involves the differences in procedure for each tracer. The CI incubating solution has a pH of 1.1-1.3 (Mowry, 1958), therefore the tissue must be prefixed before exposure to the tracer. At this pH the carboxyl groups of membrane glycoproteins are sufficiently dissociated to permit CI staining (DeBruyn et al., 1978), and should also show CF staining at physiological pH. Burry and Wood (1979) demonstrated that glutaraldehyde fixation prior to tracer binding, increases the number of anionic groups on the membrane. Since all ferritin binding experiments preceded fixation, the extensive CI binding may be attributed to the exposure of new anionic sites on the membrane. If this interpretation is correct we must conclude that the germ cell syncytial membrane has few charged sites at physiological pH. Another explanation for the paucity of CF binding, is that during tryptic basal lamina digestion,

protease sensitive anionic sites have been removed. This has been observed in mammalian cells, where glycopeptides and glycosaminoglycans are the primary anionic stes (Chiarugi et al., 1974; Anderson and Hein, 1977; Simionescu et al., 1981). Trypsin insensitive anionic sites have been observed on retinal cells (Jokoi et al., 1982), and in the present study basal lamina remnants still bind CF. Regions of follicle cell contact and the inner sheath cells both bound CF and therefore these sites must be trypsin insensitive.

The concentration of ferritin tracer was intentionally kept low to reduce any osmotic effects on the denuded ovariole. Larger oocytes exhibit some shrinkage during denuding (Watson et al., in preparation) and an attempt was made to minimize this. Anderson and Hein (1977) reported a concentration dependent binding increase of CF to the oviduct ciliary membrane. At low concentrations (0.16 mg/ml) CF bound predominantly on the cilia tips; not unlike CF binding to the oocyte microvilli (Fig. 12). Future experiments with higher CF concentrations may demonstrate greater oocyte binding than observed in this study.

Therefore, there are at least 3 possible explanations for the lack of anionic sites on the germ cell syncytial membrane; (1) Trypsin removal of anionic sites, (2) at physiological pH there are no charged sites on the membrane accessible to the tracers and (3) low tracer concentrations. It is clear that the basal lamina must be removed in order to gain access to the somatic and germ tissues (Figs. 33-36). Mechanical removal is very difficult and often damaging to the underlying cells. Unfortunately, more specific enzymes such as collagenase and elastase do not digest the basal lamina (Watson et al., in preparation). Shorter trypsin digestions, followed by trypsin inhibitors, combined

with these other enzymes and mechanical removal may help solve this problem. It may be necessary to examine the binding characteristics of CF at a range of pH, to allow charged sites with high pK_a values to become dissociated. By using a higher pH and more cationic ferritins, cell surfaces will increase the binding of tracer (Rennke et al., 1975; DeBryun et al., 1978; Brac, 1983; Dermietzel et al., 1983).

CF binding to the dissociated somatic cells does demonstrate heterogeneous charge distributions. Follicle cells bound CF primarily in regions of follicle cell-follicle cell contact and ocasionally between follicle cells and oocyte microvilli, indicating these areas contain anionic sites. This may be related to the location of gap junctions between follicle cells in a patent epithelium, or gap junctions found between the oocyte and follicle cells (Huebner and Injeyan, 1981). CF bound to free surfaces (Fig. 17), may indicate former regions of contact, disrupted during the denuding procedure.

The extensive CF binding between inner sheath cells indicates a regular, often linear arrangement of anionic sites in areas of cell-cell contact. A similar, although more latice-like binding pattern has been found on retinal cell plasma membranes (Jokoi et al., 1982) and macrophages (Ben-Ishay et al., 1975). These authors have attributed this pattern to ligatin, a linear polymeric protein, able to anchor extrinsic membrane proteins. Its presence in areas of cell contact suggests it may play a role in cell recognition or adhesion. There is no evidence for a similar protein in insects.

In Rhodnius there have not been any detailed examinations for the presence of junctional complexes between inner sheath cells, although there is evidence for gap junctions between the inner epithelial cells surrounding the

nurse cell cap in cecropia (Woodruff et al., 1984b). These cells have been implicated in a hypothesis explaining the extracellular electrical current flow around the follicle (Woodruff et al., 1984a; see Chapter 2), which may be applicable to the Rhodnius ovariole, extracellular current pattern (Sigurdson and Huebner, 1984; see Chapter2). It is therefore important to fully characterize the interactions between Rhodnius inner sheath cells. Locke and Huie (1983) have proposed a function for the anionic sites on insect plasma membrane reticular systems, which involves selective passage of proteins based upon charge. The close apposition of anionic sites between inner sheath cells may restrict the passage of negatively charged molecules, thus acting as a charge sieve for proteins or smaller charged species attempting to reach the nurse cells. This would regulate the nurse cell environment to some extent.

In a recent review Ashhurst (1982) distinguishes between the basal lamina found around insect muscle and fat body from thicker nonfibrous layers of connective tissue, on the basis of morphological differences and the lack of information on the composition of these layers. Based upon morphological differences (absence of lamina rara and densa), the Rhodnius ovariole basal lamina falls into this latter category. It is clear the basal lamina contains anionic sites, often in clusters similar to those found in fat body basal lamina (Brac, 1983). CF binding to the basal lamina implies that negatively charged sites may act as a charge sieve for hemolymph proteins (Brac, 1983), which, in the case of Rhodnius, would have free access to the oocyte surface in patent follicles. The greater number of CF molecules binding to the basal lamina from previtellogenic and vitellogenic follicles lends support to this hypothesis. Anionic sites on mammalian glomerular and capillary endothelial basal laminae,

have been shown to affect the movement of charged proteins (Rennke et al., 1975; Simionescu et al., 1982). The basal lamina of the Rhodnius ovariole, although morphologically different, may be functionally similar to basal lamina of conventional structure, in playing a role as a charge dependent permeability barrier.

General Conclusion

The telotrophic ovariole of the hemipteran Rhodnius prolixus has proven to be a very useful model system for the study of oogenesis in insects (see Huebner, 1984b). Although there remains much useful morphological research to be done on this system, a new approach was required before an understanding of the physiological processes taking place during oogenesis could occur. The meroistic ovariole is polarized, both structurally and functionally. This has led to the discoveries by Woodruff and Telfer (1973; Telfer et al., 1981) that this ovariole type can also be electrically polarized. These observations have suggested a mechanism for the intercellular transport of nurse cell products to the oocyte and other charged species which may control the state of differentiation of the germ cells within the syncytium. The use of intracellular electrodes to characterize the electrophysiological features of the ovariole suffers from the disadvantages of cell damage during penetration by the electrodes and an inherent lack of sensitivity to very small electric fields. Therefore the timely development of the vibrating probe has permitted a highly sensitive, non-invasive technique to be applied to insect ovaries. Previous work has demonstrated that tiny steady electric fields exist around meroistic ovarioles, but these studies did not attempt to examine the modulation of these fields during a cycle of oogenesis or the effects of oogenesis controlling hormones. The Rhodnius ovariole is uniquely suited for both of these observations, first because of its highly regulated vitellogenesis cycle and secondly because of the known effects of JH on vitellogenic follicles.

There is a great deal of research to be done in the detailed description of the ovariole's structural asymmetries. The distribution of membrane surface charge and basal lamina charged sites have provided clues to the nature of cell interaction and possible function for the basal lamina acting as a charge-selective permeability barrier.

In this study, the examinations of these aspects of the Rhodnius ovariole have expanded upon the present knowledge concerning oogenesis in insects. It has been shown that steady extracellular electrical currents flow in predictable patterns around the ovariole. The consistency of current efflux from the posterior, anterior and interfollicular connective of the terminal follicle, and current influx over the tropharium throughout oogenesis, suggests the importance of some as yet undefined, electrophysiological process(es). It is not known however, if these electrical currents are simply indicators of vitellogenic stage, representing changes in membrane electrical properties or are the result of mechanisms which are regulating and "driving" oogenesis. As an example of the former case, is the action of JH on follicle cell Na^+-K^+ ATPase resulting in follicle cell volume changes and presumably increased ionic flux across the cell membrane. Evidence for the latter case is more circumstantial. There are no observable structural changes in the interfollicular connective cells and yet extracellular current efflux increases in response to JH. The same can be said for the increases in current influx over the tropharium. The increase in current efflux at the anterior end of the terminal follicle as it enters vitellogenesis and the increase in current efflux at the presumptive T-1 follicle connective as the T follicle finishes vitellogenesis, are both examples of large scale changes in

ovariole physiology. The changes are likely related to intraovariole regulation, but how this regulation takes place is not known.

The electrophoretic transport of membrane bound and cytoplasmic proteins may be one of the primary effects of electrically polarized tissues. Electrophoresis of membrane electrogenic pumps to common domains will tend to increase the electrical polarity within a cell. If applied on a large scale this process could result in polarized areas within tissues. This may be the case in polytrophic and telotrophic ovarioles, where differentially located electrogenic pumps could produce the observed potential differences between the oocyte and nurse cells.

Steady electric currents flowing through a tissue may result in the redistribution of the ionic species which carry the current. Nothing is known about the ionic composition of the extracellular currents surrounding insect ovarioles. In other systems calcium often plays an important role in regulation of the current, even if it is not the primary current species (Robinson and Jaffe, 1975; Nuccitelli et al., 1977; Jaffe, 1981; Kline et al., 1983). The wide-ranging affects of intracellular calcium could produce profound changes in cell physiology if its tissue distribution is altered.

How the electrophysiological properties of the ovariole relate to the surface charge distribution is unknown. The extensive number of anionic sites located within the intercellular space between inner sheath cells may function in cell adhesion or perhaps as a charge barrier to anionic species, preventing access to the nurse cells.

Clearly, there are many questions to be answered. Of immediate interest is the elucidation of the stage specific response to juvenile hormone and its

analogues and inhibitors, the determination of the ionic composition of the extracellular current, the location of the electrogenic pumps and conductance pathways which produce the electrophysiological polarity and a resolution of the variable current properties observed in the previtellogenic region.

Finally, it may be possible to synthesize this information into an understanding of the role of bioelectricity in developing systems such as the telotrophic ovariole.

References

Abu-Hakima, R. and Davey, K.G., 1977. The action of juvenile hormone on the follicle cells of Rhodnius prolixus: The importance of volume changes. J. exp. Biol. 69: 33-44.

Abu-Hakima, R. and Davey, K.G., 1979. A possible relationship between ouabain sensitive (Na^+-K^+) dependent ATPase and the effect of juvenile hormone on the follicle cells of Rhodnius prolixus. Insect. Biochem. 9: 195-198.

Anderson, R.G. and Hein, C.E., 1977. Distribution of anionic sites on the oviduct cilliary membrane. J. Cell Biol. 72: 482-492.

Ashhurst, D.E., 1982. The structure and development of insect connective tissues. In Insect Ultrastructure R.C. King and H. Akai (Eds.) Plenum Press. New York pgs. 313-350.

Bearer, E.L. and Friend, D.S., 1981. Domains in the guinea pig sperm membrane. J. Cell Biol. 91: 266a.

Ben-Ishay, Z., Reichert, F. and Gallily, R., 1975. Crystalline-like surface charge array of murine macrophages and lymphocytes: visualization with cationized ferritin. J. Ultrastruct. Res. 53: 119-127.

Berridge, M.J., Lindley, B.D. and Prince, W.T., 1975. Membrane permeability changes during stimulation of isolated salivary glands of Calliphora by 5-hydroxytryptamine. J. Physiol. 244: 549-567.

Betz, W.J., Caldwell, J.H., Ribchester, R.R., Robinson, K.R. and Stump, R.F., 1980. Endogenous electric fields around muscle fibers depends on the Na^+-K^+ pump. Nature. 287: 235-237.

Bier, K., 1963. Synthese, interzelluläre transport, und abbau von ribonukleinsäure im ovar der stubenfliege Musca domestica. J. Cell BIol. 16: 436-440.

Bohrmann, J., Heinrich, U.R., Dorn, A., Sander, K and Gutzeit, H., 1984. Electrical phenomena and their possible significance in vitellogenic follicles of Drosophila melanogaster. In Proceedings of the European Developmental Biology Congress. In press.

Borgens, R.B., Jaffe, L.F. and Cohen, M.J., 1980. Large and persistant electrical currents enter the transsected lamprey spinal cord. Proc. Natl. Acad. Sci. USA. 77: 1209-1213.

Borgens, R.B., Rouleau, M.F. and DeLanney, L.E., 1983. A steady efflux of ionic current predicts hind limb development in the Axolotl. J. Exp. Zool. 228: 494-503.

Borgens, R.B., Vanable, J.W. and Jaffe, L.F., 1977. Bioelectricity and regeneration: Large currents leave the stumps of regenerating newt limbs. Proc. Natl. Acad. Sci. USA. 74: 4528-4532.

Borgens, R.B., Vanable, Jr. J.W. and Jaffe, L.F., 1979. Bioelectricity and regeneration. Bioscience. 29: 468-474.

Brac, T., 1983. Charged sieving by the basal lamina and the distribution of anionic sites of the external surfaces of fat body cells. Tissue and Cell. 15: 489-498.

Brower, D.L. and Gidding, T.H., 1980. The effects of applied electric fields on Microsterias II. The distribution of cytoplasmic and plasma membrane components. J. Cell Sci. 42: 279-290.

Bünning, J., 1978. Development of telotrophic-meroistic ovarioles of polyphage beetles with special reference to the formation of nutritive cords. J. Morph. 156: 237-256.

Bünning, J., 1979a. The trophic cords of telotrophic ovarioles in polyphage coleoptera. Zoomorphologie. 93: 33-50.

Bünning, J., 1979b. The telotrophic-meroistic ovary of megaloptera. I. The ontogenetic development. J. Morph. 162: 37-66.

Bünning, J., 1984. Differences in RNA synthesis between polytrophic and telotrophic meroistic ovaries: Do they exist? In Advances in Invertebrate Reproduction, Vol. 3, W. Engels (Ed.) Elsevier North Holland and Biomedical Publishers. Amsterdam pgs. 565.

Burgos, M.H. and Fawcett, D.W., 1955. Studies on the fine structure of the mammalian testis. I. Differentiation of the spermatids in the cat (Felis domestica). J. Biophys. and Biochem. Cyto. 1: 287-301.

Burry, R.W. and Wood, J.G., 1979. Contributions of lipids and proteins to the surface charge of membranes: An electron microscopy study with cationized and anionized ferritin. J. Cell Biol. 82: 726-741.

Capco, D. and Jeffrey, W., 1979. Origin and spatial distribution of maternal messenger RNA during oogenesis of an insect, Oncopeltus fasciatus. J. Cell Sci. 39: 63-76.

Chiarugi, V.P., Vannucchi, S. and Urbano, P., 1974. Exposure of trypsin-removable sulfated polyanions on the surface of normal and virally transformed $BHK^{21/C13}$ cells. Biochim. Biophys. Acta. 345: 283-293.

Danon, D., Goldstein, L. Marikovsky, Y. and Skutelsky, E., 1972. Use of cationized ferritin as a label of negative charge on cell surfaces. J. Ultrastruct. Res. 38: 500-510.

Davenport, R., 1974. Synthesis and intercellular transport of ribosomal RNA in the ovary of the milkweed bug Oncopeltus fasciatus. J. Insect Physiol. 20: 1949-1956.

Davenport, R., 1976. Transport of ribosomal RNA into the oocytes of the milkweed bug, Oncopeltus fasciatus. J. Insect Physiol. 22: 925-926.

Davey, K.G., 1981. Hormonal control of vitellogenesis uptake in Rhodnius prolixus Stal. Amer. Zool. 21: 701-705.

Davey, K.G. and Huebner, E., 1974. The response of the follicle cells of Rhodnius prolixus to juvenile hormone and antigonadotropin in vitro. Can. J. Zool. 52: 1407-1412.

DeBruyn, P.P.H., Michelson, S. and Becker, R.P., 1978. Nonrandom distribution of sialic acid over the cell surface of bristle-coated endocytic vesicles of the sinusoidal endothelium cells. J. Cell Biol. 78: 379-389.

DeLoof, A., 1983. The meroistic insect ovary as a miniature electrophoresis chamber. Comp. Biochem. Physiol. 74: 3-9.

DeLoof, A., Briers, T., Huybrechts, R., Ollevier, F., Peferoen, M. Stoppie, P. and Stynen, D., 1982. Hormones, ions pumps and control of gene expression. The cell as a miniature electrophoresis chamber? Annls. Soc. r. zool. Belg. 112: 3-22.

Dermietzel, R. Thürauf, N. and Kalweit, P., 1983. Surface charges associatd with fenestrated brain capillaries. II. In vivo studies on the role of molecular charge in endothelial permeability. J. Ultrastruct. Res. 84: 111-119.

Dittmann, F., Ehni, R. and Engels, W., 1981. Bioelectric aspects of the hemipteran telotrophic ovariole (Dysdercus intermedius). Wilhelm Roux's Archives. 190: 221-225.

Dorn, A. and Weisinseel, M.H., 1982. Advances in vibrating probe techniques. Protoplasma. 113: 89-96.

Engelmann, F., 1979. Insect vitellogenin: Identification, biosynthesis and role in vitellogenesis. In Advances in Insect Physiology, Vol. 14, J.E. Treherne, M.J. Berridge and V.B. Wigglesworth, (Eds.) Academic Press. New York. pgs. 49-108.

Erickson, C.A. and Nuccitelli, R., 1984. Embryonic fibroblast motility and orientation can be influenced by physiological electric fields. J. Cell Biol. 98: 296-307.

Farmer, J., Maddrell, S.H.P. and Spring, J.H., 1981. Absorption of fluid by the midgut of Rhodnius. J. exp. Biol. 94: 301-316.

Fawcett, D.W., Ito, S. and Slautterback, D., 1959. The occurrence of intercellular bridges in groups of cells exhibiting synchronous differentiation. J. Biophys. and Biochem. Cyto. 5: 453-460.

Foskett, J.K. and Scheffy, C., 1981. The chloride cell: Definitive identification as the salt-secretory cell in teleosts. Science, 215: 164-166.

Franchi, L.L. and Mandl, A.M., 1962. The ultrastructure of oogonia and oocytes in the foetal and neonatal rat. Proc. Roy. Soc. B. 157: 99-114.

Gasic, G.J., Berwick, L. and Sorrentino, M., 1968. Positive and negative colloidal iron as cell surface electron stains. Lab. Invest. 18: 63-71.

Grinnel, F., Tobleman, M.Q. and Hackenbrack, C.R., 1975. The distribution and mobility of anionic sites on the surfaces of baby hamster kidney cells. J. Cell Biol. 66: 470-479.

Huebner, E., 1981a. Nurse cell-oocyte interaction in the telotrophic ovarioles of an insect, Rhodnius prolixus. Tissue and Cell. 13: 105-125.

Huebner, E., 1981b. Oocyte-follicle cell interaction during normal oogenesis and atresia in an insect. J. Ultrastruct. Res. 74: 95-103.

Huebner, E., 1982. Ulrastructure and development of the telotrophic ovary. In The Ultrastructure and Functioning of Insect Cells, H. Akai, R.C. King and S. Morohoshi (Eds.) Soc. for Insect Cells. Japan. pgs. 9-12.

Huebner, E., 1983. Oostatic hormone-antigonadotropin and reproduction. In Endocrinology of Insects, R.G.H. Downer and H. Laufer. (Eds.) Alan R. Liss. New York. pgs. 319-329.

Huebner, E., 1984a. Developmental cell interactions in female reproductive organs. In Advances in Invertebrate Reprodution, Vol. 3, W. Engels. (Ed.) Elsevier North Holland and Biomedical Publishers. Amsterdam pgs. 97-105.

Huebner, E., 1984b. The ultrastructure and development of the telotrophic ovary. In Insect Ultrastructure, Vol. 2, R.C. King and H. Akai (Eds.) Plenum Press. New York. pgs. 3-48.

Huebner, E. and Anderson, E., 1970. The effects of vinblastine sulfate on the ovary fo Rhodnius prolixus. J. Cell Biol. 46: 191-198.

Huebner, E. and Anderson, E., 1972a. A cytological study of the ovary of Rhodnius prolixus. I. The ontogeny of the follicular epithilium. J. Morph. 136: 459-494.

Huebner, E. and Anderson, E., 1972b. A cytological study of the ovary of Rhodnius prolixus. II. Oocyte defferentiation. J. Morph. 137: 385-416.

Huebner, E. and Anderson, E., 1972c. A cytological study of the ovary of Rhodnius prolixus. III. Cytoarchitecture and development of the trophic chamber. J. Morph. 138: 1-40.

Huebner, E, and Davey, K.G., 1973. An antigonadotropin from the ovaries of the insect Rhodnius prolixus Stal. Can. J. Zool. 51: 113-120..

Huebner, E. and Injeyan, H., 1980. Patency of the follicular epithelium in Rhodnius prolixus: A rexamination of the hormone response and technique refinement. Can. J. Zool. 58: 1617-1625.

Huebner, E. and Injeyan. H., 1981. Follicular modulation during oocyte development in an insect: Formation and modification of septate and gap junctions. Dev. Biol. 83: 101-113.

Huebner, E. and Sigurdson, W.J., 1984. Comparative aspects of extracellular current in insect ovaries. Abstract accepted by J. Cell Biol.

Huebner, E., Tobe, S.S. and Davey, K.G., 1975. Structural and functional dynamics of oogenesis in Glossina austeni: General features, previtellogenesis and nurse cells. Tissue and Cell. 7: 297-317.

Hyams, J.S. and Stebbings, H., 1977. The distribution and function of microtubules in nutritive tubes. Tissue and Cell. 9: 537-545.

Hyams, J.S. and Stebbings, H., 1979a. The formation and breakdown of nutritive tubes: massive microtubular organelles associated with cytoplasmic transport. J. Ultrastruct. Res. 68: 46-57.

Hyams, J.S. and Stebbings, H., 1979b. The mechanism of microtubule associated cytoplasmic transport. Cell Tissue Res. 196: 103-116.

Ilenchuk, T.T. and Davey, K.G., 1982. Some properties of Na^+-K^+ ATPase in the follicle cells of Rhodnius prolixus. Insect. Biochem. 12: 675-679.

Ilenchuk, T.T. and Davey, K.G., 1983. Juvenile hormone increases ouabain-binding capacity of microsomal preparations from vitellogenic follicles cells. Can. J. Biochem. Cell Biol. 61: 826-831.

Jaffe, L.F., 1966. Electrical currents through the developing Fucus egg. Proc. Natl. Acad. Sci. USA. 56: 1102-1109.

Jaffe, L.F., 1977. Electrophoresis along cell membranes. Nature. 256: 600-602.

Jaffe, L.F., 1981. The role of ionic currents in establishing developmental pattern. Phil. Trans. R. Soc. Lond. B. 295: 553-566.

Jaffe, L.F. and Nuccitelli, R., 1974. An ultrasensitive vibrating probe for measuring steady extracellular currents. J. Cell Biol. 63: 614-628.

Jaffe, L.F. and Nuccitelli, R., 1977. Electrical controls of development. Ann. Rev. Biophys. and Bioeng. 6: 445-476.

Jaffe, L.F. and Stern, C.D., 1979. Strong electrical currents leave the primitive streak of chick embryos. Science. 206: 569-571.

Jaffe, L.F. and Woodruff, R.I., 1979. Large electrical currents traverse developing cecropia follicles. Proc. Natl. Acad. Sci. USA. 76: 1328-1332.

Jakoi, E.R., Marchase, R.B. and Reedy, M.C., 1982. Distribution of anionic sites on surfaces of retinal cells: A study using cationized ferritin. J. Ultrastruct. Res. 76: 96-106.

King, R.C. and Aggarwal, S.K., 1965. Oogenesis in Hyalophora cecropia. Growth. 29: 17-83.

Kinosita, H., 1963. Electrophoretic theory of pigment migration within fish melanophores. Ann. N.Y. Acad. Sci. 100: 992-1004.

Kline, D., Robinson, K.R. and Nuccitelli, R., 1983. Ion currents and membrane domains in the cleaving Xenopus egg. J. Cell Biol. 97: 1753-1761.

Koch, E.A. and King, R.C., 1966. The origin and early differentiation of the egg chamber of Drosophila melanogaster. J. Morph. 119: 283-304.

Kropf

Lane, N.J., 1982. Insect intercellular junctions: Their structure and development. In Insect Ultrastructure, R.C. King and H. Akai. (Eds.) Plenum Press. New York. pgs. 402-433.

Locke, M. and Huie, P., 1983. A function for plasma membrane reticular systems. Tissue and Cell. 15: 885-902.

Lund, E.J., 1923. Electrical control of organic polarity in th egg of Fucus. Bot. Gaz. 76: 288-301.

Luther, P.W, Peng, H.B. and Lin, J.J-c., 1983. Changes in cell shape and actin distribution induced by constant electric fields. Nature. 305: 61-64.

Lutz, D. and Huebner, E., 1980. Development and cellular differentiation of an insect telotrophic ovary (Rhodnius prolixus). Tissue and Cell. 12: 773-794.

Lutz, D. and Huebner, E., 1981. Development of nurse cell-oocyte interactions in the insect telotrophic ovary (Rhodnius prolixus). Tissue and Cell. 13: 321-335.

Maddrell, S.H.P., 1969. Secretion by the malpighian tubules of Rhodnius. The movement of ions and water. J. exp. Biol. 57: 71-98.

Mendenhall, W., 1975. Introduction to Probability and Statistics. Duxbury Press. Mass. 460 pgs.

McLaughlin, S. and Poo, M-m., 1981. The role of electro-osmosis in the electric field-induced movement of charged macromolecules on the surfaces of cells. Biophys. J. 34: 85-93.

Mowry, R.W., 1958. Improved procedure for the staining of acidic polysaccharides by Müller's colloidal (hydrous) ferric oxide and its combination with the Feulgen and

Pollack, S.B. and Telfer, W.H., 1969. RNA in cecropia moth ovaries: Sites of synthesis, transport and storage. J. exp. Zool. 170: 1-24.

Poo, M-m., 1981. In situ electrophoresis of membrane components. Ann. Rev. Biophys. Bioeng. 10: 245-276.

Poo, M-m. and Robinson, K.R., 1977. Electrophoresis of concanavalin A receptors along embryonic muscle cell membrane. Nature. 265: 602-605.

Pratt, G.E and Davey, K.G., 1972a. The corpus allatum and oogenesis in Rhodnius prolixus (Stal). I. The effects of allatectomy. J. exp. Biol. 56: 201-214.

Pratt. G.E. and Davey, K.G., 1972b. The corpus allatum and oogenesis in Rhodnius prolixus (Stal). II. The effects of starvation. J. exp. Biol. 56: 215-221.

Pratt, G.E. and Davey, K.G., 1972c. The corpus allatum and oogenesis in Rhodnius prolixus (Stal). III. The effect of mating. J. exp. Biol. 56: 223-237.

Regis, L., 1979. The role of the blood meal in egg-laying periodicity and fecundity in Triatoma infestans. Int. J. Invert. Reprod. 1: 187-195.

Rennke, H.G., Cotran, R.S. and Venkatachalsm, M.A., 1975. Role of molecular charge in glomerular permeability: Tracer studies with cationized ferritins. J. Cell Biol. 67: 638-646.

Robinson, K.R., 1979. Electrical currents through full-grown and maturing Xenopus oocytes. Proc. Natl. Acad. Sci. USA. 76: 837-841.

Robinson, K.R. and Jaffe, L.F., 1975. Polarizing fucoid eggs drive a calcium current through themselves. Science. 187: 70-72.

Rodan, G.A., Bourret, L.A. and Norton, L.A., 1978. DNA synthesis in cartilage cells is stimulated by oscillating electric fields. Science. 199: 690-692.

Rose, B., 1980. Introduction to techniques in Davey, K.G., 1979. The effect of C18 juveni Altosid on the efficiency of egg producton in Rhodnius prolixus. Iness. Toronto. pgs. 1

Ryan, T.A., 1959. Multiple comparisons in psychological research. Psychological Bulletin. 56: 26-47.

Scheffy, C., Foskett, J.K. and Machin, T.E., 1983. Localization of ionic pathways in the teleost opercular membrane by extracellular recording with a vibrating probe. J. Membrane Biol. 75: 193-203.

Sigurdson, W.J. and Huebner, E., 1984. Extracellular currents during oogenesis in an insect. Abstract accepted by the J. Cell Biol.

Simionescu, N., Simionescu, M. and Palade, G., 1981. Differentiated microdomains on the luminal surface of the capillary endothelium. I. Preferential distribution of anionic sites. J. Cell Biol. 90: 605-613.

Simionescu, M., Simionescu, N. and Palade, G.E., 1982. Preferential distribution of anionic sites on the basement membrane and abluminal aspect of the endothelium in fenestrated capillaries. J. Cell Biol. 95: 425-434.

Singer, S.J. and Nicolson, G., 1972. The fluid mosaic model of the structure of cell membranes. Science. 175: 720-731.

Slayman, C.L. and Slayman, C.W., 1962. Measurement of membrane potentials in Neurospora. Science. 136: 876-877.

Stump, R.F., Robinson, K.R., Harold, R.L. and Harold, F.M., 1980. Endogenous electrical currents in the water mold Blastocladiella emersonii during growth and sporulation. Proc. Natl. Acad. Sci. USA. 77: 6673-6677.

Telfer, W.H., 1975. Development and physiology of the oocyte-nurse cell syncytium. In Advances in Insect Physiology, Vol. 11, J.E. Treherne, M.J. Berridge and V.B. Wigglesworth. (Eds.) Academic Press. New York. pgs. 223-319.

Telfer, W.H., Huebner, E. and Smith, D.S., 1982. The cell biology of vitellogenic follicles in Hyalopohora and Rhodnius. In Insect Ultrastructure, Vol. 1, R.C. King and H. Akai. (Eds.) Plenum Press. New York. pgs. 118-149.

Telfer, W.H., Woodruff, R.I. and Huebner, E., 1981. Electrical polarity and cellular differentiation in meroistic ovaries. Am. Zool. 21: 675-686.

Thürauf, N., Dermietzel, R. and Kalweit, P., 1983. Surface charges associated with fenetrasted brain capillaries. I. In vitro labelling of anionic sites. J. Ultrastruct. Res. 84: 103-110.

Vanderburg, J.P., 1963. Synthesis and transfer of DNA, RNA and proteins during vitellogenesis in Rhodnius prolixus (Hemiptera). Biol. Bull. 125: 556-575.

Waller, R.A. and Duncan, D.B., 1969. A Bayes rule for the symmetric multiple comparisons problem. J. Am. Statistical Association. 64: 1484-1503.

Weisinseel, M.H., Dorn, A. and Jaffe, L.F., 1979. Natural H^+ cuttents traverse growing roots and root hairs of barley (Hordeum vulgare). Plant Physiol. 64: 512-518.

Weisinseel, M.H., Nucciteeli, R. and Jaffe, L.F., 1975. Large electrical currents traverse growing pollen tubes. J. Cell Biol. 66: 556-567

Weinstein, S.P., Kostellow, A.B., Ziegler,D.H. and Morril, G.A., 1982. Progesterone-induced down-regulation of an electrogenic Na^+-K^+ ATPase during the first meiotic division in amphibian oocytes. J. Membrane Biol. 69: 41-48.

Woodruff, R.I. and Telfer, W.H., 1973. Polarized intercellular bridges in ovarian follicles of the ececropia moth. J. Cell Biol. 58: 172-188.

Woodruff, R.I. and Telfer, W.H., 1974. Electrical properties of ovarian cells linked by intercellular bridges. Ann. N.Y. Acad. Sci. 238: 408-419.

Woodruff, R.I. and Telfer, W.H., 1980. Electrophoresis of proteins in intercellular bridges. Nature. 286: 84-86.

Woodruff, R.I., Huebner, E. and Telfer, W.H., 1984a. The origin of electrical currents in insect ovaioles, Abstract. In Advances in Invertebrate Reproduction, Vol. 3, W.Engels. (Ed.) Elsevier North Holland and Biomedical Publishers. Amsterdam. pg. 562.

Woodruff, R.I., Huebner, E. and Telfer, W.H., submitted to Dev. Biol. 1984.

Zamboni, L. and Gondos, B., 1967. Intercellular bridges and synchronization of germ cell differentiation during oogenesis in the rabbit. J. Cell Biol. 36: 276-282.

Zinsmeister, P.P. and Davenport, R., 1971. An autoradiographic and cytochemical study of cellular interactions during oogenesis in the milkweed bug, Oncopeltus fasciatus. Exp. Cell Res. 67: 273-278.

Appendix 1

The Vibrating Probe

Principles of Operation

The principle of operation is based upon the reduction of electrode noise to the theoretical minimum, the Johnson noise, by using a low access resistance platinum electrode which is vibrated within the electric field at a frequency which reduces the impedance at the saline-platinum interface to extremely small values (Jaffe and Nuccitelli, 1974). This allows the electrode to detect nV electric fields in highly conductive physiological salines. The entire probe assembly (Fig. 6; see Jaffe and Nuccitelli, 1974) is vibrated at 320 to 450 Hz by a piezoelectric reed causing the probe tip (Pt ball) to oscillate between two points in a horizontal plane. The presence of an electric field will be converted by the probe tip into a sinusoidal output, whose peak to peak amplitude is equal to the potential difference between the extremes of vibration (Jaffe and Nuccitelli, 1974). This AC signal is amplified by a lock-in amplifier tuned to the vibration frequency, thus filtering out noise at all other frequencies. The AC signal is converted to DC and is used to drive a chart recorder. This method overcomes the disadvantages of high noise levels due to high resistance and sensitivity to gradients in medium composition found in conventional static microelectrodes. The mixing action of the probe tip (see Jaffe and Nuccitelli, 1974) makes the probe insensitive to gradients in composition of the saline.

Equipment Set-Up

The general layout of the vibrating probe equipment is shown in Fig. 1. The room requirements are minimal, consisting of a plastic enclosure which prevents air currents from disturbing the probe-saline interface. Ideally, the equipment could be placed in a controlled environment room. The modified Leitz inverted microscope (IM) and micromanipulator (Line Tool Co., Allentown, PA) assembly (M) are bolted to a 200 kg steel plate, which rests on a partially inflated motorcycle inner tube. This arrangement provides an excellent and inexpensive vibration free table (VT, Fig. 1).

The sensing tip of the probe can be seen in typical measuring positions in Figs. 2 and 3. The probe electrode is secured and positioned by its insertion into a plastic block, the meniscus setter (MS) which is waxed to the distal end of the piezoelectric reed (PR, Figs. 4, 5 and 6). The piezoelectric reed is kept dry with a gentle stream of dried, filtered air (20 cm^3/min), via an air line connected to an air guide (Fig. 4). The probe electrode is connected to the lock-in amp (LA, Fig. 1) by a coaxial signal cable (S, Figs. 5 and 6). The probe assembly is positioned with a non-rotating XYZ micromanipulator (M) which means the specimen must be rotated and free to move along any X-Y axis. This is accomplished with a simple 1 cm thick plexiglass gliding stage (ST) greased (Dow Corning silicone grease) to the fixed stage of the inverted microscope (Fig. 4). Specimen chambers are constructed from 1 mm thick plexiglass rings cemented to #1 coverslip bottoms and are positioned as seen in Fig. 5.

Probe Calibration and Use

The phase of the probe AC signal must be matched to the vibration frequency phase in order to produce the maximum signal. The reference signal phase from the vibrator power supply (VP, Fig. 1; #5, Fig. 10) is compared to the phase of the probe output by passing a known current (of known polarity) through a saline filled calibration chamber. The phase angle control on the lock-in amp is first adjusted to produce the maximum signal and then switched 180° to produce the desired chart deflection for a given polarity. Typically in our set-up, positive current moving from the top of the microscope field down (the inverted microscope produces a non-inverted image) produces a deflection to the right on the chart recorder.

In use the probe tip is brought near the surface of the tissue under study (Figs. 2 and 3) and then moved to a reference position several hundred μM from the specimen, to provide a baseline reading (Fig. 11). The specimen should not touch the vibrating tip since the tissue may be damaged. The Rhodnius ovariole's basal lamina is very resilient and accidental contact with the vibrating tip did not affect either the tissue or current measurement. Preliminary experiments using denuded ovarioles (see Chapter 4) proved that plasma membranes can easily be disrupted by the probe if touched.

Given the medium resistivity and vibration amplitude, the small voltage changes (typically nano-volts) can be converted to current values (typically tenth's of a $\mu A/cM^2$) using formula 1,

$$I = \frac{2.83V}{pL} \qquad (1)$$

where I=current in $\mu A/cM^2$, $V=10^{-9}$ volts, p=resistivity in Ω-cm, L=vibration amplitude in 10^{-3} cm and 2.83 converts RMS output to peak output. This allows comparisons between systems independent of medium resistivities. The probe can determine the direction of current flow. Measurements made perpendicular to the cell surface will indicate current entry or exit, while parallel measurements provide tangential current directions. By convention, all current measured is considered to be positive.

Probe Electrode Description and Fabrication

The probe consists of a short tapered glass micropipette which has a 30 μM platinum black ball fixed to the tip (1, see Fig. 9). The ball is connected to an internal low resisitance connector (3 and 4) to which the internal conductor of coaxial cable (8) is attached. The gold coated glass exterior (5) provides the connection between the platinum black reference electrode (2) and the external conductor (9) of the signal cable. The reference electrode is separated from the platinum ball by the uncoated shaft of the micropipette.

The glass shell used to form the electrode is a modified version of the original published description (Jaffe and Nuccitelli, 1974). Short tapered pipettes (3.5 mm shoulder to tip) were pulled from 0.86 mm ID X 1.31 mm OD pyrex glass stock. The closed tip diameter can range from 1-5 μM, and has an off axis wobble of less than 0.15 mm. Using a specially constructed mask, shells were coated in gold vapour at 10^{-6} Torr for 10-15 minutes and then examined for

completeness and the extent of gold-coating towards the tip. Shells were discarded if the coating was less than 1.5-2.0 mm from the tip.

The 0.5 mm wide epoxy stop ring (24 hour epoxy)(6, Fig.9) and the 1.0 mm wide conductive silver epoxy (ACME Chemicals and Insulation, New Haven, Conn.) ring (7. Fig. 9) were applied after gold-coating. Completed shells were stored until required for the final stages of fabrication.

The shell is firmly clamped in the stage clamp (Vibrating Probe Company, Davis, CA) as seen in Fig. 8. The shell tip is broken open to a diameter of 5 μM by touching the tip to a piece of coverslip resting on the heating filament and empty cuvette attached to the micromanipulator (Figs. 7 and 8). The tip's own reflection will be seen approaching the tip as the coverslip is raised, and while touching, a gentle tap on the micromanipulator causes the tip to break squarely. A 2.5-3.0 mm long piece of Cerrotru (Cero Corp. New York) solder is inserted into the shell, followed by a #24 Twistcon socket (Vibrating Probe Company, Davis, CA). A nichrome loop (HF, Fig. 8) is raised concentrically to the shell, about 0.5-1.0 mm above the tip. A teflon coated syringe needle (Fig. 8) is then used to push the socket into the shell to a depth of 1.0 mm as the solder is melted by the heating filament. The solder should exit from the tip and form a 0.2-0.3 mm ball which is often connected by a neck of solder from the tip. The solder bead is placed in a 0.2% AuKCN plating solution at 1.5 V, and the coax cable (from the probe maker; PM, Fig. 7) connected to the shell. The solder bead is knocked off and gold plating starts immediately on the fresh solder break at the tip. Plating should start at 5 nA current and continue until a 10 μM bead has formed. The tip is withdrawn from the plating solution with the current on and then (with the current off) placed into the platinizing solution

(1% chloroplantinic acid plus 0.01% lead acetate). The voltage on the probe maker is set to maximum, the current to minimum, and then turned on. The current is slowly raised until 0.14-0.16 μA and allowed to plate for 2 minutes. The voltage should be about 0.7 V. For a 30 μM tip, after the initial 2 minutes, the voltage is raised 0.1 V and plating allowed to continue for another 2 minutes. Usually this is repeated for another 2 minutes to obtain the correct tip diameter. Smaller tips require fewer voltage increases. A final 10 second plating at an additional 0.1 V will improve probe performance. The probe is then immersed until the shoulder of the shell enters the solution and the reference electrode is plated at 0.3 mA for 7 minutes. The probe is then washed in distilled water, placed in 60 mM NaCl and checked for noise using the lock-in amp at its maximum sensitivity. On a good day approximately a third of the shells can be made into working electrodes. These can be stored indefinitely.

Appendix 1 Plate Abbreviations

Inverted Microscope	IM
Vibrating Power Source	VP
Lock-in Amplifier	LA
Calibrator Power Source	CS
Chart Recorder	R
Vibration Free Table	VT
Probe Electrode	P
Piezoelectric Reed	PR
Micromanipulator Holder	MH
Signal Cable	S
Meniscus Setter	MS
Air Line	A
Microscope Stage	ST
Petri Dish	PD
Stage Clamp	SC
Heating Filament	HF
Plating Solution	PS
Probe Maker	PM

NOTICE/AVIS

PAGE(S) Figures 1-8 IS/ARE EST/SONT black and white photos.

PLEASE WRITE TO THE AUTHOR FOR INFORMATION, OR CONSULT THE ARCHIVAL COPY HELD IN THE DEPARTMENT OF ARCHIVES AND SPECIAL COLLECTIONS, ELIZABETH DAFOE LIBRARY, UNIVERSITY OF MANITOBA, WINNIPEG, MANITOBA, CANADA, R3T 2N2.

VEUILLEZ ECRIRE A L'AUTEUR POUR LES RENSEIGNEMENTS OU VEUILLEZ CONSULTER L'EXEMPLAIRE DONT POSSEDE LE DEPARTEMENT DES ARCHIVES ET DES COLLECTIONS SPECIALES, BIBLIOTHEQUE ELIZABETH DAFOE, UNIVERSITE DU MANITOBA, WINNIPEG, MANITOBA, CANADA, R3T 2N2.

Figure 1. The general layout of vibrating probe equipment, consisting of the inverted microscope (IM) and the micromanipulator-probe assembly (M, P) which are attached to the vibration free table (VT). The lock-in amp (LA), vibrator power source (VP) and calibration power source (CS) are conveniently located within easy reach.

Figures 2 and 3. The probe electrode in typical measuring positions around the Rhodnius ovariole.

Figure 2. The probe measuring extracellular current at the base of the tropharium, P7.

Figure 3. Here the probe is measuring current at the interfollicular connective, P3.

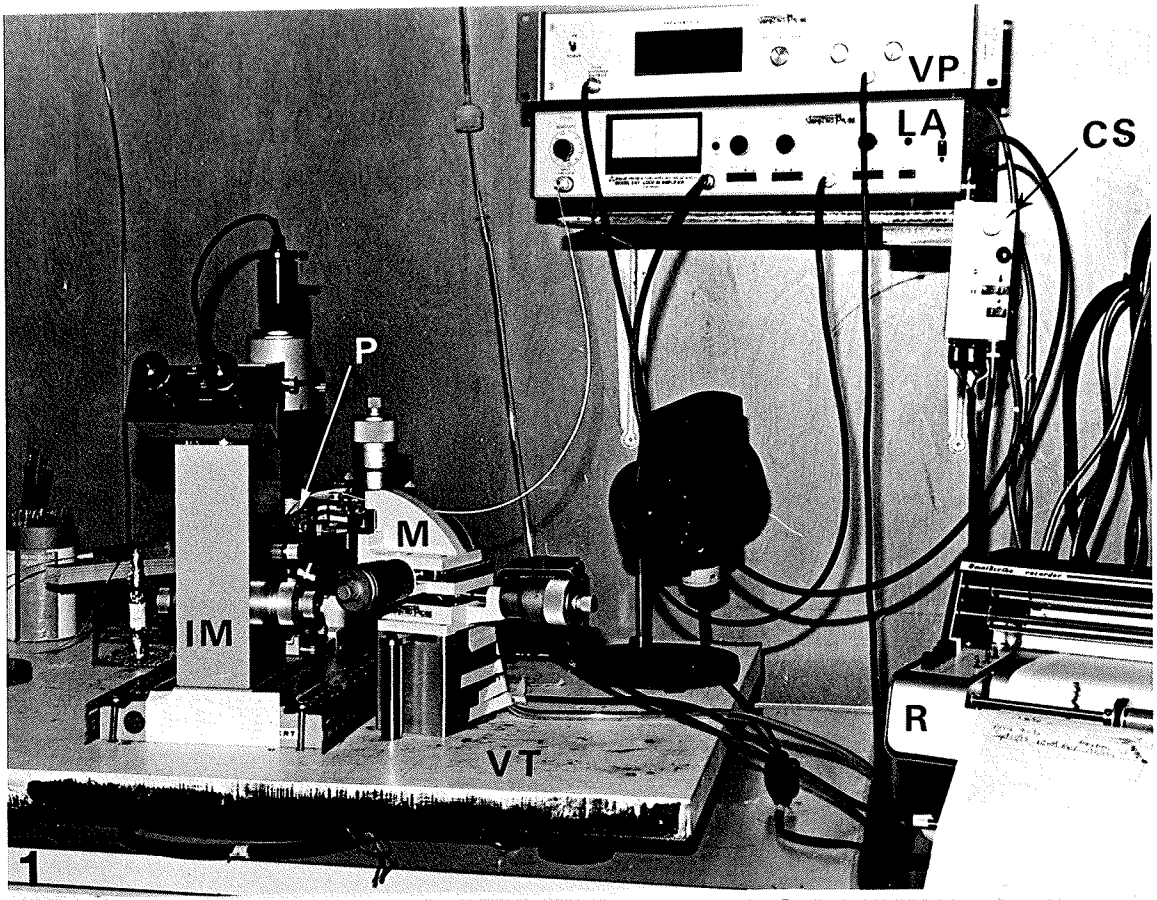
VP
LA
CS
P
M
IM
R
VT
1

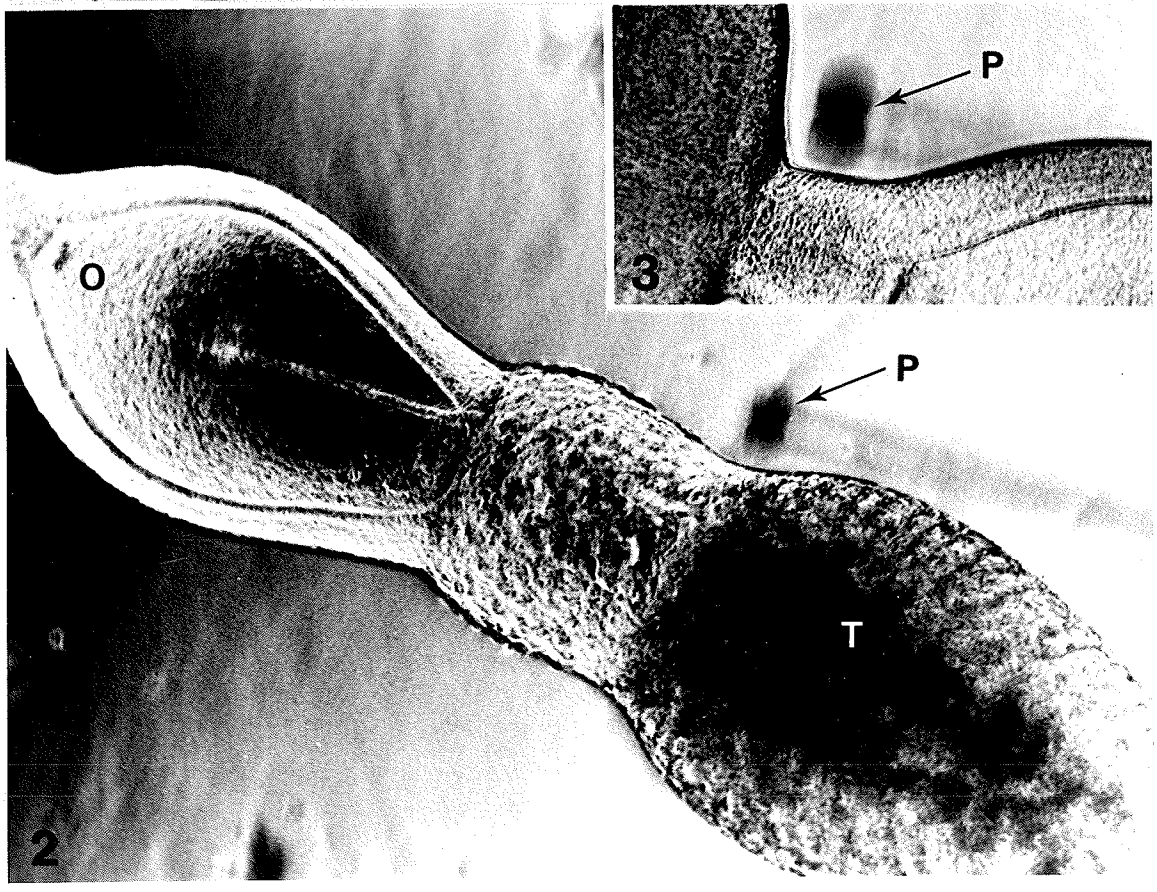
O
P
T
2

P
3

Figures 4, 5 and 6. The probe electrode and piezoelectric reed assembly.

Figure 4. The probe electrode (P) and reed are held by a stainless steel tube attached to the micromanipulator holder (MH). The air line (A) and signal cable can then be attached or clamped securely without interfering with the probe.

Figure 5. The probe seen with a petri dish (PD) in position on the gliding stage (ST).

Figure 6. The probe is inserted into the meniscus setter (MS) which is waxed to the piezoelectric reed (PR). The signal cable is bent and clamped in a position which does not produce any lateral strain when attached to the probe electrode.

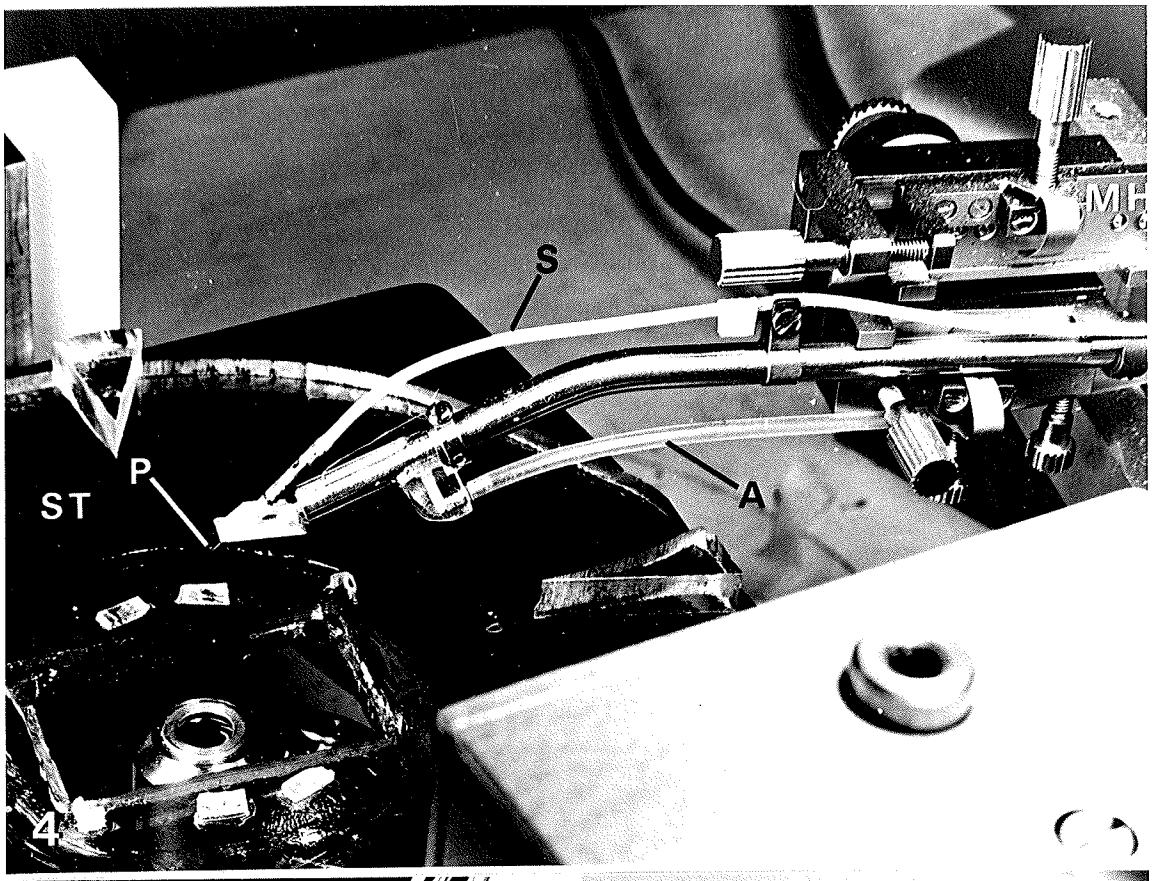
S
P
ST
A
4

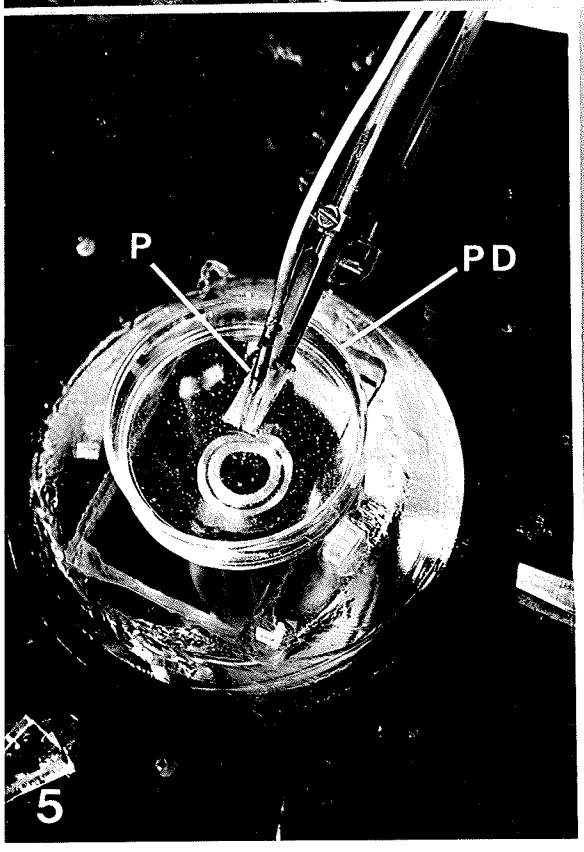
P
PD
5

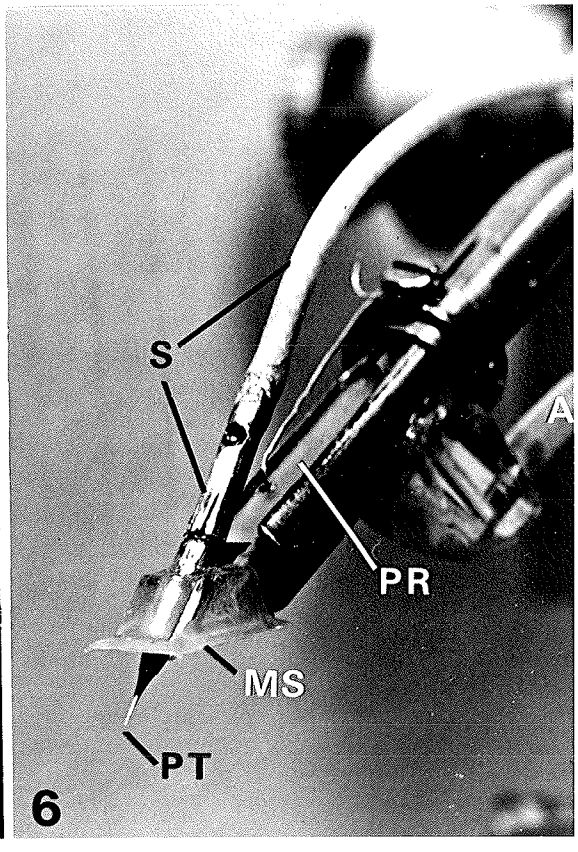
S
A
PR
MS
PT
6

Figure 7. The probe electrode fabrication equipment consisting of the probe maker (PM) which furnishes power to the heating filament and the current for the plating procedures. The plating solutions and heating filament are positioned by the micromanipulator (M).

Figure 8. Detail of the stage clamp holding the gold-coated shell (P). The heating filament (HF) is positioned to melt the solder inside the shell and form the connection with the internal socket. The syringe needle is removed and a coax cable (similar to the signal cable) is plugged into the shell (just visible at the top of the stage clamp in Fig. 5). The microscope allows observation of the probe tip during all plating procedures.

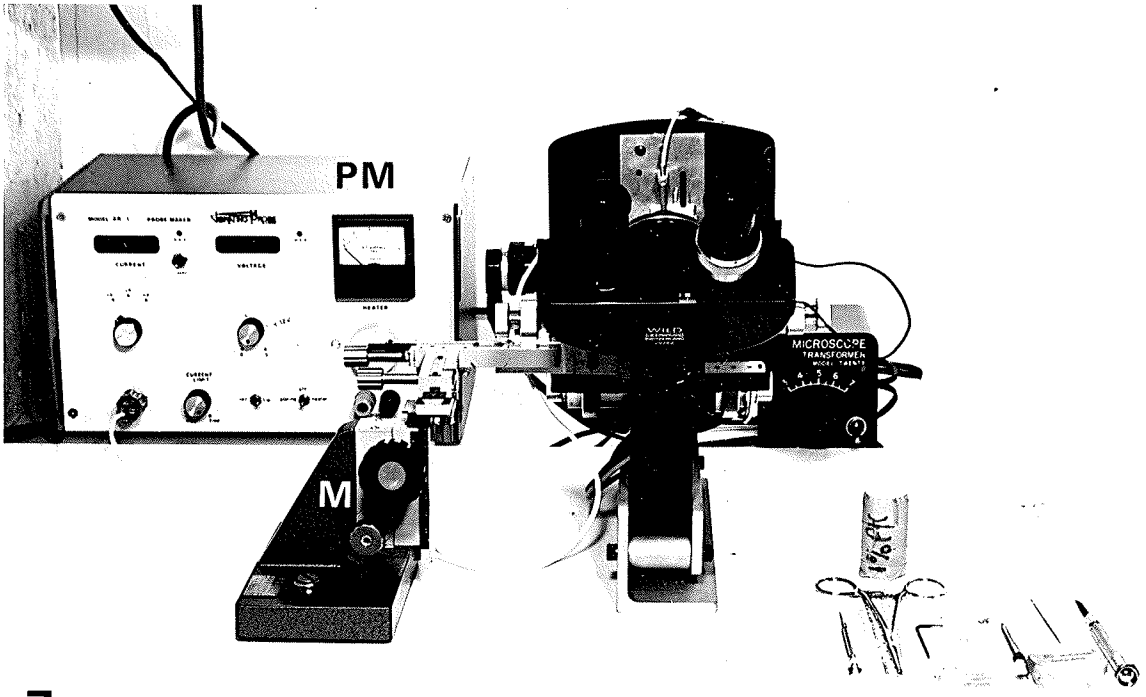

7

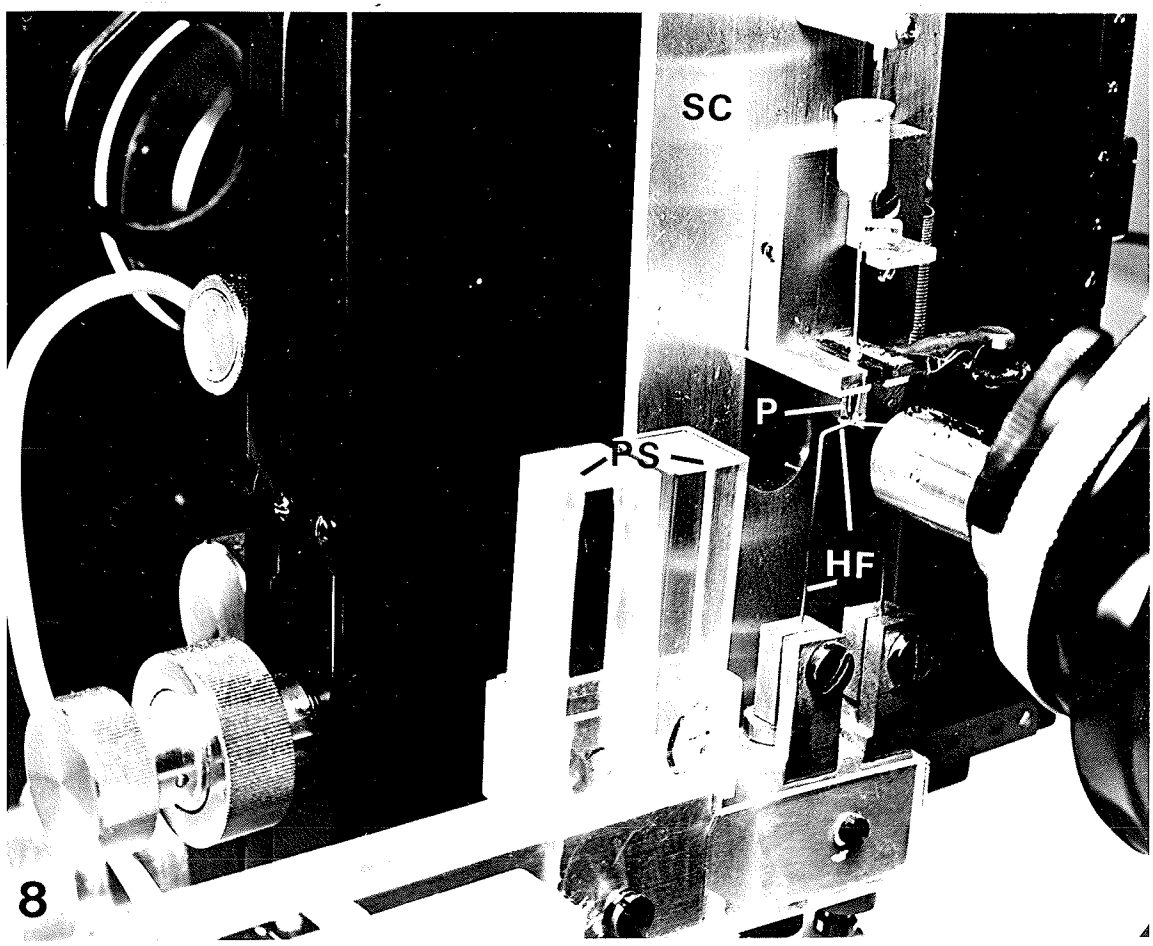

8

Figure 9. Schematic of probe electrode showing the platinum ball, (1); platinum reference electrode, (2); Cerrotru solder, (3); the #24 Twistcon socket, (4); the gold-coated exterior of the micropipette, (5); the epoxy stop ring, (6); and the silver epoxy coating which protects the gold coating when the signal cable is plugged into the probe (8 and 9).

Figure 10. The connections between the probe electrode (1) and the rest of the electronic equipment. The meniscus setter (2) is vibrated by the piezoelectric reed (3) which is powered by the vibrator power supply (5). The lock-in amp (4) receives the reference signal from the vibrator power supply at connection 9, the probe signal via the signal cable (12) at connection 8 and then sends the amplified DC signal from 10 to the chart recorder (6), resulting in the tracing (7).

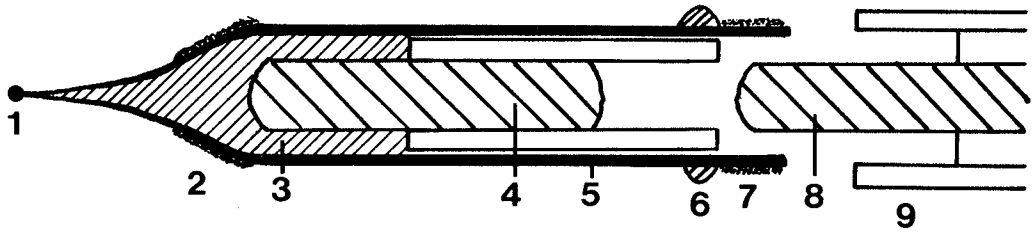
1
2
3
4
5
6
7
8
9

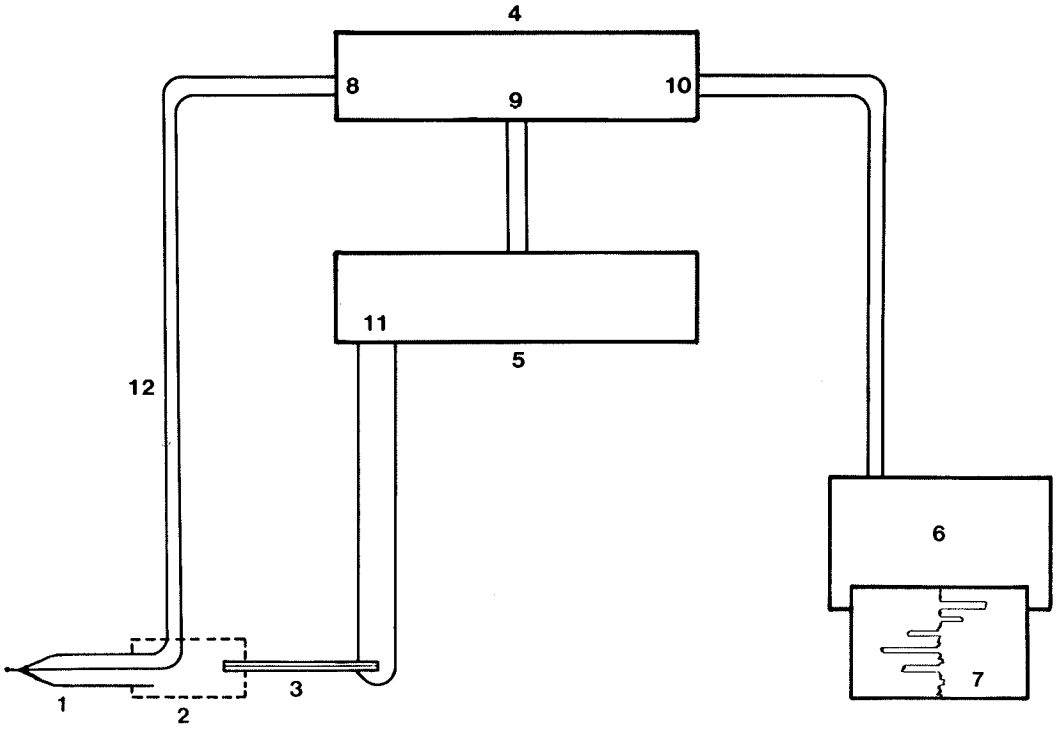
4
8
9
10
11
5
12
6
7
1
2
3

Figure 11. An example of the vibrating probe output. Peaks at the left represent influx current, while peaks to the right efflux current. After each measurement the probe is moved to a reference position to obtain a baseline. The numbered peaks represent the ovariole positions described in Fig. 1, Chapter 2.

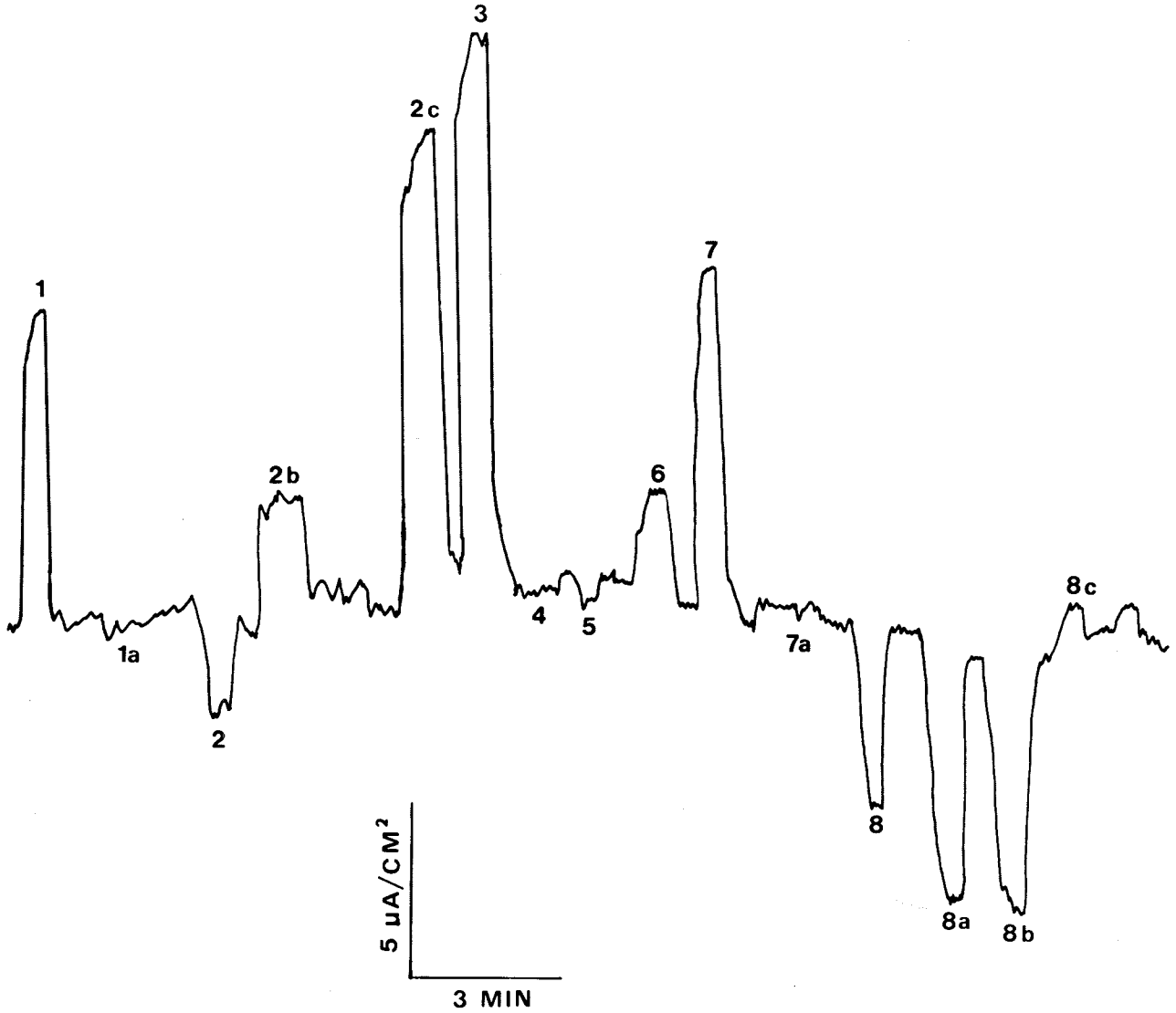
1
1a
2
2b
2c
3
4
5
6
7
7a
8
8a
8b
8c
5 µA/CM²
3 MIN

Appendix 2

Oocyte Growth Characteristics

Oocyte growth rate is determined by plotting T oocyte length versus days post feed (Fig. 1). Data in Fig. 1 represent ovarioles subsequently examined for extracellular currents (see Chapters 2 and 3). The large degree of scatter in the data indicates little correlation between the T follicle size and days post feed. A linear regression analysis bears this out producing a correlation coefficient of r=0.11. This unexpected result must be seen in relation to the feeding history of the individual insect. Detailed records of individual feeding histories were not kept, although in most cases the animals would have been starved for 2-3 weeks before feeding and subsequent use of the ovarioles.

The relation between T oocyte length and the penultimate (T-1) oocyte length demonstrates intraovariole regulation in Rhodnius. T-1 oocytes initially increase in length until the T oocyte attains a length of 600-800 μM, at which point the T-1 oocyte slows its growth (Fig. 2). This two stage process is illustrated by statistical analysis using linear and logarithmic curve fitting. The logarithmic curve fits the data better (r= 0.78) than the linear regression line (r= 0.69, Fig. 2).

The terminal follicle's trophic cord length can be indirectly monitored by measuring the distance between the anterior end of the T follicle and the tropharium base. The linear growth of the trophic cord and previtellogenic tissues anterior to the T-1 follicle as the T follicle increases in size is shown in Fig. 3. There is little difference in the linear and logarithmic curve fits, r= 0.80 and 0.86 respectively.

The assessment of the reproductive parameter; oocyte growth rate, permits the comparison between the colony of insects used in this study and other colonies used in this line of research. Because the insects are highly inbred in most laboratories, this would provide some indication that the timing of events during the oogenesis cycle can be applied to other Rhodnius colonies and be seen in light of previously published work.

The normal course of oocyte growth starts with a rapid size increase as the T oocyte enters vitellogenesis on day 3 post feed (Pratt and Davey, 1972a). By day 5 vitellogenesis is mostly completed and chorion formation begun. This is followed by the completion of chorionation on day 6 post feed (Pratt and Davey, 1972a). The scatter of data seen in Fig. 1 was unexpected but can be partially explained in relation to the individual insect feeding history. The large follicles found in ovarioles from animals only 1 or 2 days post feed is in disagreement with the work of Pratt and Davey (1972a) who found completion of oocyte growth occurred at 5 to 6 days post feed and may be explained as follicles left over from the previous cycle of oogenesis. Therefore these animals were not completely devoid of the previous blood meal and were still able to produce eggs. The number of early vitellogenic eggs ie, 400-500 μM seen at days 3, 4 and 6 is also not indicative of what appears to occur normally (Pratt and Davey, 1972a). Again if the previous blood meal had not been finished and the ovarioles were still producing eggs, a new blood meal would not initiate a new cycle of egg production, but simply prolong the first cycle. Therefore the number of days post feed would have little bearing on the stage of oogenesis; thus the Rhodnius ovariole will continuously produce eggs, if the blood meals are closely spaced.

This has been observed in the closely related species, Triatoma infestans (Regis, 1979) as well. In some cases ovarioles were obtained form animals which had been starved for 3-4 weeks before feeding. Pratt and Davey (1972b) report that in these animals, vitellogenesis is delayed for 2 to 3 days which would also contribute to the above results. The T follicle does not show the expected size increase after 6-10 days post feed, which is not in agreement with Pratt and Davey (1972a). At present this is not completely understood.

The comparisons of T-1 and T oocyte lengths (Fig. 2), agrees with the conclusions drawn by Pratt and Davey (1972a) showing the initial growth of the T-1 oocyte until reaching the "activation" size, and then holding at this point until the terminal oocyte becomes chorionated. Our data do not clearly show the initiation of T-1 vitellogenesis since ovarioles with a completely chorionated terminal oocyte (length >2000 μM) were not used in the electrophysiological part of the study. The discrepency of sizes which Pratt and Davey (1972a) state the T-1 oocyte attains during the arrested growth stage may be attributed to shrinkage of the ovariole caused by fixation prior to their measurements. All measurements made in this study were on live ovarioles which did not exhibit any signs of shrinkage.

The linear size increase of the previtellogenic region (Fig. 3) provides a clear indication that the trophic cord to the T oocyte lengthens throughout vitellogenesis until cord separation (Huebner, 1981a). Fig. 3 when compared with Fig. 2, also demonstrates the growth of the previtellogenic region anterior to the T-1 follicle, since before the T oocyte trophic cord loss, the T-1 follicle remains constant in length .

Therefore the coordinated growth of oocytes within the Rhodnius ovarioles used in this study resembles that observed by other reseachers and subsequent comparisons can be made with confidence.

Figure 1. T oocyte growth rate. The lack of correlation is discussed in the text. The regression line (not shown) has a correlation coefficient, r= 0.11.

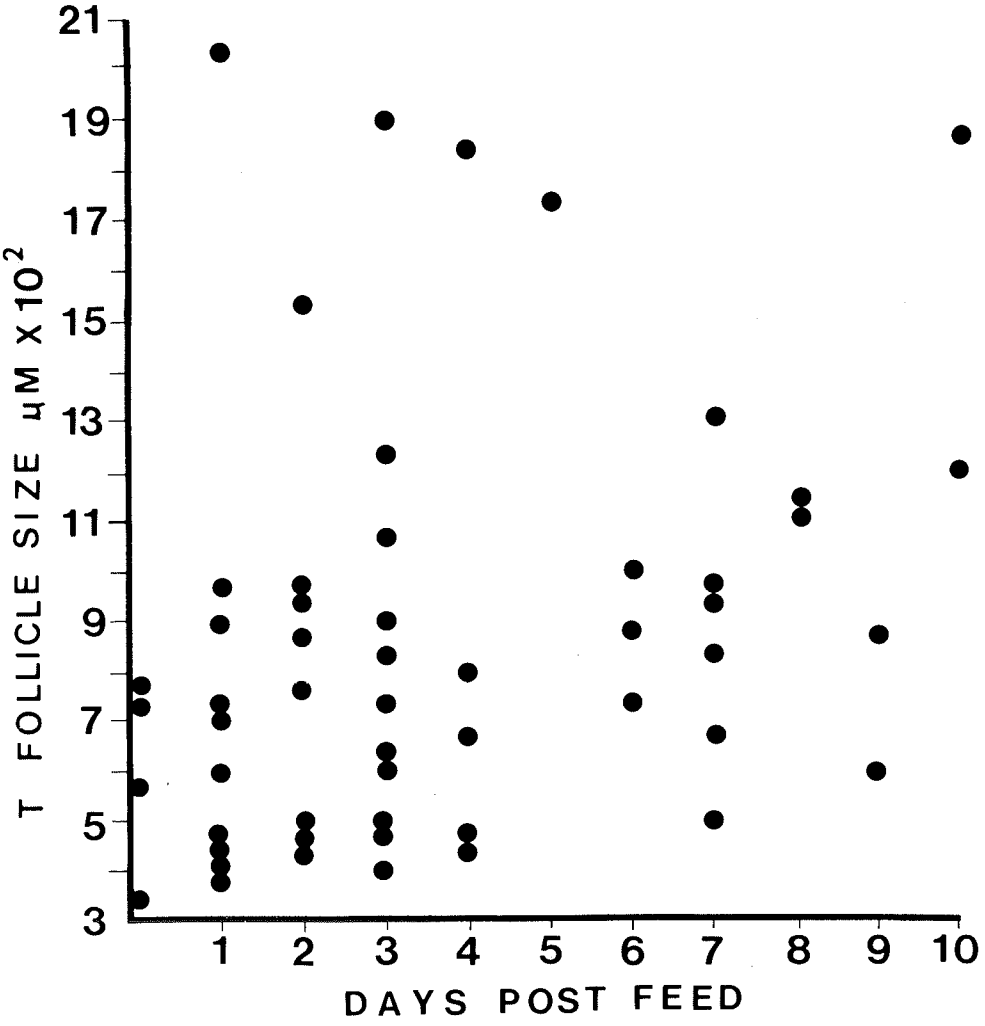
T FOLLICLE SIZE μM X10²
21
19
17
15
13
11
9
7
5
3
1
2
3
4
5
6
7
8
9
10
DAYS POST FEED

Figure 2. The relationship between T follicle and T-1 follicle size during oogenesis. The T-1 follicles have an initial growth increase which stops upon reaching a length of 300-450 μM. The logarithmic curve (solid circles) fits the data better than the linear regression line (open triangles), r= 0.78 versus 0.69 respectively.

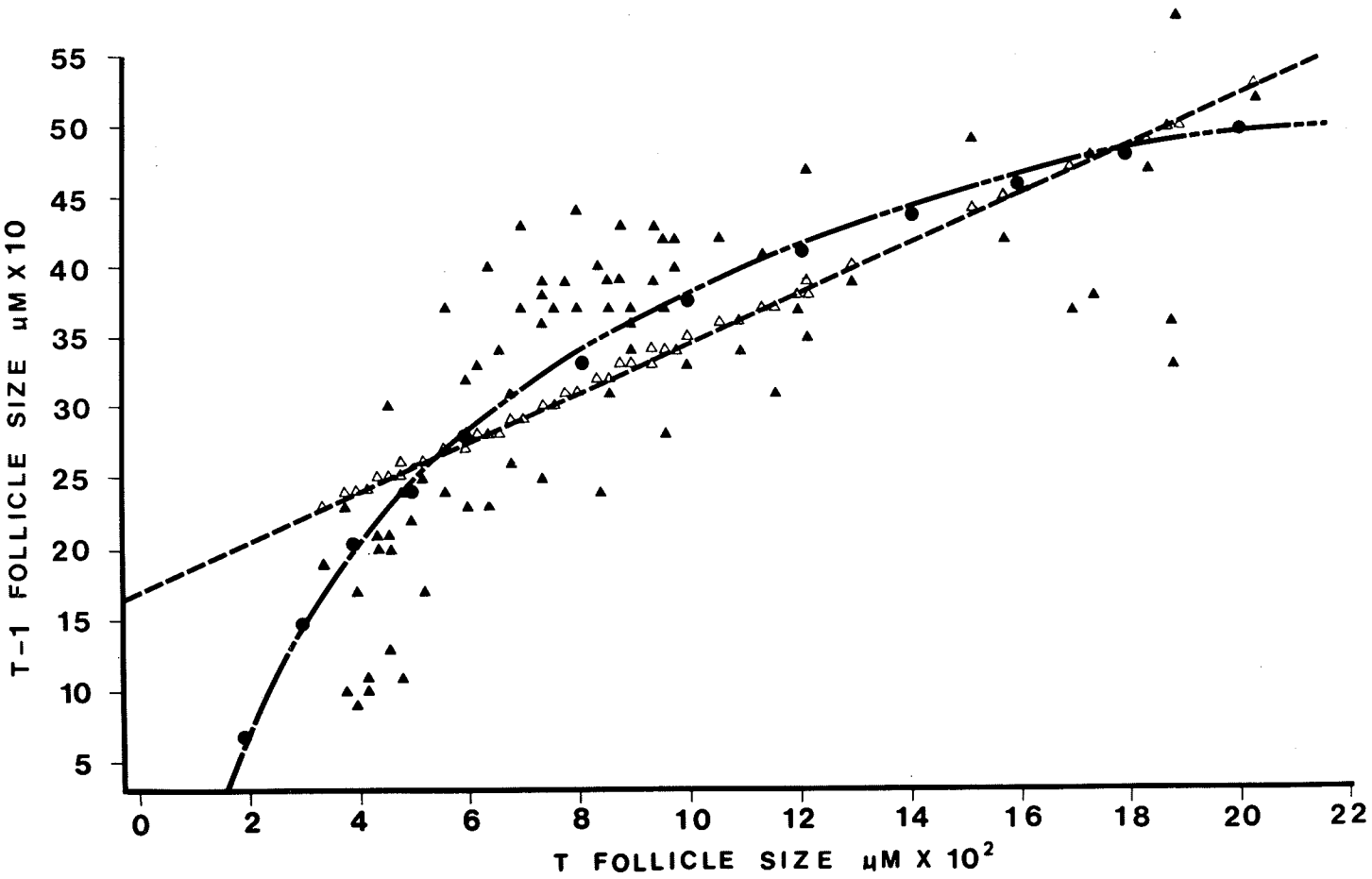
55
50
45
40
35
30
25
20
15
10
5
T-1 FOLLICLE SIZE µM X 10
0
2
4
6
8
10
12
14
16
18
20
22
T FOLLICLE SIZE µM X 10²

Figure 3. The relation of the entire previtellogenic region (including T-1 follicle) length and the T follicle size during oogenesis. The entire previtellogenic region lengthens as the T oocyte proceeds with vitellogenesis, thus giving a crude indication of the length increase of the T oocyte trophic cord. The relationship is approximately linear (open circles) with a correlation of r= 0.8 although the logarithmic curve (solid circles) also fits well, r= 0.86.

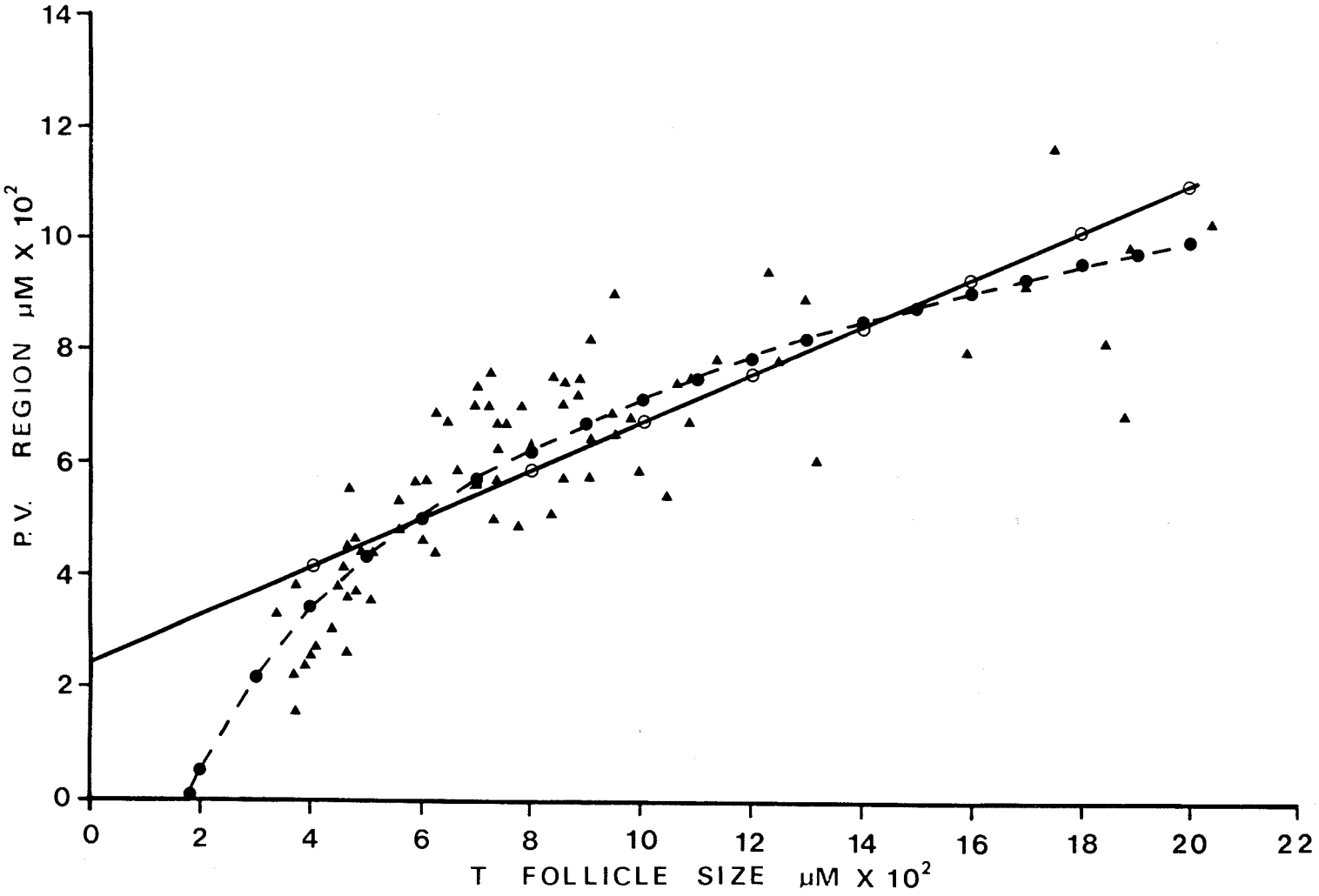
14
12
10
8
6
4
2
0
P.V. REGION µM X 10²
0
2
4
6
8
10
12
14
16
18
20
22
T FOLLICLE SIZE µM X 10²

Appendix 3

Statistical Analysis Techniques and Results

The analysis of the vibrating probe measurements presented in Chapter 2 required the comparisons of many means with each other. One way analysis of variance (F test) is the classical method of determining significant differences in a group of means, but does not indicate which means are different. For 2 or 3 means a standard Student's t test suffices, but as the number of means increases, so do the number of comparisons. For example, if 10 means are compared with each other, there will be 45 comparisons. If the significance level of each comparison is 0.01, then the probability of making a wrong decision concerning one of the comparisons is 0.45. an unacceptably high error rate (Ryan, 1959). A variety of multiple comparisons tests have been developed to overcome this problem, each having its own characteristics concerning how liberal or conservative the decision making process will be. The test chosen in this study is based on a "Bayes Rule for the Symmetric Multiple Comparisons Problem" (Waller and Duncan, 1969). The test was developed from the process of taking into account the "weighted average of the decision errors ie., the Bayes risk" (Waller and Duncan, 1969) and determining the "seriousness" of these errors. The approach is also intuitively appealing since it bases the Bayes t (t_B) value (which is similar to Student's t) on the F value from a standard analysis of variance. As the F value increases, the test becomes more liberal, and as it decreases the test becomes highly conservative, a response which tends to detect differences based upon the heterogeneity of the means (Waller and Duncan, 1969). A F value of 1 or less produces a t_B which approaches infinity.

The level of significance is determined by an error-seriousness ratio or k-ratio, which is the ratio between Type 1 and Type 2 errors ie., the probability of rejecting the null hypothesis when it is true versus the probability of accepting the null hypothesis when it is false. A k-ratio of 50:1, 100:1 or 500:1 is closely correlated with the common α levels of 0.1, 0.05 and 0.01 respectively (Waller and Duncan, 1969).

The test is applied as follows: the F value plus its degrees of freedom is entered into a table which determines the t_B for the selected k-ratio. This value is then entered into formula 1 (Waller and Duncan, 1969), which determines the least significant difference, LSD,

$$LSD = t_B [(2/r) s_e^2]^{\frac{1}{2}} \qquad (1)$$

where t_B is the Bayesan t value obtained above, r = number of means minus 2 and s_e^2 = sum of squares for the error (from the ANOVA table). The LSD is then compared with the difference between each pair of means being compared. If this difference exceeds the LSD, the means are considered significantly different at an error seriousness ratio k.

The following are the summary of analyses of the vibrating probe data. The first group consists of comparisons between the means for all the positions for one ovariole size class, the second consists of comparisons between the means for one position for all ovariole size classes. The comparisons can be conveniently presented by underlining the means which are not significantly different from each other.

Group 1

Ovariole Class = 1

r = 13 q = 14 F = 1.75 s_e^2 = 5.94 k = 100

f = 28 LSD = 2.62

P7a P8a P8 P8c P1a P8b P2 P4 P5 P7 P2a P1 P6 P3 P2c P2b

Ovariole Class = 2

r = 14 q = 15 F = 5.05 s_e^2 = 12.09 k = 100

f = 145 LSD = 260

P8a P6 P8 P5 P7a P8b P7 P8c P1a P4 P2 P2a P1 P2b P2c P3

Ovariole Class = 3

r = 14 q = 15 F = 4.70 s_e^2 = 3.45 k = 100

f = 60 LSD = 4.04

P5 P8 P8a P2 P7a P8b P2a P7c P6 P1a P7 P2b P4 P1 P2c P3

Ovariole Class = 4

r = 14 q = 15 F = 10.39 s_e^2 = 2.10 k = 100

f = 136 LSD = 1.8

P8 P8a P8b P7a P6 P8c P7 P2 P4 P2a P1a P5 P2b P1 P2c P3

Ovariole Class = 5

r = 14 q = 15 F = 10.13 s_e^2 = 1.09 k = 100

f = 87 LSD = 2.09

P8a P8 P8b P8c P2 P1a P4 P7a P6 P2a P5 P7 P1 P2b P2c P3

Ovariole Class = 6

r = 14 q = 15 F = 16.74 s_e^2 = 126 k = 100

f = 93 LSD = 27

P8 P7a P8a P8b P8c P4 P7 P2 P6 P5 P1a P2a P2b P1 P3 P2c

Ovariole Class = 7

r = 14 q = 15 F = 1.68 s_e^2 = 1.35 k = 100

f = 134 LSD = 480

P2 P8 P8a P6 P7 P7a P8b P4 P5 P2a P8c P1a P2b P1 P2c P3

Ovariole Class = 8

r = 14 q = 15 F = 14.28 s_e^2 = 314 k = 100

f = 102 LSD = 3.32

P6 P8 P8a P8b P2 P7a P4 P7 P5 P8c P1a P2a P2b P1 P2c P3

Ovariole Class = 9

r = 14 q = 15 F = 6.68 s_e^2 = 2.93 k = 100

f = 97 LSD = 3.30

P8 P8a P2 P8b P4 P6 P8c P7a P7 P1a P2a P2b P5 P1 P3 P2c

Group 2

Position P1

r = 7	q = 8	F = 1.08	s_e^2 = 38.41	k = 100
	f = 52			LSD = ___

No Significant Difference Between Means

Position P1a

r = 7	q = 8	F = 0.87	s_e^2 = 3.16	k = 100
	f = 50			LSD = ___

No Significant Differene Between Means

Position P2

r = 7	q = 8	F = 1.05	s_e^2 = 12.21	k = 100
	f = 61			LSD = 5.6

No Significant Difference Between Means

Position P2a

r = 7	q = 8	F = 0.28	s_e^2 = 5.68	k = 100
	f = 50			LSD = ___

No Significant Difference Between Means

Position P2b

r = 7	q = 8	F = 0.89	s_e^2 = 26.63	k = 100
	f = 55			LSD = ___

No Significant Difference Between Means

Position P2c

r = 7	q = 8	F = 3.21	s_e^2 = 50.85	k = 100
	f = 43			LSD = 8.39

6 8 7 9 4 3 5 2 1

Position P3

r = 7 q = 8 F = 4.06 s_e^2 = 63.3 k = 100

f = 64 LSD = 8.74

8	7	3	5	6	4	9	2	1

Position P4

r = 7 q = 8 F = 1.97 s_e^2 = 7.83 k = 100

f = 61 LSD = 3.86

8	9	7	5	6	2	1	4	3

Position P5

r = 7 q = 8 F = 1.6 s_e^2 = 30.34 k = 100

f = 60 LSD = 8.14

3	2	8	7	6	1	5	4	9

Position P6

r = 7 q = 8 F = 1.43 s_e^2 = 20.4 k = 100

f = 65 LSD = 6.81

8 2 7 6 9 4 3 5 1

Position P7

r = 7 q = 8 F = 0.19 s_e^2 = 51.37 k = 100

f = 65 LSD = ___

No Significant Difference Between Means

Position P7a

r = 7 q = 8 F = 0.37 s_e^2 = 9.79 k = 100

f = 41 LSD = ___

No Significant Difference Between Means

Position P8

r = 7	q = 8	F = 0.8	s_e^2 = 3.6	k = 100
	f = 65			LSD = ___

No Significant Difference Between Means

Position P8a

r = 7	q = 8	F = 0.34	s_e^2 = 4.16	k = 100
	f = 47			LSD = ___

No Significant Difference Between Means

Position P8b

r = 7	q = 8	F = 0.86	s_e^2 = 4.06	k = 100
	f = 46			LSD = ___

No Significant Difference Between Means

Position P8c

r = 7	q = 8	F = 1.06	s_e^2 = 0.69	k = 100
	f = 42			LSD = ___

No Significant Difference Between Means